MAGNETIC BEHAVIOR IN METAL TETRACYANOETHYLENE MOLECULE-BASED MATERIALS

by

Amber Clarice McConnell

A dissertation submitted to the faculty of
The University of Utah
in partial fulfillment of the requirements for the degree of

Doctor of Philosophy

Department of Chemistry

University of Utah

August 2012

The University of Utah Graduate School

STATEMENT OF DISSERTATION APPROVAL

The dissertation of _____

has been approved by the following supervisory committee members:

_____ , Chair _____
Date Approved

_____ , Member _____
Date Approved

_____ , Member _____
Date Approved

_____ , Member _____
Date Approved

_____ , Member _____
Date Approved

and by _____ , Chair of

the Department of _____

and by Charles A. Wight, Dean of The Graduate School.

ABSTRACT

Several compounds in the metal-tetracyanoethylene (TCNE) family of molecule-based magnets have been studied. The first two are compounds that exhibit similar magnetic behavior as well as share an almost identical synthetic route, namely, $Mn^{II}(TCNE)_{3/2}(I_3)_{1/2}$ and $Mn^{II}(TCNE)I(OH_2)$. They both have a critical temperature of 171 K and exhibit bulk ferrimagnetism. $Mn^{II}(TCNE)_{3/2}(I_3)_{1/2}$ is the first known structure of a molecule based magnet to possess μ_4-$[TCNE]^{\cdot -}$ in all three dimensions. $Mn^{II}(TCNE)_{3/2}(I_3)_{1/2}$ was also shown to exhibit a pressure-induced reversible enhancement of the critical temperature up to a maximum of 273 K. Suprisingly 2-D $Mn^{II}(TCNE)I(OH_2)$ has the same critical temperature as 3-D $Mn^{II}(TCNE)_{3/2}(I_3)_{1/2}$ which may be attributed to significant dipolar interactions between the layers due to the relatively short interlayer separation. The next two compounds are the isostructural $M^{II}(TCNE)[C_4(CN)_8]_{1/2}$ (M = Mn, Fe). It was shown via detailed magnetic susceptibility measurements that they both possess an antiferromagnetic ground state with T_cs of 67 and 84 K, respectively. They also both exhibit a reversible ferri- or ferromagnetic pressure-induced magnetic transition. Finally, through a Mean Field (MF) theory analysis, it was shown that expressions that relate the exchange coupling to the critical temperature could be generated for several structure-types of the metal-TCNE family of materials. Using these expressions allowed for the estimation of the exchange coupling for several metal-TCNE compounds.

This dissertation is dedicated to my girls: my mother Charline, my sister Cira and my daughter Adelaide.

TABLE OF CONTENTS

LIST OF TABLES

LIST OF FIGURES

LIST OF SYMBOLS AND ABBREVIATIONS

MBM	molecule-based magnet
M	magnetization
H	applied magnetic field
E	energy
μ_n	microscopic magnetization
N_A	Avogadro's number
k_B	Boltzmann's constant
χ	molar magnetic susceptibility
C	Curie constant
g_e	Landé g-factor
S	total spin
θ	Weiss constant
T	temperature
E_T	thermal energy
E_J	magnetic coupling energy
T_c	critical ordering temperature
T_N	Néel temperature
J	exchange coupling
1-D	one-dimensional
2-D	two-dimensional
3-D	three-dimensional
MF	Mean Field

z	coordination number
Oe	Oersted
M_{ZFC}	zero field cooled magnetization
M_{FC}	field cooled magnetization
T_b	bifurcation temperature
M_r	remnant magnetization
B	Brillouin function
T	Tesla
H_{cr}	coercive field
M_s	saturation magnetization
AC	alternating current
DC	direct current
ω	frequency
χ'	in-phase AC susceptibility
χ''	out-of-phase AC susceptibility
TCNE	tetracyanoethylene
TPP	tetraphenylporphrin
THF	tetrahydrofuran
MeCN	acetonitrile
MPMS	magnetic properties measurement system
SQUID	superconducting quantum interference device
IR	infrared
ν	infrared absorption
emu	electromagnetic unit
EPR	electron paramagnetic resonance
$OCMe_2$	acetone
RT	room temperature

f	frustration
H_c	critical field
T_t	tricritical temperature
K	interlayer exchange coupling between M and M
M	metal ion
L^S	spin bearing ligand
L^{NB}	non-spin bearing, non-bridging ligand
L	non-spin bearing, bridging ligand
J'	interlayer exchange coupling between M and L^S or L^{S1}
$M1$	average spin on M
$M2$	average spin on L^S or L^{S1}
$M3$	average spin on L^{S2}
H_{eff}	effective field
$\boldsymbol{H}$	effective Hamiltonian
P	pressure
AFM	antiferromagnetic
FM	ferromagnetic
FI	ferrimagnetic
PM	paramagnetic

ACKNOWLEDGEMENTS

As the final pages of my dissertation come to completion, I find myself facing the most difficult challenge: how can I possibly express the gratitude I have for the people in my life? I am reminded of a quote from Stephen King's 'The Body' that says: "The most important things are the hardest to say…because words diminish them – words shrink things that seem limitless." So I find that I cannot express the words that accurately represent how I feel; nonetheless, here is my clumsy attempt.

First, I would like to thank my best friend, Adam, for the incredible amount he has sacrificed, especially in this last year and for all of the support and understanding he has given me. Next, I would like to thank my mom, Charline, for her undying love and encouragement and for supporting me no matter what I do in life. I would also like to thank my dad, Scott, for his humor, his wisdom, and for his uncanny ability to understand me. I would especially like to thank my daughter Adelaide; although she doesn't know it yet, she inspires me to do better. During the most difficult times, her smiling face was my daily reminder of why I had to push through and finish.

I would next like to express my gratitude toward my mentor, Professor Joel Miller for his guidance, knowledge and expertise about magnetism and about life. His vast knowledge in the area of molecule-based magnets has given me very valuable insight into a field of research that is notoriously complicated. He has helped me become a better chemist, scientist and critical thinker. I would also like to thank him for giving me the opportunity to manage and maintain one of the most state-of-the-art instruments in our

field of research, which has resulted in experience that will help me become successful in my career.

In addition to my graduate mentor, special thanks must be given to my undergraduate mentor, Dr. Jamie Manson. His leadership and guidance were the motivation for me to attend graduate school. Without his support and encouragement I would not have pursued an advanced degree.

In addition, there are several members of the Miller group that have given me their guidance, advice and support. I especially would like to thank Dr. William Shum for giving me a solid foundation of understanding of magnetism and for teaching me everything I know about SQUID magnetometry. I would also like to thank Dr. Chris Kareis for sharing his incredible synthetic intuition and for his friendship (although some may say that it is more like a sibling rivalry!). I would also like to give special thanks to Jack DaSilva for dedicating large portions of his time to edit this dissertation. Also, I would like to thank current group members, Andrew Simonson, Josh Sussman, Josh Bell, Lan Vo, Zach Fox, Kevin Seigel, Casey Hawkins, Royce Davidson; and past group members, Brian Lefler, Jason Schaller, Preston Erickson, Dr. Kendric Nelson, Dr. Kostia Pokhodnya, Dr. Bretni Kennon, Dr. Endrit Shurdha, and Dr. Jordan Arthur.

I would also like to thank: Dr. Randy Fishman for his collaboration and for teaching me everything I know about mean field theory; Jo Hoovey for her friendship and guidance; and Dr. Carrie Kelley for the valuable and candid conversations about first-year teaching strategies. I would also like to thank my friends from back home, Jennifer Dunn and Michaela Lindsay whose friendships have been two of the most solid relationships I have had in my life. I would like to thank all of the friends I have gained

during my time here in Utah, especially Paige Sidwell, Jennifer Williams and Jessica Johnston.

Finally, I would like to thank the University of Utah for the opportunity to pursue my degree, all of the members of my research committee, and for research funding provided by the Department of Energy Division of Material Science (Grant No. DE-FG03-93ER45504).

CHAPTER 1

MAGNETIC MATERIALS, INTRODUCTION TO MAGNETISM, AND TETRACYANOETHYLENE-BASED MOLECULE-BASED MAGNETS

Magnetic Materials

The design and investigation of new materials that have potential technological application is an expanding facet of research. In particular, the study of magnetism and magnetic materials has led to discoveries that have developed into exciting fields of study such as molecule-based magnets (MBM), spintronics, spin-cross over, photomagnetics, single molecule magnets, and nanomagnetism, to name a few.[1] Magnets are ubiquitous components of technology and contribute significantly to the current economy. Therefore, the study of magnetism and magnetic materials has become an essential aspect of research worldwide.[2]

Traditionally, magnets are atom-based materials comprised of metal and/or metal-oxides. These magnets are expensive, due to their energy-intensive syntheses, and have limited synthetic diversity; however, they are useful due to their high magnetic densities. An advantage that MBMs have over their traditional counterparts is that their synthesis can be performed at ambient conditions. Also, the properties of MBMs can be fine-tuned

due to the "building block" approach taken in their syntheses through which one can envision the deliberate inclusion of particular molecules so that specific magnetic behaviors are achieved. Also, several MBMs have exhibited interesting magnetic properties that, in tandem with other properties, result in new phenomena like photo-induced magnetism.[3] Although, MBMs may present an exciting alternative to traditional magnets, they have several limitations. Due to MBMs containing more "non-magnetic bulk" than traditional magnets, they usually exhibit lower magnetic densities, and therefore lower ordering temperatures. Also, many MBMs are air sensitive readily decomposing upon exposure. However, recent work in the field of MBMs has led to discoveries of several room temperature magnets that show promising technological applications.[4]

Introduction to Magnetism

Magnetism is the response of a material to an applied magnetic field. The type of response is determined by the occupancy of the electrons in the orbitals of the material. If the electrons are all spin-paired, the material will repel a magnetic field, resulting in diamagnetism. This is the most common type of magnetic response found in everyday materials, such as rubber, plastic and clothing. In fact, every material exhibits some diamagnetism due to spin-paired core electrons. On the other hand, if a material contains unpaired electrons it will be attracted to a magnetic field, resulting in paramagnetism. In an ideal paramagnet, the unpaired electrons are non-interacting and exhibit random orientations due to thermal energy. More commonly, however, short-range interactions occur in which the electrons within the material will tend to align in a particular fashion.

When the interactions become strong enough to overcome thermal energy, long-range interactions occurs, resulting in magnetic ordering.

Curie-Weiss law. The magnetic behavior of a material is measured as a response to an applied magnetic field. When a sample is perturbed by an external magnetic field, in classical mechanics the magnetization, *M*, can be written as

$$M = -\frac{\partial E}{\partial H}, \tag{1.1}$$

in which *M* is the molar magnetization, *H* is the applied field, and *E* is the energy. In quantum mechanics, the energy, *E*, of a system can be rewritten as E_n in which *n* is the principle quantum number ($n = 1, 2, 3, \ldots$) and eqn. (1.1) becomes

$$\mu_n = -\frac{\partial E_n}{\partial H}, \tag{1.2}$$

in which μ_n is the microscopic magnetization.[5] According to the Boltzmann distribution law,[5] the macroscopic magnetization is the summation of the population-weighted average of the microscopic magnetizations giving

$$M = \frac{N_A \sum_n \left(-\frac{\partial E_n}{\partial H}\right) e^{\left(-\frac{E_n}{k_B T}\right)}}{\sum_n e^{\left(-\frac{E_n}{k_B T}\right)}}, \tag{1.3}$$

in which N_A is Avogadro's number and k_B is the Boltzmann constant. The molar magnetic susceptibility can thus be determined[5] by

$$\chi = \frac{\partial M}{\partial H}. \tag{1.4}$$

In an ideal paramagnet, with uncorrelated spins, the magnetic susceptibility is inversely proportional to temperature and can be described by the Curie Law[6]

$$\chi = \frac{C}{T}, \tag{1.5}$$

in which C is the Curie constant and equal to

$$C = \frac{N_A g_e^2 \mu_B^2 S(S+1)}{3k_B}, \tag{1.6}$$

in which g_e is the Lande g-factor for the electron, μ_B is the Bohr magneton, and S is the total spin.

When spins within a material exhibit short-range interactions, a deviation from the Curie law occurs in which the magnetic susceptibility dependence on temperature becomes

$$\chi = \frac{C}{T - \theta}, \tag{1.7}$$

which is the Curie-Weiss law,[6] in which θ is the Weiss constant and takes into consideration the type of magnetic interactions that occur within the material. A plot of $\chi^{-1}(T)$, (See Figure 1.1) shows a linear relationship between χ^{-1} and T in which the temperature axis intercept can reveal the nature of interactions. For example, a negative Weiss constant reveals antiparallel alignment between neighboring spins (antiferromagnetic interactions) and a positive Weiss constant reveals parallel alignment between neighboring spins (ferromagnetic interactions). It must be noted that these interactions, described by the Curie-Weiss Law are short-range pair-wise interactions and are not indicative of long-range magnetic ordering.

Magnetic ordering. When interactions between neighboring spins lead to a bulk phenomenon and exhibit long-range correlation, the system is said to be magnetically ordered. As previously stated, there are two types of coupling: (1) antiferromagnetic coupling, in which spins align antiparallel, and (2) ferromagnetic coupling, in which spins align parallel. These two coupling interactions can lead to a vast array of magnetic behavior (see Figure 1.2).[7] The three most common are: (1) ferromagnetic, (2) antiferromagnetic, and (3) ferrimagnetic ordering. Ferromagnetic ordering is present when long-range alignment of magnetic moments occurs in a parallel fashion, leading to a spontaneous net magnetic moment. This suggests that the individual molecule magnetic moments are arranged in a regular manner. Antiferromagnetic ordering is present when long-range alignment of magnetic moments occurs in an antiparallel fashion, which does not lead to a spontaneous magnetic moment due to the net cancellation of the individual magnetic moments. Ferrimagnetic ordering can be considered a special case of antiferromagnetism in which the material exhibits a spontaneous magnetic moment even

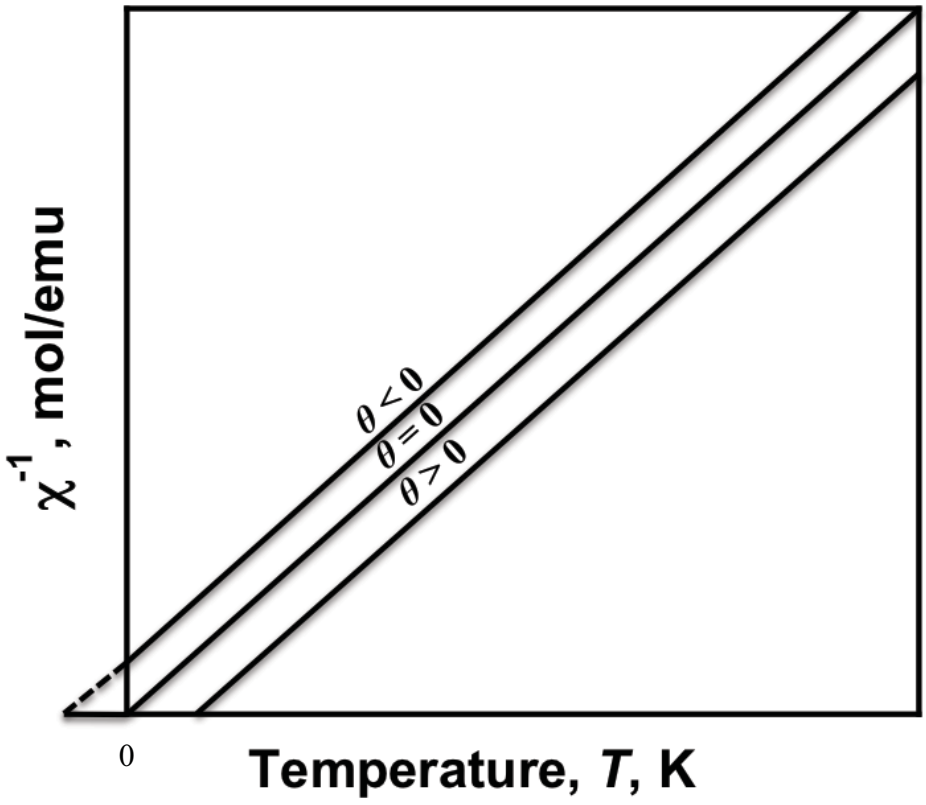

Figure 1.1. Plot of $\chi^{-1}(T)$ showing the effect of intermolecular interactions in paramagnets.

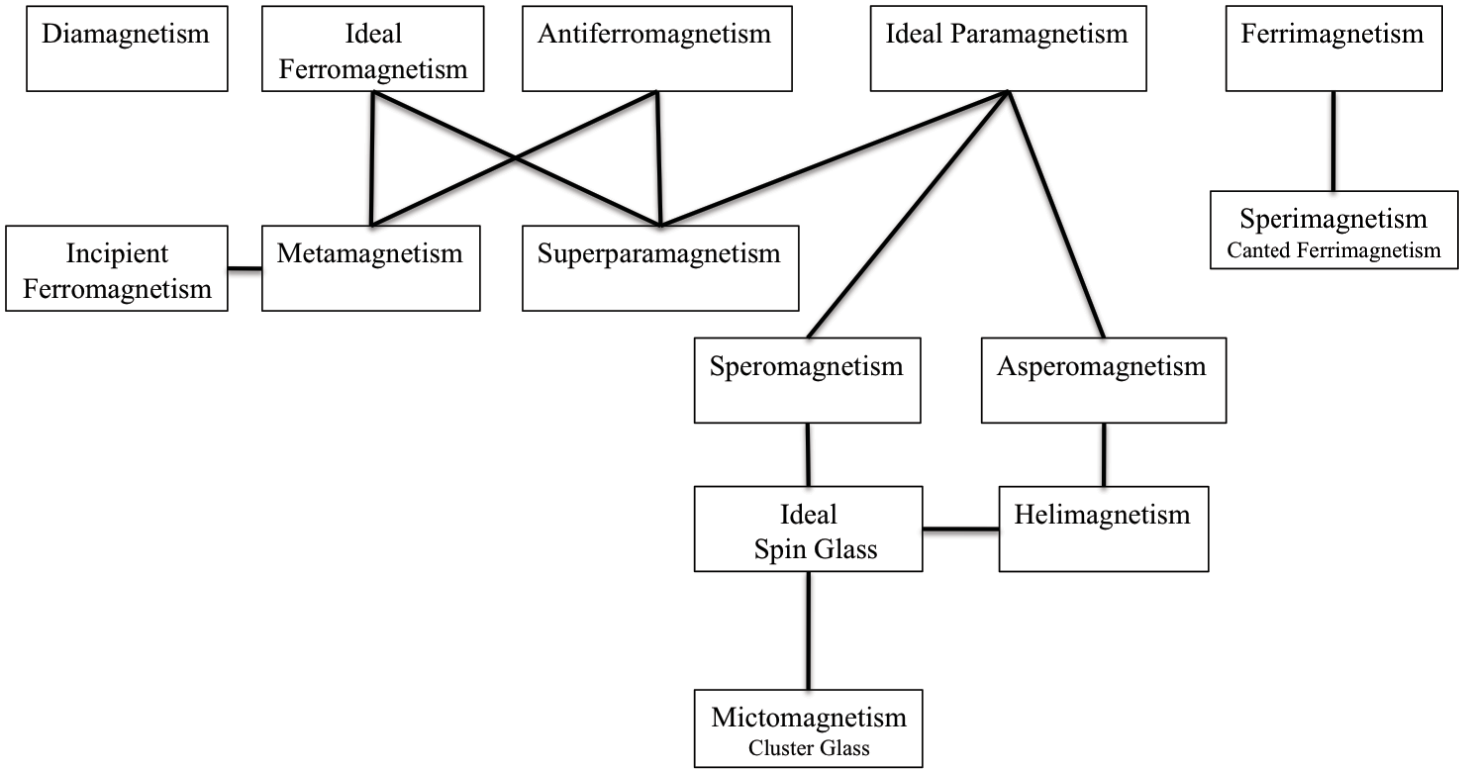

Figure 1.2. Hierarchy of magnetic behavior (adapted from ref. 7).

though long-range antiparallel alignment of magnetic moments occurs. This is because the moments are nonequivalent and therefore complete cancelation of spins does not occur.

The magnetic behaviors that occur in a material are determined by the competition of two energies: the thermal energy, $E_T \sim k_B T$, and the magnetic coupling energy, $E_J \sim J/K$. For magnetically ordered materials at high temperatures, thermal energy dominates ($E_T >> E_J$) and the system is in its paramagnetic phase and, typically, the material behaves according to the Curie- or Curie-Weiss Law. At low temperatures, the magnetic coupling energy dominates ($E_J >> E_T$) and the system is in its magnetic phase. A magnetic phase change occurs at the temperature at which the thermal and magnetic energies are equivalent. This is commonly referred to as the critical temperature, T_c (or sometimes as the Neél temperature, T_N for antiferromagnets).

There are several types of interactions that facilitate magnetic ordering that are referred to as magnetic exchange pathways. The types of magnetic exchange pathways that are present in a material is governed by its structural and electronic properties. The strongest type of exchange pathway is a direct exchange interaction, in which magnetic moments communicate directly through a bond.[8a] The type of coupling that occurs between magnetic moments, whether antiferromagnetic or ferromagnetic, is governed by Coulombic interactions and the Pauli exclusion principle.[8a] Typically, this can be determined by evaluating the magnetic orbitals. Magnetic orbitals are defined as the orbitals on a species that are occupied by unpaired electrons.[5] If the magnetic orbitals on neighboring ions are orthogonal, then due to the Pauli principle the electrons can occupy the same spin state and couple ferromagnetically in order to minimize electronic

repulsion. On the other hand, if the magnetic orbitals between neighboring magnetic ions are not orthogonal then the moments are restricted to align antiparallel and couple antiferromagnetically. A weaker pathway that is similar to direct exchange is superexchange.[9] Superexchange also occurs when magnetic moments communicate through bonds, however the magnetic ions are separated by a diamagnetic species that does not contain a magnetic orbital(s), and therefore it creates a weaker interaction.

The weakest type of exchange pathway that can occur is an indirect exchange interaction, which occurs through space. One type of indirect exchange is dipole-dipole interaction.[2,8a] Compared with the direct exchange pathways, this is typically very weak and therefore insignificant. However, as will be discussed in Chapter 2, if present in the right environment, the dipole-dipole interaction may contribute significantly to the overall coupling and therefore can have a large role in magnetic ordering. Another type of indirect exchange involves the so-called RKKY interaction[8b] in which the polarization of conduction electrons in transition metals by interaction with local spins contributes to the spin-spin interaction.

The magnitude and the sign of the coupling constant, *J*, which is a measure of the strength of the magnetic interaction, can be calculated by the use of several mathematical models. Typically, these models are limited to systems with only one spin-bearing species or with isotropic magnetic interactions. For example, the Fischer-Chain model[10] is used to calculate the magnetic coupling in 1-D chain systems. The Heisenberg, XY and Ising models[11] have all been used to describe 2-D layered compounds. Also, Mean Field (MF) theory [6,12] has been used extensively to describe 3-D cubic systems and is the basis

for the Curie and Curie-Weiss Laws. Using MF theory for an ordered system, the relationship between T_c and J is estimated as

$$T_c = \frac{2JzS(S+1)}{3k_B}, \tag{1.8}$$

in which z is coordination number of the magnetic ion. In a subsequent chapter, it will be shown how the use of MF theory can be applied to more complicated ordered systems that contain more than one magnetic ion and type of interaction, J.

Magnetic Measurements

In order to correctly probe the magnetic properties of a system, the appropriate measurements must be taken. The most useful is to measure the magnetization as a function of temperature, $M(T)$, Figure 1.3. This measurement is carried out by placing the sample in the magnetometer, cooling the sample in zero field and then measuring the magnetization upon warming in a constant applied field (usually 1000 Oe). A measurement with a small enough applied field, H, allows for the relationship in eqn. 1.4 to be simplified to eqn. 1.9 and the magnetization, M to become linearly proportional to the field, H, by a scalar which is called the susceptibility,

$$M = \chi H. \tag{1.9}$$

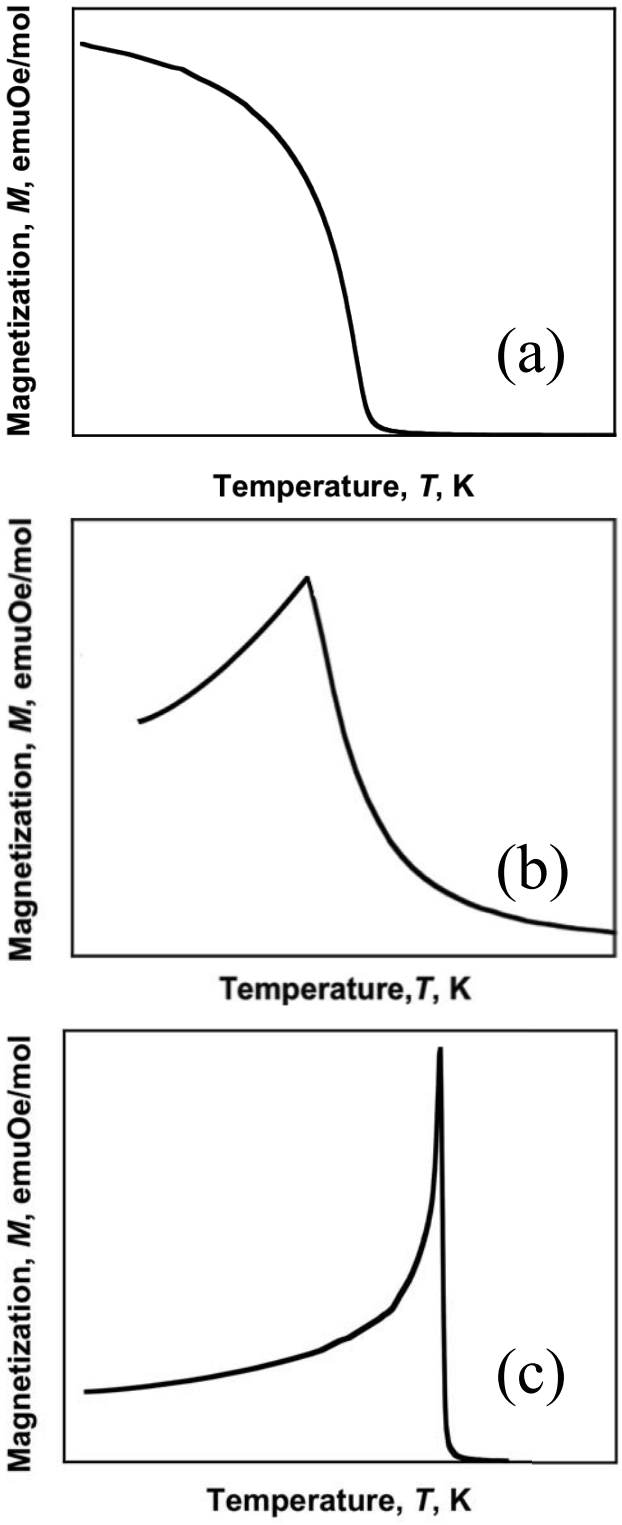

Figure 1.3. Diagram of magnetization as a function of temperature for ferromagnet (a), antiferromagnet (b), ferrimagnet (c).

For an ordered material, in addition to an $M(T)$ measurement, a useful probe to understand the magnetic ground state, and thus into the magnetic interactions, is zero-field-cooled, $M_{ZFC}(T)$ and field-cooled, $M_{FC}(T)$ measurement, Figure 1.4. This is carried out by cooling the sample in zero field and then measuring the magnetization upon warming in a small applied field (usually < 5 Oe) followed by cooling the sample in the same field as the zero-field measurement and then remeasuring the magnetization. When the $M_{ZFC}(T)$ and $M_{FC}(T)$ data are overlapped, for magnetically ordered materials that have a spontaneous magnetic moment (ferro- or ferrimagnetic), a bifurcation temperature, T_b, will be revealed. This temperature represents a point of irreversibility within the system and indicates a magnetic transition is present at that temperature. A typical response of $M_{ZFC}(T)$ and $M_{FC}(T)$ measurements for antiferromagnetic MBMs is not well-known. However, an analysis of data from $M_{ZFC}(T)$ and $M_{FC}(T)$ measurements of two antiferromagnetic MBMs is discussed in Chapter 3.

A well-established method for determining the T_c of a material is to perform a remanant magnetization measurement, $M_r(T)$, Figure 1.5. This is carried out by cooling the sample in an applied magnetic field (typically the same field used for the $M_{ZFC}(T)$ and $M_{FC}(T)$ measurements)then turning the field off and measuring the magnetization upon warming. Materials that have a spontaneous magnetic moment (i.e. ferri- or ferromagnetic ordering) will exhibit magnetization values that are not trivial, in the low temperature region. Upon warming, the data will exhibit a sharp decline in value as the magnetic transition is approached, after which, it will approach zero once T_c is exceeded. T_c is determined by an extrapolation of the linear-most region of the data as $M_r(T)$ approaches zero.

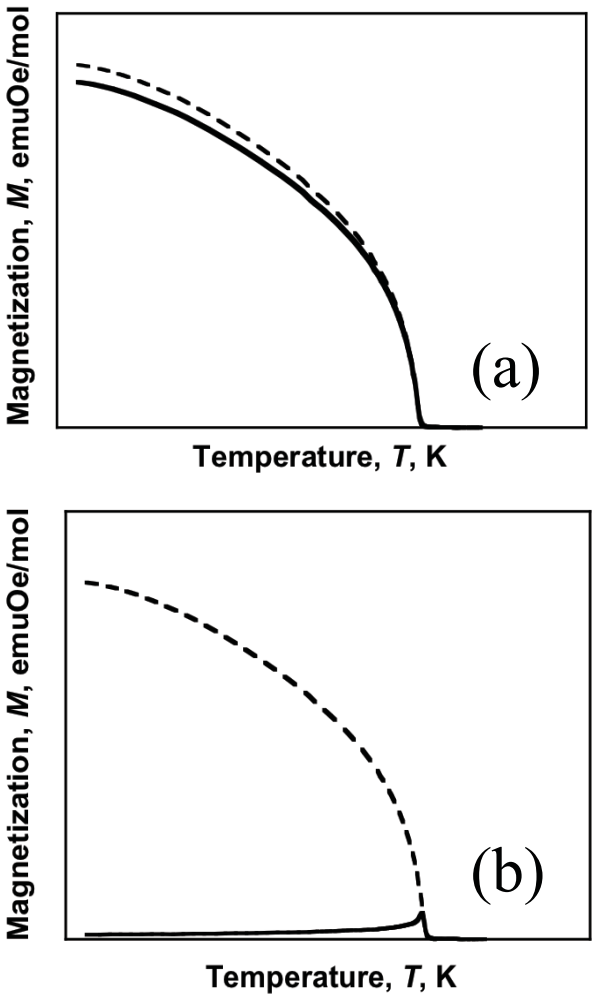

Figure 1.4. Diagram of zero-field cooled (–) and field-cooled (--) magnetization for ferromagnet (a) and ferrimagnet (b).

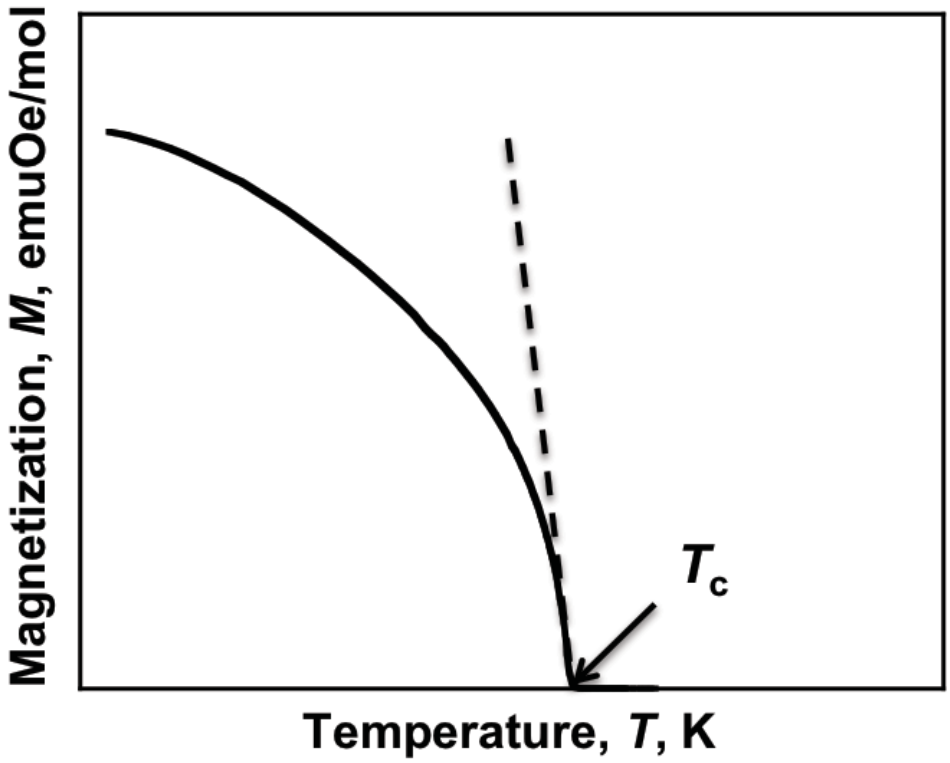

Figure 1.5. Plot of remanant magnetization, $M_r(T)$ with extrapolated critical temperature, T_c.

Another method of probing the magnetic properties of a material is to perform an isothermal field dependent magnetization, $M(H)$, measurement. For paramagnetic material, the measurement is carried out at low temperatures at which the magnetization is measured as a function of applied field ($H > 0$). The magnetization data can then be fitted using

$$M = N_A g_e \mu_B S B, \tag{1.10}$$

in which B is the Brillouin function,[5] given by

$$B = \frac{2S+1}{2S}\coth\left(\frac{2S+1}{2S}x\right) - \frac{1}{2S}\coth\left(\frac{x}{2S}\right) \quad \text{and} \quad x = \frac{g_e \mu_B S H}{k_B (T-\theta)}. \tag{1.11}$$

For ordered materials, the measurement is carried out in the magnetic temperature region (below T_c) as a function of applied field (H ± 5T, or ± 9T depending on the instrument), Figure 1.6. Materials that exhibit a spontaneous magnetic moment will reveal irreversibility in the measurement, typically referred to as hysteresis, in which three key magnetic properties can be extracted: (1) remanant magnetization, M_r, which represents the magnetization that remains with no applied field after the material is brought to saturation, (2) coercive field, H_{cr}, which is the field required to demagnetize a sample and is a useful indicator for the type of potential technological application and (3) saturation magnetization, M_s, which is the maximum magnetization a sample can exhibit. Antiferromagnetically ordered materials will not exhibit hysteretic behavior in an isothermal field dependent measurement, however, if the coupling is weak enough, they

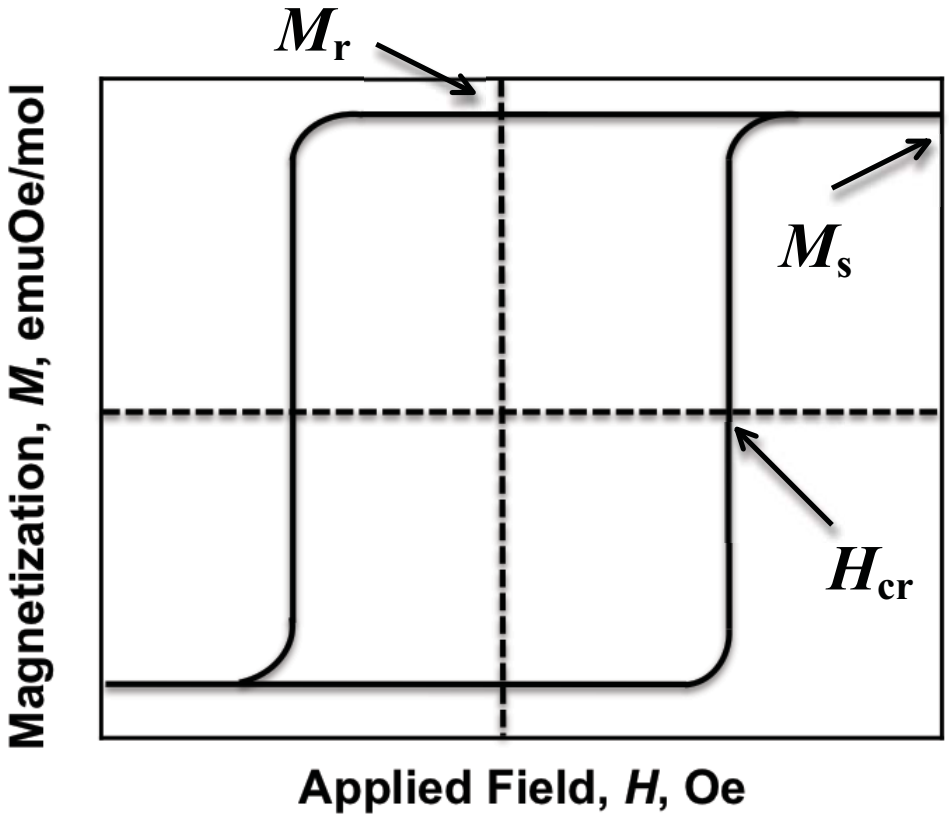

Figure 1.6. Diagram showing isothermal field dependent magnetization with typical hysteretic shape for ferro- or ferrimagnets depicting M_s, M_r, and H_{cr}.

will exhibit a saturation magnetization indicating a spin-flop transition. This type of transition typically occurs with isotropic systems in which there are rotations of the local spin directions. For anisotropic systems, the so-called "spin-flop" transitions are typically characterized by simple reversal of spin directions due to competing interactions. These materials are commonly referred to as metamagnetic. Previously, isothermal field dependent measurements have been shown to reveal exotic magnetic phenomena including interpenetrating ferrimagnetic cubic lattices[13] and metamagnetism.[14]

The last measurement that will be discussed is AC susceptibility, Figure 1.7. The previously mentioned measurements are all performed with a direct current and are referred to as DC magnetometry. In DC magnetometry, the sample is magnetized in a constant magnetic field. In an AC measurement, an alternating current is superimposed on a small DC field, which causes a time-dependent moment in the sample. The induced magnetic moment is

$$M_{AC} = (dM/dH)H_{AC}\sin(\omega t), \tag{1.12}$$

in which H_{AC} is the driving field, ω is the driving frequency, and dM/dH is slope of the isothermal field dependent curve, or commonly referred to as the susceptibility, equation 1.4.[15] At very low frequencies, AC magnetometry approaches its DC counterpart. However, since the AC measurement is a function of the *slope* of $M(H)$ and not the absolute value (like in DC magnetometry), it is very sensitive to small changes and can detect small magnetic shifts. At higher frequencies, the magnetization of the sample may lag behind the drive field due to dynamic effects in the sample. As a consequence of the

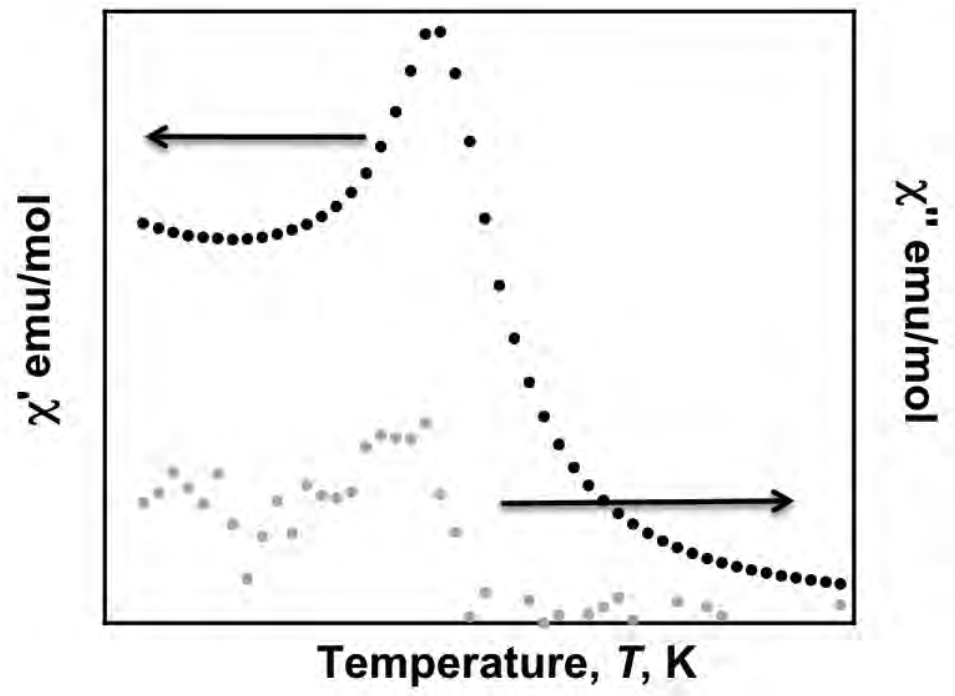

Figure 1.7. Sample plot of in-phase, $\chi'(T)$ and out-of-phase, $\chi''(T)$ AC responses.

dynamic nature of the measurement, two quantities are yielded: the magnitude of the susceptibility, χ and the phase shift, φ. This creates an in-phase, or real component, χ' and out-of-phase or imaginary component, χ'' given by the following relationships,[15]

$$\chi' = \chi\cos\varphi \tag{1.13}$$

$$\chi'' = \chi\sin\varphi \tag{1.14}$$

$$\chi = \sqrt{\chi'^2 + \chi''^2} \tag{1.15}$$

$$\varphi = \arctan(\frac{\chi'}{\chi''}). \tag{1.16}$$

At low frequencies, the χ' signal mirrors the DC susceptibility, χ. A response in the χ'' signal indicates irreversibility in the system due to dissipative properties which can arise from spin glass phenomena or domain walls in ferro- or ferrimagnetically ordered systems. Therefore, a response, or lack thereof, in χ'' can be a useful diagnostic tool in determining bulk magnetic properties. For most systems, the T_c is taken to be the temperature at which the rise in χ'' occurs, however for antiferromagnets, there is no response in χ'', and therefore, T_c is taken to be the peak in the χ' signal.

Tetracyanoethylene (TCNE)-based MBMs

A main approach taken in the synthesis of MBMs is with the deliberate inclusions of molecular building blocks. The goal is to help facilitate structural and magnetic ordering within the systems. In order to know which molecules are the best candidates for inclusion in syntheses, an understanding of the structural and electronic properties is essential. Tetracyanoethylene (TCNE), Figure 1.8, is an ideal candidate as a molecular building block for several reasons. First, it is a highly symmetrical ligand with four terminal nitrogen atoms and an olefin bond that are available for coordination. Second, TCNE is a good electron acceptor which leads to a radical anion with $S = 1/2$.[16] Therefore when TCNE, in the radical form, is coordinated to a metal ion that also carries spin, S, direct exchange interaction can occur which, as discussed earlier, can result in long-range ordering. The additional electron in the TCNE radical anion ($[TCNE]^{\cdot -}$), through polarized neutron diffraction measurements, has been shown to be delocalized throughout, Figure 1.9.[17] Therefore, the terminal nitrogen atoms carry significant spin density that is available to couple with spin residing on metal ion sites. The consequence of these two properties leads to versatile bonding modes for TCNE, its radical anion(s), and its dimer, Figure 1.8.[18]

The structural diversity of the TCNE ligand is best evident within the variety of structural motifs that have been observed with various TCNE-based MBMs. These motifs include so- called, 0-D electron transfer salt, $[Fe^{III}(C_5Me_5)_2]^{\cdot +}[TCNE]^{\cdot -}$;[19] 1-D chain compound, $[Mn^{II}TPP]^{+}[TCNE]^{-}$ (TPP = tetraphenylporphrin);[20] 2-D layered compounds, $[M^{II}(TCNE)(NCMe)_2]^{+}[X]^{-}$ (M = Mn, Fe, Ni, X = SbF_6[21]; M = Fe, X = $Fe^{III}Cl_4$[22]) and $Mn(TCNE)I(OH_2)$ (Chapter 2); 3-D compounds $M^{II}(TCNE)[C_4(CN)_8]_{1/2}$ (M = Mn, Fe,

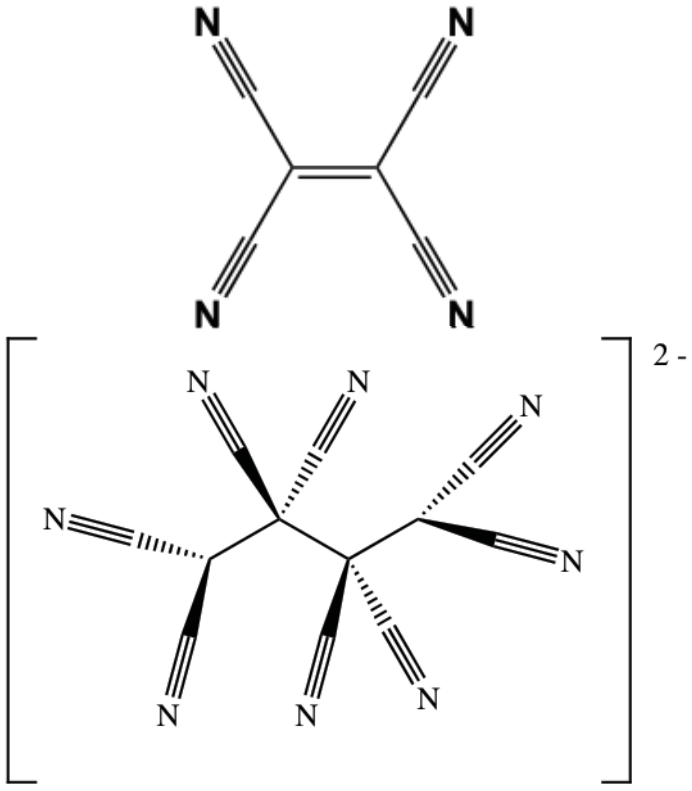

Figure 1.8. Structure of TCNE and the diamagnetic σ-dimer of its radical anion, $[C_4(CN)_8]^{2-}$.

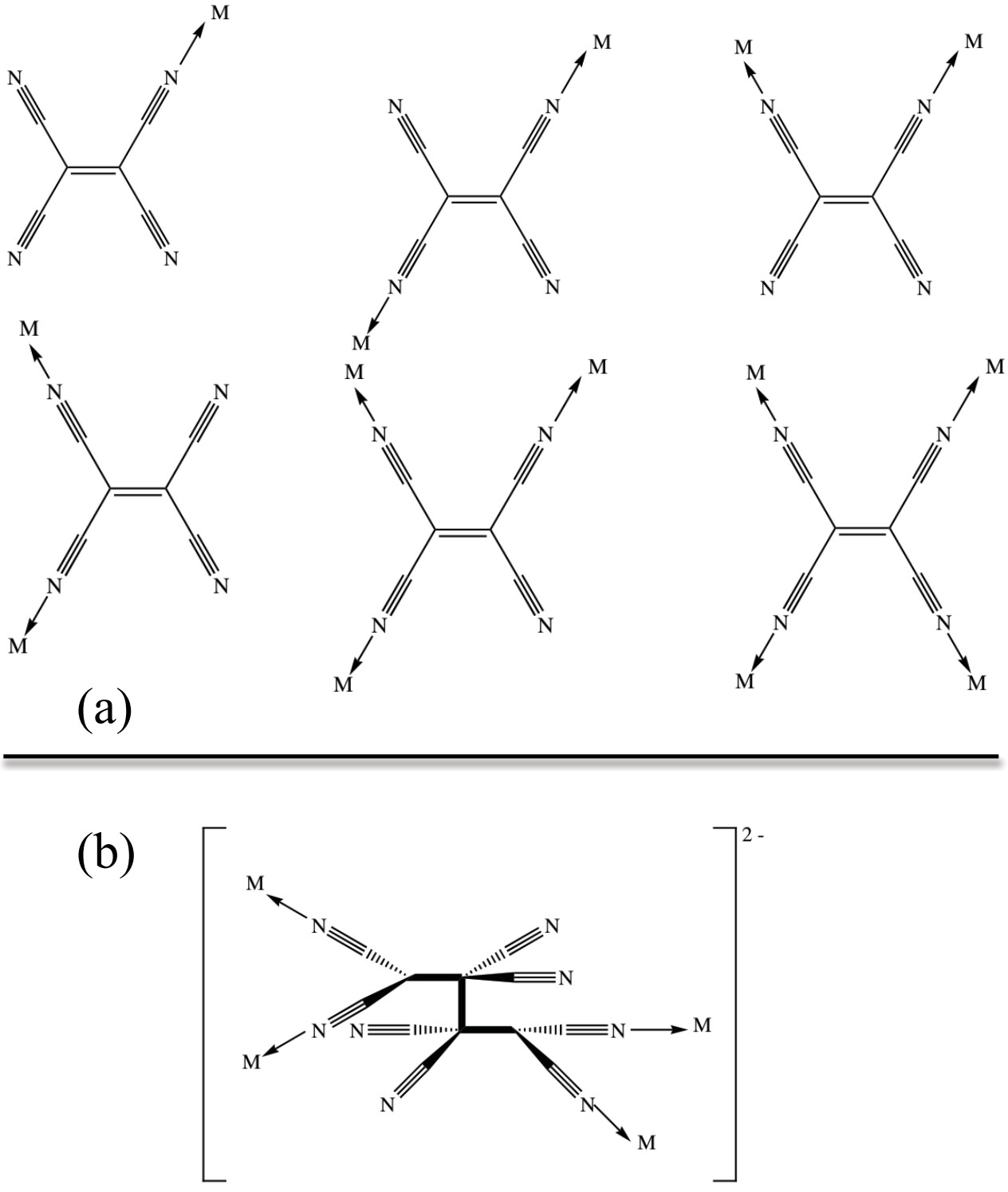

Figure 1.9. Schematic of the various bonding modes for TCNE and $TCNE^{\bullet -}$ (a) and $[C_4(CN)_8]^{2-}$ (b).

Ni, Co) (Chapter 3) and $M^{II}(TCNE)_{3/2}(I_3)_{1/2}$ (Chapter 2) and amorphous room-temperature magnet, $V^{II}(TCNE)_x$ whose structure has continued to be elusive.[4a,23] The result of this structural diversity is a wide range of critical temperatures, T_c, in the range of 4.8 – 400 K with various bulk ferro-, ferri- and antiferromagnetic orderings.

In this dissertation, I present the synthesis and characterization of two new TCNE-based MBMs with relatively high T_cs ~ 171 K. In addition, I present several investigations into the nature of the magnetic interactions of several TCNE-based MBMs via magnetic susceptibility measurements, Mean Field theory calculations, and pressure dependent magnetization measurements.

References

(1) (a) Miller, J. S. *Chem. Soc. Rev.* **2001**, *40*, 3266. (b) Miller, J. S.; Gatteschi, D. *Chem. Soc. Rev.* **2011**, *40*, 3065. (c) Miller, J. S.; Esptein, A. J. *Angew. Chem. Int. Ed.* **1994**, *33*, 385. (d) Felser, C.; Fecher, G. H.; Balke, B. *Angew. Chem. Int. Ed.* **2007**, *46*, 668. (e) Halcrow, M. A. *Chem. Soc. Rev.* **2011**, *40*, 4119. (f) Bleuzen, A.; Marvaud, V.; Mathaniere, C.; Sieklucka, B.; Verdaguer, M. *Inorg. Chem.* **2009,** *48*, 3453. (g) Dei, A.; Gatteschi, D. *Angew. Chem. Int. Ed.* **2011**, *50*, 11852.

(2) *Magnetism: Molecueles to Materials I-V*, Miller, J. S. and Drillon, M., Eds.; Wiley-VCH: New York, 2001.

(3) (a) Sato, O.; Iyoda, T.; Fujishima, A.; Hashimoto, K. *Science* **1996**, *271*, 49. (b) Maxim, C.; Mathoniere, C.; Marius, A. *Dalton Trans.* **2009**, *37*, 7805. (c) Brossard, S.; Volatron, F.; Lisnard, L.; Arrio, M.-A.; Catala, L.; Mathaniere, C.; Mallah, T.; Cartier dit Moulin, C.; Rogalev, A.; Wilhelm, F. *J. Am. Chem. Soc.* **2012**, *134*, 222.

(4) (a) Manriquez, J. M.; Yee, G. T.; McLean, R. S.; Epstein, A. J.; Miller, J. S. *Science* **1991**, *252*, 1415. (b) Hatlevik, Ø.; Buschmann, W. E.; Zhang, J.; Manson, J. L.; Miller, J. S. *Adv. Mater.* **1999**, *11*, 914. (c) Holmes, S. M.; Girolami, G. S. *J. Am. Chem. Soc.* **1999**, *121*, 5593. (d) Ferlay, S.; Mallah, T.; Quahes, R.; Veillet, P.; Verdaguer, M. *Nature* **1995**, *378*, 701. (e) Dujardin, E.; Ferlay, S.; Phan, X.; Desplanches, C.; Moulin, C. D.; Sainctavit, P.; Baudelet, F.; Dartyge, E.; Veillet, P.; Verdaguer, M. *J. Am. Chem. Soc.* **1998**, *120*, 11347.

(5) Kahn, O. *Molecular Magnetism*; VCH Publisher: New York, 1993, pp. 1-29.

(6) Kittel, C. *Introduction to Solid State Physics. 6th Ed.*; John Wiley & Sons, Inc.: New York, 1986, pp. 421-428.

(7) Hurd, C. M. *Contemp. Phys.* **1982**, *23*, 469.

(8) (a) Mattis, D. C. *The Theory of Magnetism Made Simple*; World Scientific Publishing Co. Pte. Ltd.: Singapore, 2006, pp. 53-69. (b) Mattis, D. C. *The Theory of Magnetism Made Simple*; World Scientific Publishing Co. Pte. Ltd.: Singapore, 2006, p. 287.

(9) (a) Curely, J.; Bernard, B. *Struct. Bond.* **2006**, *122*, 207. (b) Curely, J. *Mont. Chem.* **2005**, *136*, 1013.

(10) Bonner, J. C.; Fisher, M. E. *Phys. Rev. A* **1964**, *135*, 640.

(11) *Magnetic Properties of Layered Transition Metal Compounds*, de Jongh, L. J., Ed.: Kluwer Academic Publishers: Dordrecht, 1990.

(12) (a) Carlin, R. *Magnetochemistry*; Spinger-Verlag: New York, 1986. (b) Néel, L. *Ann. Phys.* **1948**, *3*, 137. (c) Smart, J. S. *Am. J. Phys.* **1955**, *23*, 356.

(13) Miller, J. S.; Vos, T. E.; Shum, W. W. *Adv. Mater.* **2005**, *17*, 2251.

(14) (a) Stryjewski, E.; Giordano, N. *Adv. Phys.* **1977**, *26*, 487. (b) Taliaferro, M. L.; Palacio, F.; Miller, J. S. *J. Mater. Chem.* **2006**, *16*, 2677. (c) Shum, W. W.; Schaller, J. N.; Miller, J. S. *J. Phys. Chem. C.* **2008**, *112*, 7936. (d) Schmidt, V. A.; Friedberg, S. A. *Phys. Rev. B.* **1970**, *1*, 2250. (e) Jacobs, I. S.; Lawrence, P. E. *Phys. Rev.* **1967**, *164*, 866. (f) Vettier, C.; Alberts, H. L.; Bloch, D. *Phys. Rev. Lett.* **1973**, *31*, 1414.

(15) Martien, D. Quantum Design Technical Resources: Introduction to AC Susceptibility. http://www.qdusa.com/sitedocs.appNotes/ppms/1078-201.pdf (access March 2012).

(16) Page, F. M.; Kay, J. *Nature*, **1963**, *199*, 483.

(17) Zheludev, A.; Grand, A.; Ressouch, E.; Schweizer, J.; Morin, B. G.; Epstein, A. J.; Dixon, D. A.; Miller, J. S. *Angew. Chem. Int. Ed.* **1994**, *33*, 1397.

(18) Miller, J. S. *Angew. Chem. Int. Ed.* **2006**, *45*, 2508.

(19) (a) Miller, J. S.; Calabrese, J. C.; Epstein, A. J.; Bigelow, R. W.; Zhang, J. H.; Reiff, W. M. *J. Chem. Soc., Chem. Comm.* **1986**, *13*, 1026. (b) Miller, J. S.; Calabrese, J. C.; Rommelmann, H.; Chittipeddi, S. R.; Zhang, J. H.; Reiff, W. M.; Epstein, A. J. *J. Am. Chem. Soc.* **1987**, *109*, 769.

(20) Miller, J. S.; Calabrese, J. C.; McLean, R. S.; Epstein, A. J. *Adv. Mater.* **1992**, *4*, 498.

(21) Olson, C.; Heth, C.; Lapidus, S. H.; Stephens, P. W.; Halder, G. J.; Pokhodnya, K. *J. Chem. Phys.* **2011**, *135*, 024503.

(22) Pokhodnya, K. I.; Bonner, M.; Her, J.-H.; Stephens, P. W.; Miller, J. S. *J. Am. Chem. Soc.* **2006**, *126*, 15592.

(23) Miller, J. S. *Polyhedron* **2009**, *28*, 1596.

CHAPTER 2

SYNTHESES AND MAGNETIC BEHAVIORS OF HIGH T_c (~170 K) $Mn^{II}(TCNE)_{3/2}(I_3)_{1/2}$ AND $Mn^{II}(TCNE)I(OH_2)$

Abstract

$Mn^{II}(TCNE)_{3/2}(I_3)_{1/2}$ (**1**) and $Mn^{II}(TCNE)I(OH_2)$ (**2**) were isolated from the reactions of tetracyanoethylene (TCNE) and $MnI_2(THF)_3$ in CH_2Cl_2 after stirring for 2 days and 6 months, respectively. Both **1** and **2** are comprised of $S = 5/2$ Mn^{II} cations that are coordinated to four μ_4-$[TCNE]^{\cdot-}$ radical anions, which creates corrugated 2-D layers. However, **1** also contains an additional μ_4-$[TCNE]^{\cdot-}$ radical anion that bridges the layers, creating an extended 3-D network. While **2**, on the other hand, contains I^- and H_2O coordinated *trans* to the Mn^{II} cations, which creates an isolated 2-D structure. The magnetic susceptibility measurements for **1** and **2** reveal that they both order as ferrimagnets with critical temperatures, T_cs, at 171 K.

Introduction

Several families of metal-TCNE compounds have been studied including those with the formula $M^{II}(TCNE)_x$ (M = Mn, Fe, Co: x ~ 2).[1] These compounds exhibit a wide range of bulk magnetic properties including ferrimagnetism, antiferromagnetism and

paramagnetism with T_cs ranging from 67 - 84 K. The structure of these compounds consist of corrugated layers of μ_4-$[TCNE]^{\cdot-}$ bonded to four M^{II} ions and these layers are connected by the diamagnetic μ_4-$[C_4(CN)_8]^{2-}$ anion that is also bonded to four M^{II} ions. Therefore these compounds are best described as $M^{II}(TCNE)[C_4(CN)_8]_{1/2}$. In addition to the family of $M^{II}(TCNE)_x$ (x ~ 2) magnets, several compounds with a M^{II} to TCNE ratio of 1:1 have been studied, including the compounds with formula $[M^{II}(TCNE)(NCMe)_2]^+[X]^-$ (M = Mn, Fe, Ni, X = SbF_6[2]; M = Fe, X = $FeCl_4$[3]). This family of magnets also possesses similar 2-D corrugated layers comprised of M^{II} bonded to four μ_4-$[TCNE]^{\cdot-}$, however each M^{II} ion has two *trans* N-bound MeCN solvent molecules above and below the layer. These magnets order as ferrimagnets with T_cs ranging from 20 – 96 K.

With the goal to explore other M:TCNE materials the reaction of TCNE and $MnI_2(THF)_3$ (THF = tetrahydrofuran) in CH_2Cl_2 for 3 days led to the isolation of material with the formula of $Mn^{II}(TCNE)_{3/2}(I_3)_{1/2}$ (**1**) (T_c = 171 K) while the same reaction left to stir for 6 months led to the discovery of material with the formula of $Mn^{II}(TCNE)I(OH_2)$ (**2**) (T_c = 171 K). Detailed magnetic susceptibility measurements were performed on these materials and presented herein.

Experimental Section

General procedure. $MnI_2(THF)_3$[4] was prepared via literature methods while TCNE was purchased from Aldrich and purified by sublimation. All operations were carried out under a dry N_2 atmosphere (< 1 ppm O_2) using a Vacuum Atmosphere DriLab. Dichloromethane (CH_2Cl_2) was purified through an activated alumina dual

column purification system under a positive pressure of N_2. The solids were isolated on a glass frit with porosity of 4-5.5 μm.

Polycrystalline samples for magnetic measurements were loaded in gelatin capsule holders and sealed with minimal amounts of heavy Nujol© (Aldrich) to protect the sample from the atmosphere. The DC magnetization measurements were carried out by cooling in zero applied field and then data were collected on warming in an applied field (5 or 1000 Oe) using a Quantum Design MPMS-5XL 5T SQUID magnetometer equipped with a reciprocating sample measurement system, low field option, and continuous low temperature control with enhanced thermometry features. Core diamagnetic susceptibility corrections of -168 and -138 x 10^{-8} emuOe/mol were used for samples **1** and **2**, respectfully. The crystal structures were determined from high-resolution powder diffraction patterns collected at beamline X16C at the National Synchrotron Light Source at Brookhaven National Laboratory at ambient temperature by Saul Lapidus, Kevin Stone, and Peter Stephens. The powdered samples were sealed in a thin-walled glass capillary of about 1 mm diameter, which was rotated during data collection. A Si(111) double-crystal monochromator selected a highly collimated incident beam of $\lambda \sim 0.7$ Å X-rays. Structures were solved and refined at Brookhaven using TOPAS-Academic[5] and the structures were visualized with the program VESTA.[6] Infrared spectra were recorded between 400 and 4000 cm^{-1} on a Bruker Tensor 37 spectrometer with ± 1 cm^{-1} resolution operated with an OPUS computer interface. Samples were prepared as a Nujol mull on KBr salt plates.

$Mn^{II}(TCNE)_{3/2}(I_3)_{1/2}$ (1). To a slurry of 198 mg (0.377 mmol) of $MnI_2(THF)_3$ in CH_2Cl_2 was added 50 mg (0.390 mmol) of TCNE dissolved in CH_2Cl_2. The slurry turned

from pink to red to black. After stirring for two days, the black precipitate was filtered and washed with CH_2Cl_2. The solid was dried in vacuo for 30 min at room temperature. IR (Nujol), 2231 (m) and 2189 cm^{-1} (s) (ν_{CN}); Raman, 110 cm^{-1} ($\nu_{I_3^-}$)[7]. This preparation was shown to form additional phases and details leading to reproducible synthesis have not been established. Combustion analysis was performed in Canada at Chemistar Laboratories Inc. Anal. Calcd. for $C_{11}H_4N_6I_{1.5}O_{0.5}Mn$ **1**: C, 27.9; H, 0.85; N, 17.75; O, 1.69; I, 40.2; Mn, 11.6. Found: C, 27.76; H, 1.08; N, 16.60; O, 1.90; I, 37.61; Mn, 10.85.

Mn^{II}(TCNE)I(OH_2) (2). On one occasion, to a slurry of 190 mg (0.362 mmol) of $MnI_2(THF)_3$ in CH_2Cl_2 was added 47 mg (0.367 mmol) of TCNE dissolved in CH_2Cl_2. The slurry turned from pink to red to black. After stirring for six months, the black precipitate was filtered and washed with CH_2Cl_2. The solid was dried in vacuo for 30 min at room temperature. IR (Nujol), 2240 (m), 2222 (s), 2184 (s), and 2158 cm^{-1} (m). Insufficient material was available for combustion analysis to determine elemental percentage. Guided by this discovery, the same material was directly synthesized via the molar-equivalent reaction of TCNE, $MnI_2(THF)_3$ and H_2O in CH_2Cl_2.[8]

Results and Discussion

The variation of stir time for the reaction of $MnI_2(THF)_3$ with TCNE in CH_2Cl_2 in an inert N_2 atmosphere, of 2 days versus 6 months, led to two new materials with compositions, $Mn(TCNE)_{3/2}(I_3)_{1/2}$ (**1**) and Mn(TCNE)I(OH_2) (**2**), respectively. A determination toward the origin of the H_2O in **2** was not definitive, as has been previously observed.[9] However it was estimated to have been present in the reaction solvent CH_2Cl_2 that, due to the long reaction time, allowed for coordination of water to the metal. The

IR, powder X-ray diffraction data and magnetic data showed that compounds **1** and **2** were chemically and structurally different. The IR ν_{CN} absorptions for **1** are at 2225 and 2173 cm^{-1} which are different, albeit comparable, to the IR ν_{CN} absorptions for **2,** which occur at 2240, 2222, 2184 and 2158 cm^{-1}. The values of the IR absorptions for both **1** and **2** suggest the presence of μ_4-$[TCNE]^{\cdot-}$, additionally, a broad peak that occurs at 3444 cm^{-1} is assigned to a ν_{OH} absorption. Compound **1** also contains disordered THF solvent molecules in the lattice which was determined do be at about 50% occupancy[10] hence the composition is $Mn(TCNE)_{3/2}(I_3)_{1/2}\bullet 0.5(THF)$. All magnetic data analysis was performed assuming this composition.

Structure of $Mn(TCNE)_{3/2}(I_3)_{1/2}\bullet 0.5(THF)$ (1). Reitveld analysis of the synchrotron powder diffraction data revealed compound **1** to be of the space group *Cmmm* with, a = 13.170(2) Å, b = 15.926(3) Å, c = 7.6087 Å, V = 1595.9(3) $Å^3$, at T = 298 K. The structure revealed that each Mn^{II} is octahedrally coordinated with the octahedra being rotated by 37° (angle between the out-of-plane Mn-N bond and the *b* axis), which is much larger than the 12-15° observed for other M-TCNE family compounds,[2,3,11] Fig.2.1. Each Mn^{II} is bonded to four μ_4-$[TCNE]^{\cdot-}$ creating 2-D layers with ∠MnNC of 156.5(6)°. This angle significantly deviates from the preferred 180° bonding typical of sp-N-Mn due to the geometrical considerations of forming an extended layer structure based upon the octahedrally preferred ∠NMnN of 90°. This is also accommodated by the aforementioned rotation of the MnN_6 octahedra. Each Mn^{II} is also bonded to two other μ_4-$[TCNE]^{\cdot-}$ that bridge the layers. This connection is less strained, as the ∠MnNC of 174.3(9)° approaches linearity. I_3^- forms linear chains parallel to the *a*-axis and is also parallel to the central C-C bonds of all of the μ_4-$[TCNE]^{\cdot-}$s.

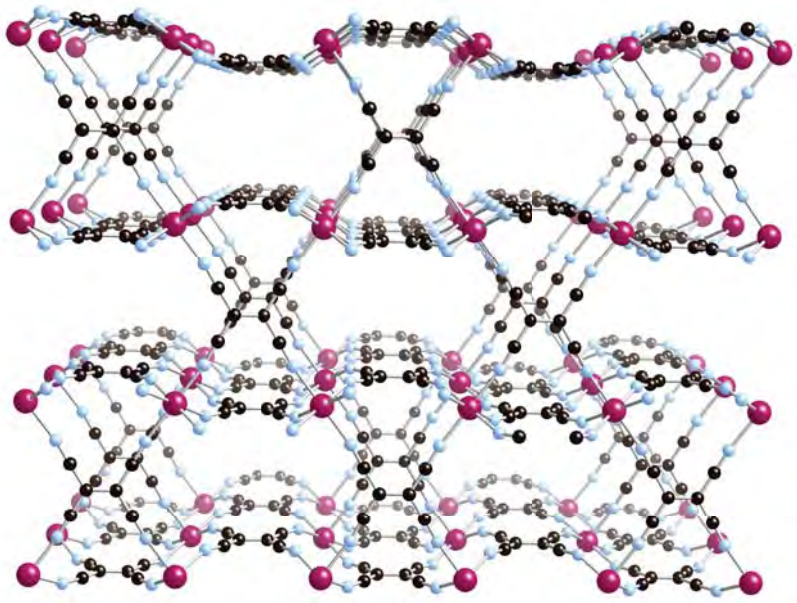

Figure 2.1. Structure of $Mn(TCNE)_{3/2}(I_3)_{1/2}$ (**1**) showing the 3-D extended covalent network (Mn is dark red; C is black; N is blue). Solvent molecules as well as I_3^- have been omitted for clarity.

The THF solvent resides in channels parallel to the *c*-axis but is disordered and cannot be crystallographically refined, Fig 2.2.

Structure of Mn(TCNE)I(OH$_2$) (2). Reitveld analysis of the synchrotron powder diffraction data revealed compound **2** to be of the space group *P*nam with, a = 12.7123(3) Å, b = 9.9961(3) Å, c = 7.6268(2) Å, V = 969.16(5) Å^3, at T = 298 K. The structure revealed each Mn^{II} is octahedrally coordinated, with the octahedral being significantly rotated, as for compound **1**, by 50°, Fig. 2.3. Each Mn^{II} is bonded to four μ_4-$[TCNE]^{-}$. The Mn^{II} are also bonded to a terminal iodide and water. This arrangement leads to parallel isolated 2-D corrugated layers. There are two different ∠MnNC [164.8(2)° and 146.4(2)°], and ∠MnNCC [157.2(2)° and 92.8(1)°], which indicates two different environments for the μ_4-$[TCNE]^{-}$. The 5.00 Å interlayer separation is substantially less than that observed for **1** and for other compounds in the M^{II}-TCNE family.[2,3,11]

Magnetic properties of Mn(TCNE)$_{3/2}$(I$_3$)$_{1/2}$•0.5(THF) (1). The temperature dependent magnetic susceptibility, $\chi(T)$ of **1** is reported as $\chi T(T)$ and $\chi^{-1}(T)$, Fig. 2.4. Compound **1** has a room temperature χT value of 6.65 emuK/mol that exceed the spin-only value of 4.75 emuK/mol suggestive of strong spin coupling. In accord with the strong coupling, $\chi T(T)$ increases gradually with decrease in temperature, and rises abruptly at ~185 K reaching 945 emuK/mol at 128 K, prior to decreasing toward zero. $\chi^{-1}(T)$ is linear between 175 and 205 K and extrapolates to zero at θ = 172 K indicative of significant short-range ferromagnetic coupling.

The zero-field cooled (M_{ZFC}) and field-cooled (M_{FC}) magnetizations for **1** rise sharply below 172 K, Fig. 2.5, indicative of a magnetic transition. $M_{ZFC}(T)$ reaches a maximum at 170 K before gradually decreasing toward zero. In contrast, $M_{FC}(T)$ rises

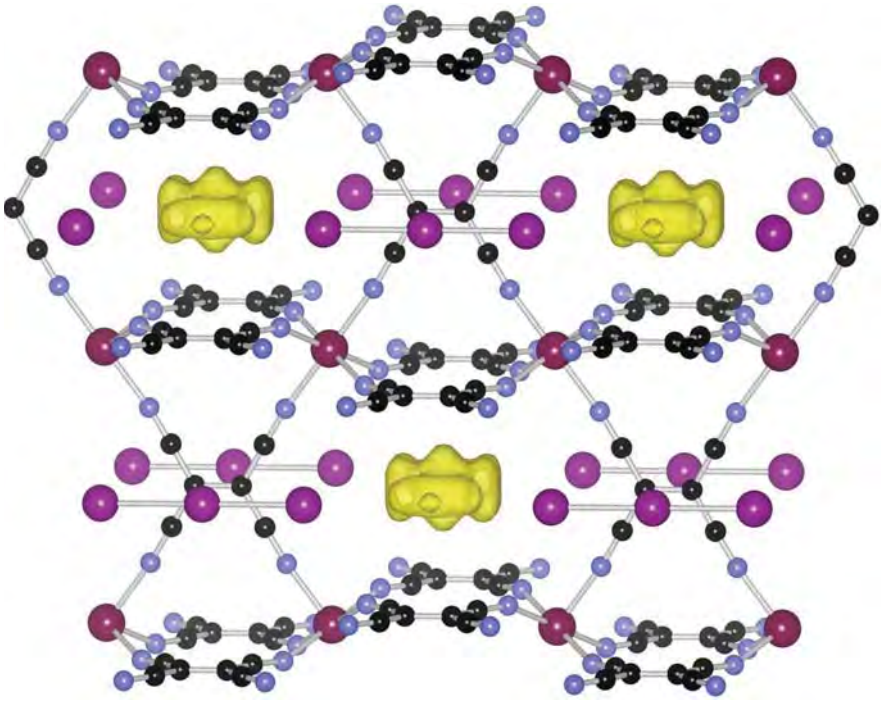

Figure 2.2. 3-D covalent network of $Mn(TCNE)_{3/2}(I_3)_{1/2}$ showing the I_3^- and the disordered solvent that reside in the channels (Mn is dark red; C is black; N is blue; I is purple, Solvent is yellow).

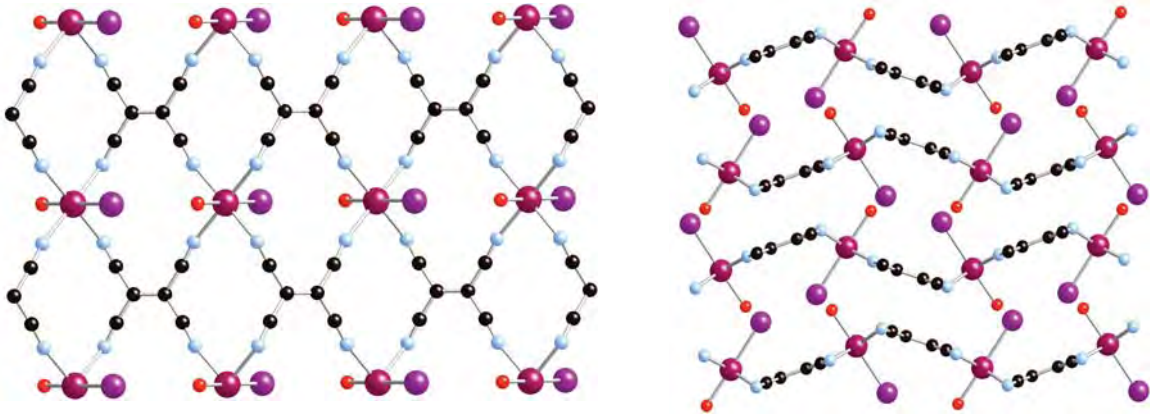

Figure 2.3. Structure of Mn(TCNE)I(OH_2) (**2**) in the *ac* plane showing a layer (left), and in the *ab* plane showing the parallel corrugated 2-D layers (right) (Mn is dark red; C is black; N is blue; O is red; I is purple).

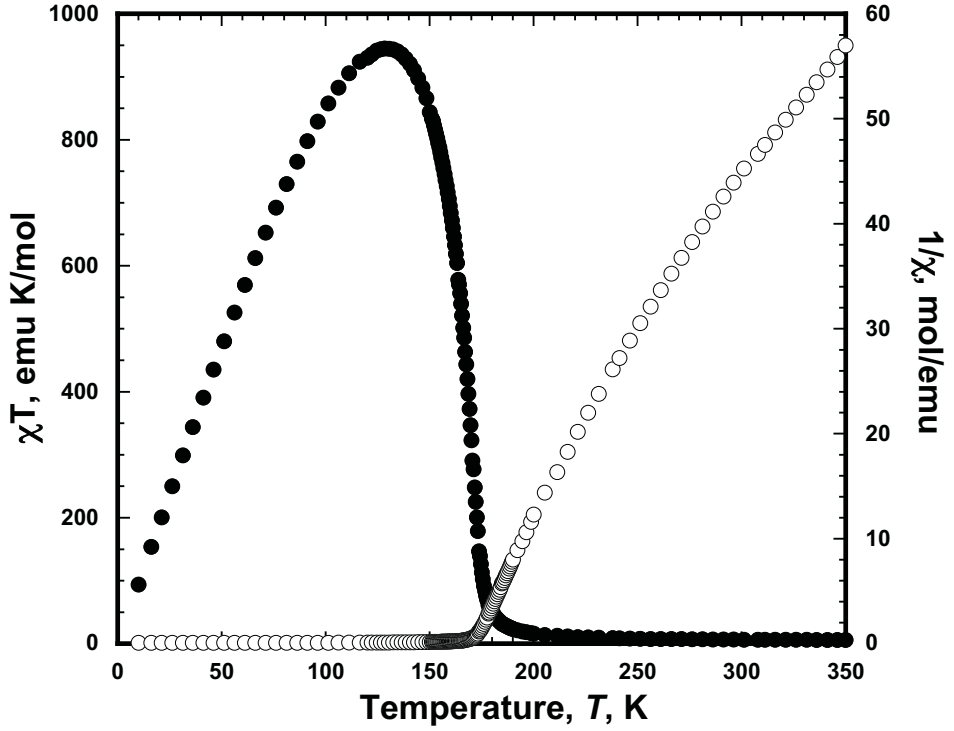

Figure 2.4. $\chi T(T)$ (•) and $\chi^{-1}(T)$ (◦) for **1**.

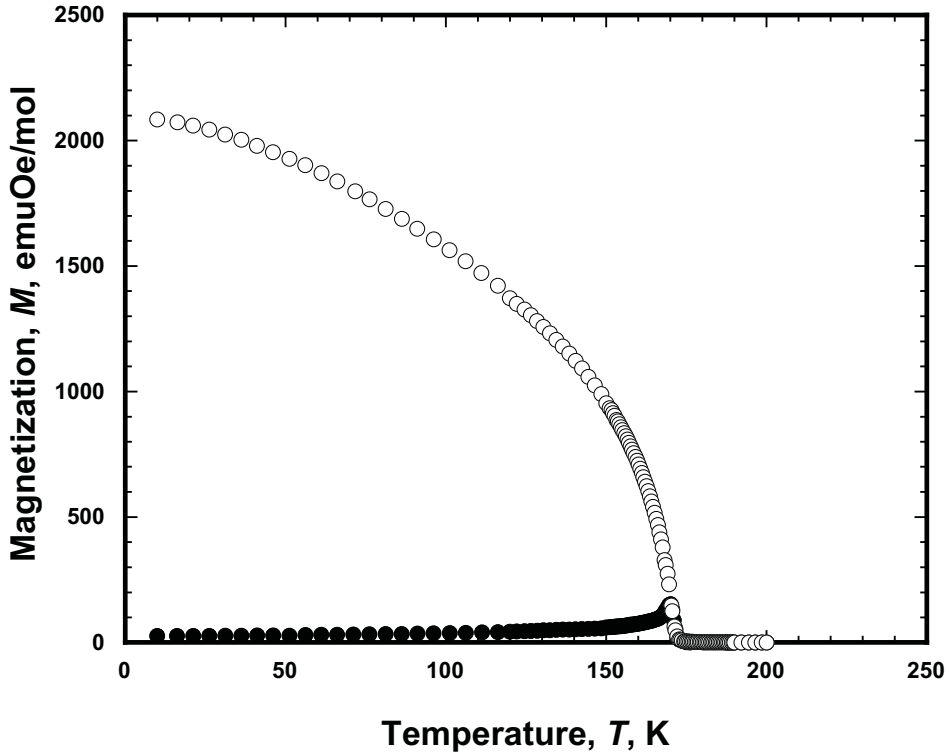

Figure 2.5. $M_{ZFC}(T)$ (•) and $M_{FC}(T)$ (◦) for **1**.

upon further cooling. These data have a bifurcation temperature, T_b of 171 K indicating a point of irreversibility. The temperature dependent remanant magnetization, $M_r(T)$ is coincident to $M_{FC}(T)$ and extrapolation of the initial rise upon cooling gave an intercept of 171 K, Fig. 2.6.

AC susceptibility studies confirmed the magnetic ordering for **1** as peaks in both the in-phase, $\chi'(T)$, and out-of-phase, $\chi''(T)$ responses were observed, Fig. 2.7. The $\chi'(T)$ data exhibit a peak at 169 K, while the rise in $\chi''(T)$ upon cooling occurs at 172 K.

The field-dependent magnetization, $M(H)$, is also characteristic of magnetic ordering and **1** exhibits hysteretic behavior with a coercive field, H_{cr} of 600 Oe, and remanant magnetization, M_r of 8000 emuOe/mol at 10 K, Fig. 2.8. H_{cr} is unexpectedly large for high spin Mn^{II}. This is ascribed to a *g* factor greater than 2, due to coupling with the $[TCNE]^{\cdot -}$, which is consistent with a powder average $\langle g \rangle \sim 2.5$ that is observed from preliminary 77 K EPR data, Fig. 2.9. The saturation magnetization, M_s at 90 kOe is 21,800 emuOe mol^{-1}. This exceeds 22,340 emuOe/mol predicted for antiferromagnetic coupling, due again to the unexpected anisotropy for Mn^{II}.

Compound **1** is attributed to have a direct-coupled 3-D magnetic motif with antiferromagnetic coupling between the Mn^{II} and μ_4-$[TCNE]^{\cdot -}$ species within a layer as well as the μ_4-$[TCNE]^{\cdot -}$ species between the layers leading to a bulk 3-D ferrimagnet. The T_c for **1** determined by the onset of the $M_r(T)$, from the $\chi'(T)$ peak, or from T_b is 171 K. It will be shown in a Chapter 5 that the T_c for **1** increases significantly under the application of pressure.

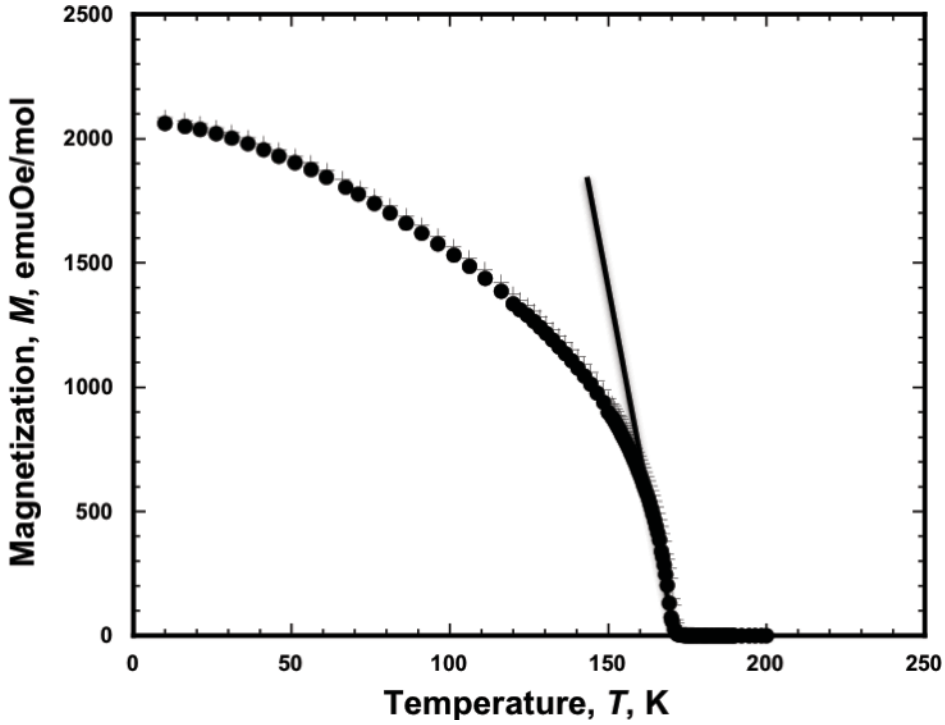

Figure 2.6. $M_r(T)$ (•) and $M_{FC}(T)$ (+) for **1** showing the extrapolated temperature intercept, T_c.

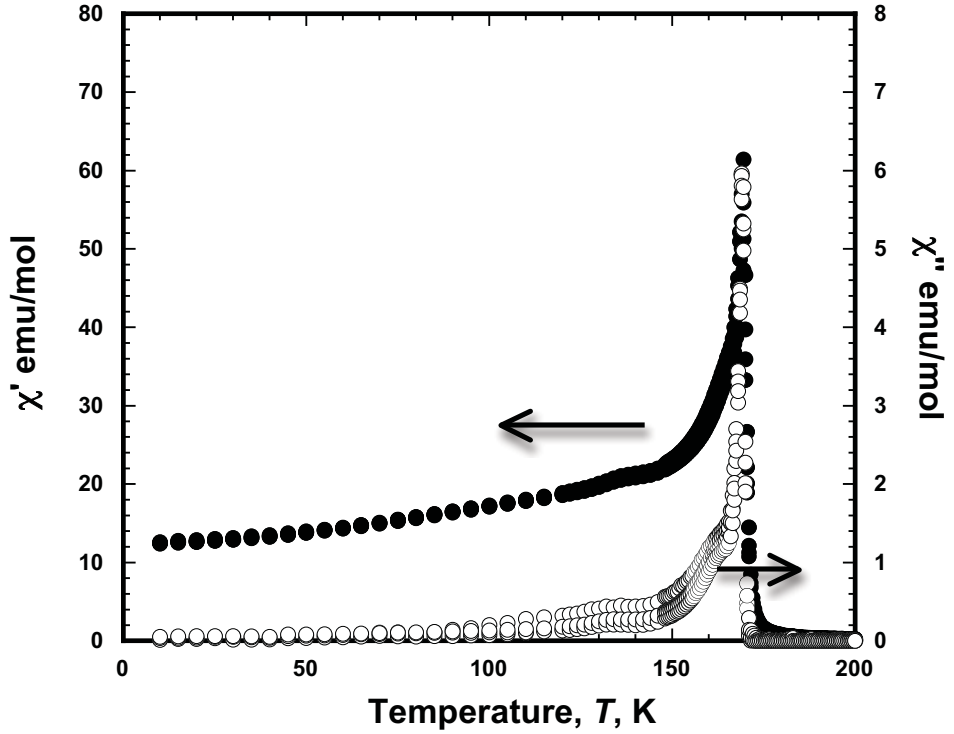

Figure 2.7. $\chi'(T)$(•) and $\chi''(T)$ (◦) for **1**.

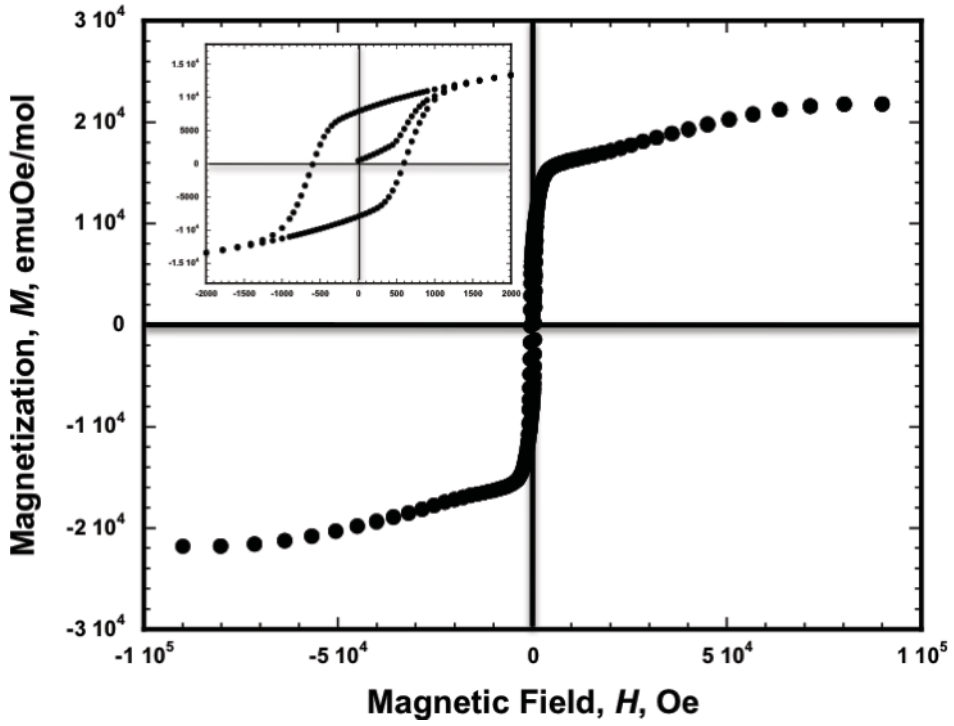

Figure 2.8. Isothermal field dependent magnetization, *M*(*H*), for **1** showing the hysteretic shape (inset).

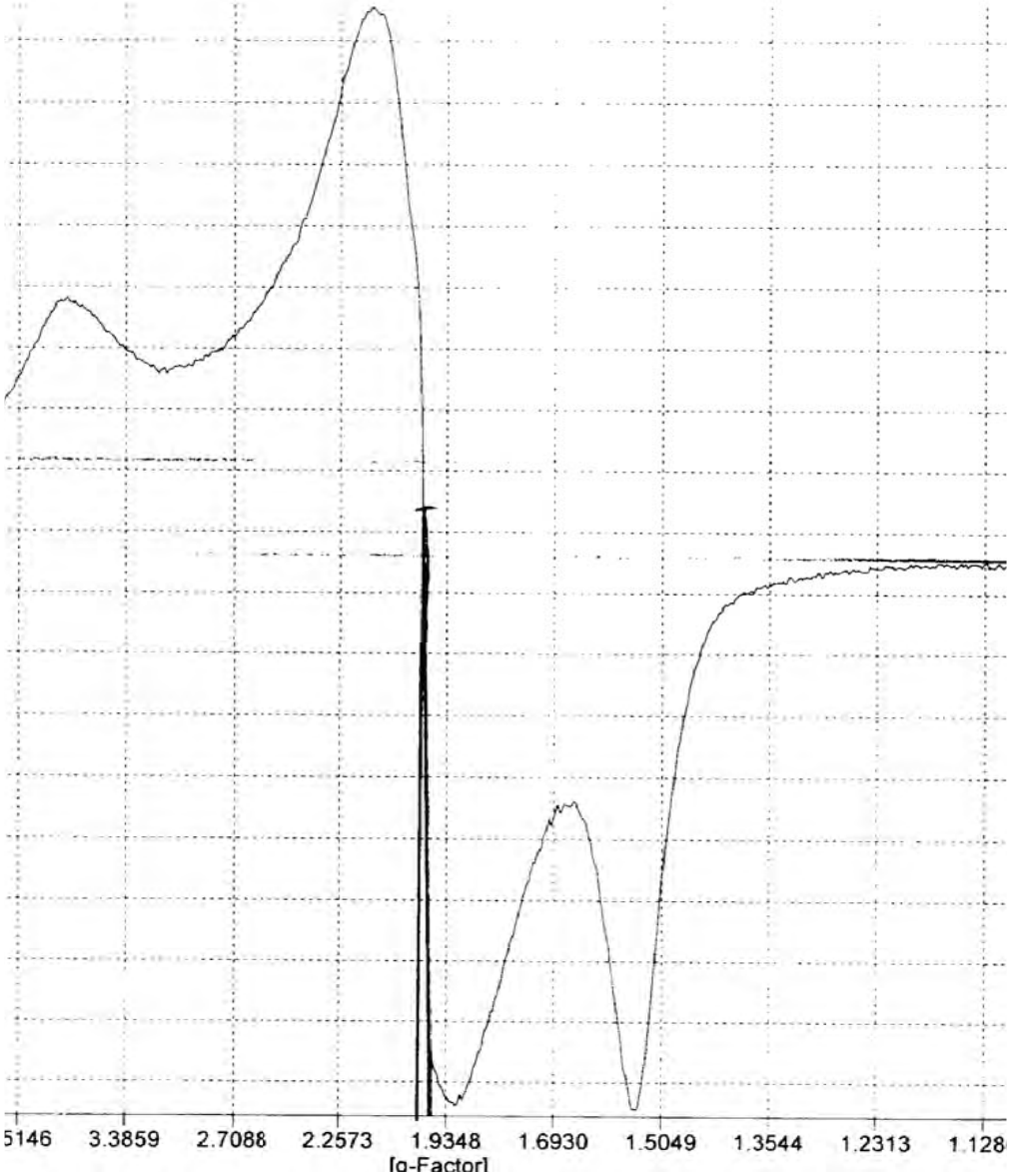

Figure 2.9. EPR spectra for **2**.

Magnetic properties of Mn(TCNE)I(OH_2) (2). The temperature dependent magnetic susceptibility, $\chi(T)$ of **2** is reported as $\chi T(T)$ and $\chi^{-1}(T)$, Fig. 2.10. Compound **2** has a room temperature χT value of 8.69 emuK/mol that significantly exceeds the expected spin-only value of 4.75 emuK mol^{-1}. This may be due to the fact that $\chi T(T)$ is not constant and is still decreasing with increasing temperature, indicating lingering interactions at room temperature. $\chi T(T)$ for **2** gradually increases with decreasing temperature until 180 K when it increases until it reaches a maximum value of 32 emuK/mol at ~137 K, below which it decreases toward zero. $\chi^{-1}(T)$ is linear above 180 K and extrapolates to zero at θ = 149 K. This is indicative of bulk magnetic ordering with considerable short-range ferromagnetic coupling, as for **1**.

The zero-field cooled (M_{ZFC}) and field-cooled (M_{FC}) magnetizations for **2** rise sharply below 175 K, Fig. 2.11, indicative of a magnetic transition. $M_{ZFC}(T)$ reaches a maximum at 170 K before gradually decreasing toward zero. In contrast, $M_{FC}(T)$ rises upon further cooling. These data have a bifurcation temperature, T_b of 172 K indicating a point of irreversibility. The temperature dependent remanant magnetization, $M_r(T)$ is coincident with $M_{FC}(T)$ and extrapolation of the initial rise upon cooling gave an intercept of 171 K, Fig. 2.12.

AC susceptibility studies confirmed the magnetic ordering for **1** as peaks in both the in-phase, $\chi'(T)$, and out-of-phase, $\chi''(T)$ responses were observed, Fig. 2.13. The $\chi'(T)$ data exhibit a peak at 167 K, while the rise in $\chi''(T)$ upon cooling occurs at 176 K. Additionally, **2** exhibits two additional weaker peaks at ~140 and ~35 K suggestive of impurities or additional magnetic transitions, but these features are not observed in the $M_{ZFC}(T)$, $M_{FC}(T)$, $M_r(T)$ data.

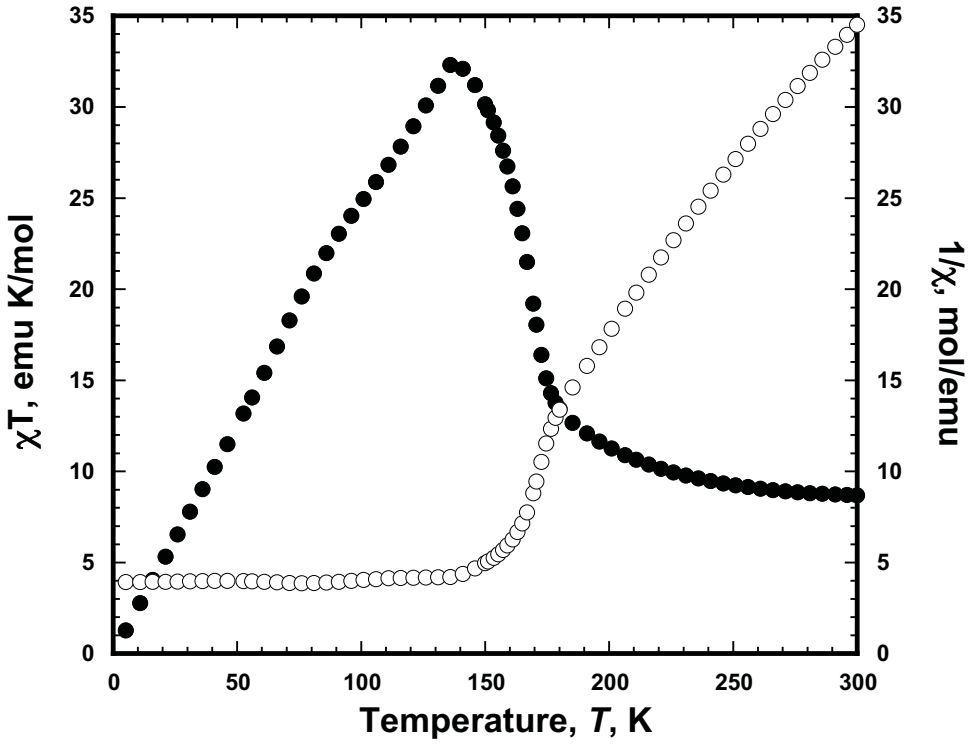

Figure 2.10. $\chi T(T)$ (•) and $\chi^{-1}(T)$ (◦) for **2**.

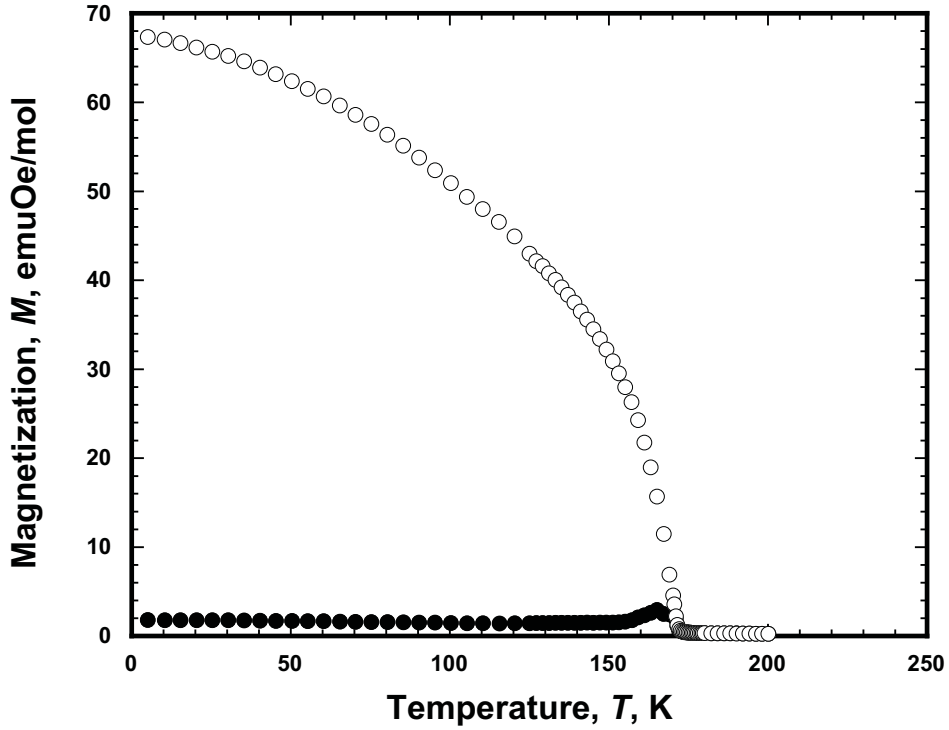

Figure 2.11. $M_{ZFC}(T)$ (•) and $M_{FC}(T)$ (◦) for **2**.

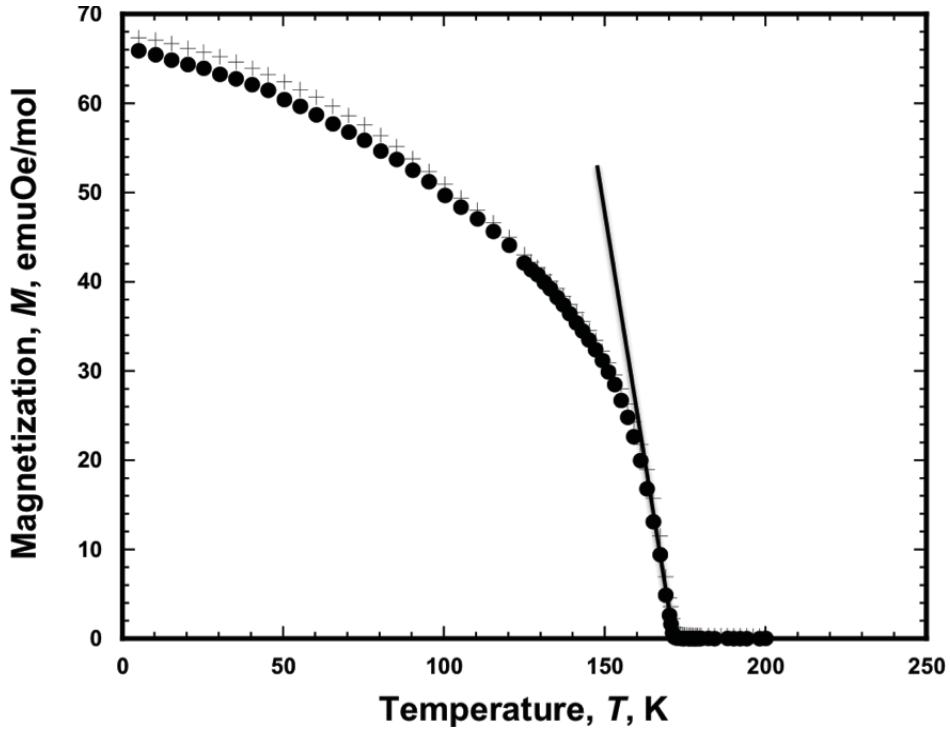

Figure 2.12. $M_r(T)$ (•) and $M_{FC}(T)$ (+) for **2** showing the extrapolated temperature intercept, T_c.

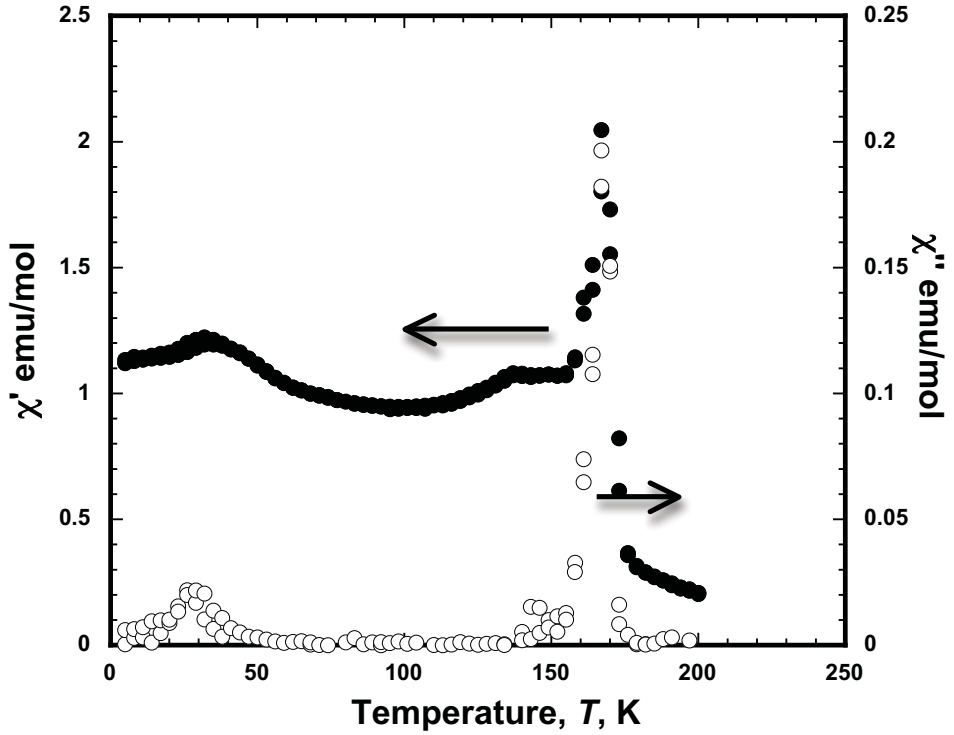

Figure 2.13. $\chi'(T)$(•) and $\chi''(T)$ (◦) for **2**.

The field-dependent magnetization, $M(H)$, is also characteristic of magnetic ordering and **2** exhibits hysteretic behavior with a coercive field, H_{cr} of 400 Oe, and remanant magnetization, M_r of 60 emuOe/mol at 10 K, Fig. 2.14. The saturation magnetization, M_s at 90 kOe is 12,200 emuOe mol^{-1}. This is significantly reduced from 22,340 emuOe mol^{-1} predicted for antiferromagnetic coupling.

Compound **2** is attributed to have a direct-coupled 3-D magnetic motif with antiferromagnetic coupling between the Mn^{II} and μ_4-$[TCNE]^-$ species within a layer, as for compound **1**. However, unlike compound **1**, compound **2** contains isolated non-bridged layers, leading to 2-D ferrimagnetic ordering. A comparison of the saturation and remanant magnetizations of **1** and **2** reveal that they deviate significantly from each other even though they share similar 2-D structural layers. The M_s and M_r values of 12,200 and 60 emuOe/mol for **2** are substantially reduced from the values of 21,800 and 8000 emuOe/mol observed for **1**. One conclusion could be that for **2**, the ferrimagnetic layers are antiferromagnetically coupled, albeit canted, leading to an incomplete cancellation of magnetic moments between the layers. This would explain the weak magnitudes observed in the $M_{ZFC}(T)$, $M_{FC}(T)$, $M_r(T)$ data for **2** compared to **1** as well as the suppressed values for M_s and M_r for **2**. Therefore compound **2** is best described as a complex weak ferrimagnet or canted antiferromagnet. The relatively high T_c for **2** is unexpected due to the low-dimensionality of the structural motif, especially since it is identical to the T_c for compound **1,** which exhibits 3-D bonding. Due to the relatively short interlayer separation of 5.00 Å observed for **2**, interlayer dipolar interactions may also contribute. Although dipolar interactions are typically considered a weak type of exchange pathway, the dipolar energy depends on the square of the effective moment,

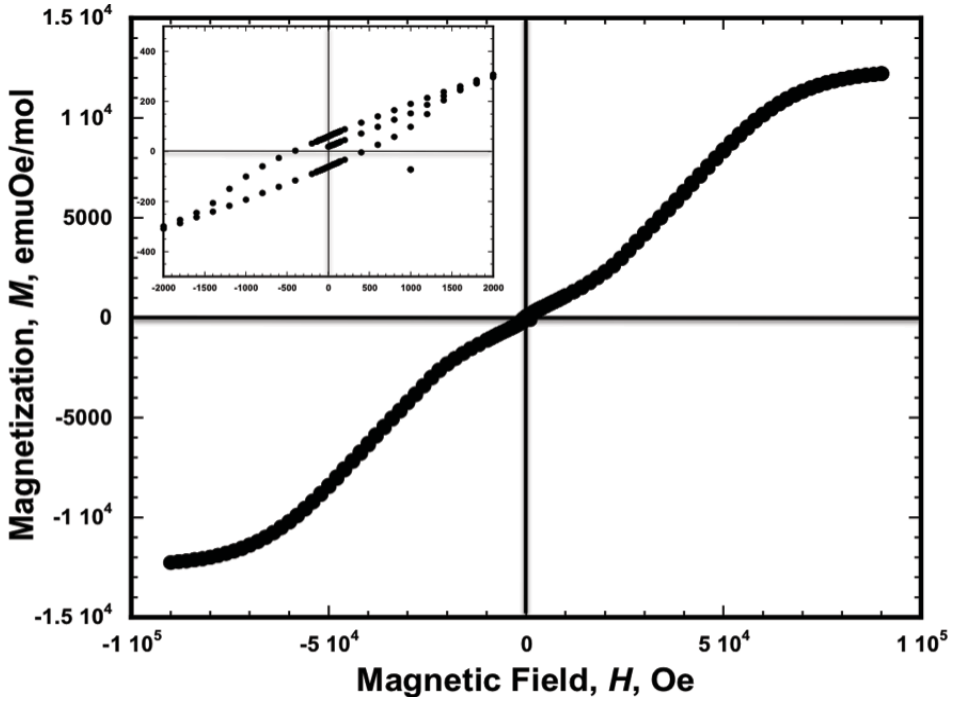

Figure 2.14. Isothermal field dependent magnetization, *M*(*H*) for **2** showing the hysteretic shape (inset).

therefore, the interaction between planes become more correlated over larger and larger distances.[12] Another possible source for the enhanced coupling lies in the intralayer coupling between Mn^{II} and $[TCNE]^{\cdot -}$ due to there being two different bonding environments for the $[TCNE]^{\cdot -}$s in which one is more linear and one is more buckled to a greater degree than other layered $M^{II}[TCNE]^{\cdot -}$ compounds. The relationship between buckling and magnetic interactions, however, is not fully understood.

Conclusion

The structural and magnetic properties of two high T_c ~171 K compounds, namely $Mn(TCNE)_{3/2}(I_3)_{1/2}$ (**1**) and $Mn(TCNE)I(OH_2)$ (**2**), were discussed. Compound **1** contains a 3-D extended covalent network of Mn^{II} bonded to four μ_4-$[TCNE]^{\cdot -}$ in which there exists direct exchange interaction between the S = 5/2 Mn^{II} and S= 1/2 $[TCNE]^{\cdot -}$ in all three dimensions that leads to bulk ferrimagnetic ordering. Compound **2** contains octahedrally coordinated Mn^{II} bonded to four μ_4-$[TCNE]^{\cdot -}$ in addition to *trans* I^- and H_2O, creating 2-D isolated layers. Direct exchange interaction occurs between the S = 5/2 Mn^{II} and S = 1/2 $[TCNE]^{\cdot -}$ however, since **2** possesses an additional dipolar interaction as a potential pathway it showed more complex behavior ordering as either a weak ferrimagnet or canted antiferromagnet.

Table 2.1 Summary of the crystallographic and magnetic properties of **1** and **2**.

	$Mn(TCNE)_{3/2}(I_3)_{1/2}$	$Mn(TCNE)I(OH_2)$
Space group	*Cmmm*	*P*nam
a, Å	13.170(2)	12.7123(3)
b, Å	15.926(3)	9.9961(3)
c, Å	7.6087(3)	7.6268(2)
V, Å^3	1595.9(3)	969.16(5)
∠MnNC, °	174.3(9)	164.8(2) and 146.4(2)
$\chi T(T)_{300\ K}$, emuK/mol	6.65	8.69
θ, K	172	149
T_b, K	171	172
T_c, K	171	171
$\chi'(T)_{peak}$, emu/mol	169	167
$\chi''(T)_{rise}$ emu/mol	172	176
M_s, emuOe/mol	21,800	12,200
H_c, Oe	600	400
M_r, emuOe/mol	8,000	60

References

(1) (a) Zhang, J.; Ensling, J.; Ksenofontov, V.; Gütlich, P.; Epstein, A. J.; Miller, J. S. *Angew. Chem. Int. Ed.* **1998**, *37*, 657. (b) Girtu, M. A.; Wynn, C. M.; Zhang, J.; Miller, J. S.; Epstein, A. J. *Phys. Rev. B.* **2000**, *61*, 492. (c) Wynn, C. M.; Girtu, M. A.; Zhang, J.; Miller, J. S.; Epstein, A. J. *Phys. Rev.* **1998**, *B58*, 8508.

(2) Olson, C.; Heth, C. L.; Lapidus, S. H.; Stephens, P. W.; Halder, G. J.; Pokhodnya, K. *J. Chem. Phys.* **2011**, *135*, 024503.

(3) Pokhodnya, K. I.; Bonner, M.; Her, J.-H.; Stephens, P. W.; Miller, J. S. *J. Am. Chem. Soc.* **2006**, *126*, 15592.

(4) Stolz, P.; Pohl, Z. *Naturforsch. B.* **1988**, *43*, 175.

(5) Coelho, A. A. *TOPAS-Academic*, available at http://www.topas-academic.net (last accessed March 2010).

(6) Momma, K.; Izumi, F. *J. Appl. Crystallogr.* **2008**, *41*, 653.

(7) Teitelbaum, R. C.; Ruby, S. L.; Marks, T. J. *J. Am. Chem. Soc.* **1978**, *100*, 3215.

(8) Bell, J. D.; McConnell, A. C.; Miller, J. S. unpublished results.

(9) Rittenberg, D. K.; Sugiura, K.-I.; Arif, A. M.; Incarvito, C. D.; Rheingold, A. L.; Sakata, Y.; Miller, J. S. *Chem.-Eur. J.* **2000**, *6*, 1811.

(10) The Mn:THF ratio would be 1:1 if the solvent sites were fully occupied, but the crystallographic and thermogravimetric analysis (TGA) points to ~50% solvent occupancy.

(11) (a) Her, J.-H.; Stephens, P. W.; Pokhodnya, K. I.; Bonner, M.; Miller, J. S. *Angew. Chem. Int. Ed.* **2007**, *46*, 1521. (b) McConnell, A. C.; Shurdha, E.; Bell, J. D.; Miller, J. S. submitted. (c) Chapter 3.

(12) (a) Drillon, M.; Panissod, P. *J. Magn. Magn. Mater.* **1998**, *188*, 93. (b) Ostrovsky, S.; Haase, W. *Phys. Rev. B.* **2001**, *64*, 134418. (c) Vauer, E. M.; Bellitto, C.; Righini, G.; Colapietro, M.; Portalone, G.; Drillon, M.; Rabu, P. *Inorg. Chem.* **2008**, *47*, 10945. (d) Drillon, M.; Panissod, P.; Rabu, P. *Phys. Rev. B.* **2002**, *65*, 104404.

CHAPTER 3

MAGNETIC BEHAVIOR OF $M^{II}(TCNE)[C_4(CN)_8]_{1/2}$ (M = Mn, Fe)

Abstract

The magnetic ground states of $M^{II}(TCNE)[C_4(CN)_8]_{1/2}$ [M = Mn (**Mn**), Fe (**Fe**)] were investigated via detailed DC and AC magnetic susceptibility measurements. Previously reported magnetic studies on **Mn** and **Fe** revealed bulk ferrimagnetic ordering; however, the materials were not pure and exhibited multiple magnetic phases with sample-to-sample variations. Herein, the properties of **Mn** and **Fe,** synthesized from a newly reported synthetic route that produced pure compounds with one magnetic phase, are reported.

Introduction

Subsequent to the discovery that $[Fe^{II}(C_5Me_5)_2]^{\cdot-}[TCNE]^{\cdot-}$ magnetically ordered as a bulk ferromagnet with a critical temperature, T_c, of 4.8 K,[1,2] several additional organic-based magnets have been reported.[3,4,5] Also, several magnets containing TCNE[6] with a wide variety of structural connectivity have been characterized, including 1-D $[Mn^{III}TPP]^{+}[TCNE]^{\cdot-}$ (T_c = 18 K),[7] 2-D $[Fe^{II}(TCNE)(NCMe)_2][Fe^{III}Cl_4]$ (T_c = 89 K)[8] and $Mn^{II}(TCNE)I(OH_2)$ (T_c = 171 K)[9] (described in Chapter 2), and 3-D $Mn^{II}(TCNE)_{3/2}(I_3)_{1/2}$

(T_c = 171 K)[10] (described in Chapter 2). In addition, the room temperature molecule-based magnet, $V(TCNE)_x$ (T_c = 400 K)[11] is amorphous; however, its structure has been elusive.[12]

The reaction of acetonitrile solvates of $M^{II}I_2$ with TCNE in CH_2Cl_2 form $M^{II}(TCNE)_2 \bullet zCH_2Cl_2$ (M = Mn, Fe, Co, Ni) with reported T_cs as high as 100 K, and coercive fields as high as 6500 Oe.[13] Additionally, $Fe(TCNE)_2 \bullet zCH_2Cl_2$ was prepared via the reaction of $Fe(CO)_5$ and TCNE in CH_2Cl_2.[14] Previous detailed studies on the Mn[15a] and Fe[15b] analogs revealed possible impurities within the material that exhibit multiphase magnetic data. However, bulk magnetic properties of the Mn and Fe analogs were attributed to antiferromagnetic coupling that leads to bulk ferrimagnetic ordering.

Recently, the reaction of $M(NCS)_2(OCMe_2)$ (M = Fe,[16] Mn,[10] Co[16]) and $(NBu_4)(TCNE)$ in CH_2Cl_2 resulted in the discovery of a new synthetic route for $M(TCNE)_2 \bullet zCH_2Cl_2$ that produced material with a single magnetic phase. The structures of $M(TCNE)_2 \bullet zCH_2Cl_2$ show that the Mn[10] (**Mn**) and Fe[17] (**Fe**) analogs are isostructural and contain corrugated layers of M^{II} bonded to four (S = 1/2) μ_4-$[TCNE]^{\cdot -}$, and these layers are bridged by the by the diamagnetic (S = 0) μ_4-$[C_4(CN)_8]^{2-}$ dimer, Figure 1.8, and is best formulated as $M^{II}[\mu_4\text{-}[TCNE]^{\cdot -}\{[\mu_4\text{-}C_4(CN)_8]^{2-}\}_{1/2}$, Figure 3.1. In addition, the reaction of $Mn^{II}I_2(THF)_3$ (THF = tetrahydrofuran) with $(NBu_4)(TCNE)$ produced material that had similar infrared and magnetic data as **Mn**, suggesting that this is also a viable synthetic route.[18]

With the availability of magnetically pure $M^{II}(TCNE)[C_4(CN)_8]_{1/2}$ (M = Mn, Fe) their magnetic properties was reinvestigated which revealed that they have an antiferromagnetic ground state, and, for **Fe**, a more complex magnetic behavior.

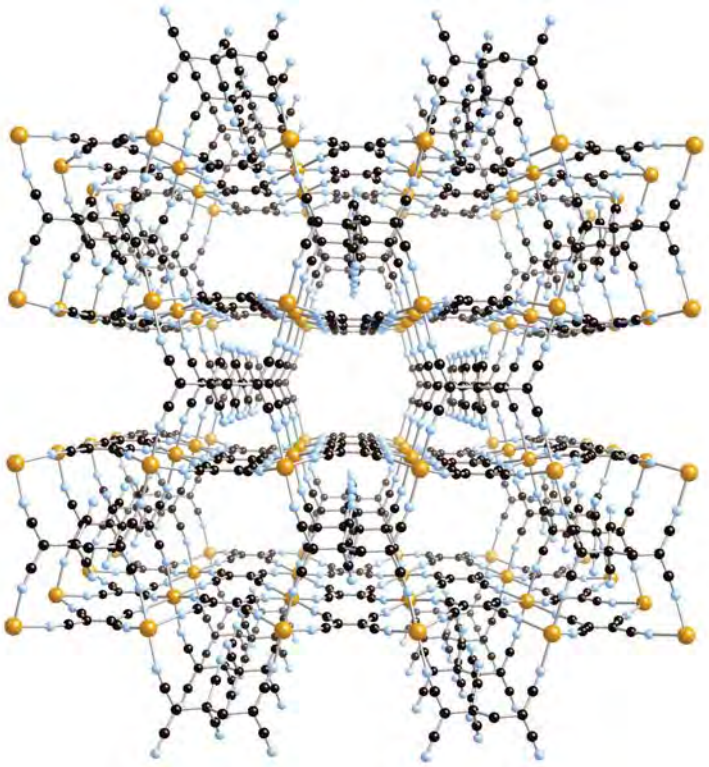

Figure 3.1. Extended network bonding via μ_4-$[TCNE]^{\bullet-}$ in 2-D in which these layers are bridged by μ_4-$[C_4(CN)_8]^{2-}$ that is observed for $M^{II}(TCNE)[C_4(CN)_8]_{1/2}\bullet zCH_2Cl_2$ (M = Mn, Fe). M is gold, N is blue, and C is black. The disordered solvent fills the channels

Experimental Section

$M^{II}(TCNE)[C_4(CN)_8]_{1/2}$ (M = Mn, Fe) were prepared as previously reported.[10,16] Polycrystalline samples for magnetic measurements were loaded in gelatin capsule holders and protected from air. The magnetic susceptibilities were measured in an 1000 Oe applied field between 5 and 300 K on a Quantum Design MPMS-5XL 5T SQUID magnetometer equipped with a reciprocating sample measurement system, low field option, and continuous low temperature control with enhanced thermometry features. The temperature dependence of the magnetization, $M(T)$, was obtained by cooling in zero-field and collecting data upon warming. The remanant magnetization was measured in zero applied field upon warming after cooling below the T_c in an applied field of 5 Oe. AC susceptibilities were measured at 33, 100 and 1000 Hz. In addition to correcting for the diamagnetic contribution from the sample holder, the core diamagnetic corrections of -134 (**Mn**), -135 (**Fe**), and – 46.6 (CH_2Cl_2) x 10^{-6} emu/mol were used. Thermogravimetric analyses (TGA) of **Mn** and **Fe** were previously measured and the average solvent content was estimated. The value of z ranged from 0.73 to 1.08 for **Mn**, and 0.60 to 0.72 for **Fe** with an average value determined to be 0.90 and 0.66 for **Mn** and **Fe** respectively.

Results and Discussion

DC and AC susceptibility measurements were performed on several samples (ca 8 each) of both **Mn** and **Fe** between 5 and 300 K, but only data in a restricted range are reported. Data from representative **Mn** and **Fe** samples are reported, and deviations are discussed. The magnetic data are summarized in Table 3.1.

Table 3.1. Summary of the magnetic data for **Mn** and **Fe**.

	$Mn(TCNE)[C_4(CN)_8]_{1/2}$	$Fe(TCNE)[C_4(CN)_8]_{1/2}$
χT (RT), emuK/mol	3.95	3.12
χT, Spin-only, emuK/mol	4.75	3.375
θ, K	89	102
$\chi T(\theta)_{calc}$, emuK/mol	6.75	5.11
T_{max}, $\chi(T)$, K	72	90
$T_c = T_{max}$, $d(\chi T)/dT$, K	67	84
T_{max}, $\chi'(T)$, K	69	86
T_{max}, $\chi T(T)$, K	72	90
T_{max}, $M(T$, 5 Oe), K	67	82
M_s, emuOe/mol (9 T, 5 K)	19,700	16,500
M_s, emuOe/mol (calc)	22,340	16,755
M_r, emuOe/mol (5 K)	0	1,850
H_{cr}, Oe (5 K)	0	4,800
H_c, Oe (5 K)	-	12,600
T, $H_c(T) \rightarrow 0$, K	-	95
T_t, K		62
$H_{SpinFlop}$, Oe (5 K)	19,500	-
Frustration, f $\{= \lvert\theta\rvert/T_c\}$	1.33	1.21

The magnetic susceptibility, $\chi(T)$, of **Mn** increases gradually with decreasing temperature until ~125 K, after which, has a more rapid rise reaching a maximum at 72 K, Figure 3.2. The magnitude and cusp-shape of $\chi(T)$ is characteristic of antiferromagnetic ordering for polycrystalline materials, as previously described.[19] The $d\chi T/dT$ data (typically referred to as the 'Fischer heat capacity'[20,21]) lacks a peak typically observed[20,21] due to the rapid drop in the $\chi T(T)$ data below 71 K, but it is estimated to occur at 67 K, Figure 3.3. Hence, T_c is 67 K for **Mn** and is minimally reduced from the 72 K obtained from the cusp in $\chi(T)$.

Mn has a room temperature χT value of 3.95 emuK/mol that is less than the expected spin-only value of 4.75 emuK/mol for one high spin, $S = 5/2$, Mn^{II} and one $S = 1/2$ $[TCNE]^{-}$. This suggests that antiferromagnetic coupling, albeit slight, occurs at room temperature. $\chi T(T)$ increases slowly with decreasing temperature until ~ 140 K when it starts to increase more rapidly, reaching a maximum at 71 K before decreasing toward zero. The peak in both $\chi(T)$ and $\chi T(T)$ indicate bulk magnetic ordering. $\chi^{-1}(T)$ is linear above 200 K and can be extrapolated to a Curie-Weiss intercept, θ, of 89 K, indicating significant short-range ferromagnetic coupling, Figure 3.4. Zero field cooled, $M_{ZFC}(T)$, and field cooled, $M_{FC}(T)$, magnetizations were measured in an applied field of 5 Oe between 5 and 150 K, Figure 3.4. The $M_{ZFC}(T)$ and $M_{FC}(T)$ data are coincident with no irreversibility, and thus lack a bifurcation temperature. Although all samples of **Mn** lacked irreversibility in the $M_{ZFC}(T)$ and $M_{FC}(T)$ data, the low temperature region for each sample showed moderate variations that suggest solvent content or the presence of impurities may effect the low temperature interactions. This is in accord with previous studies, albeit to a reduced extent.[15a] The temperature dependent remanant magnetization,

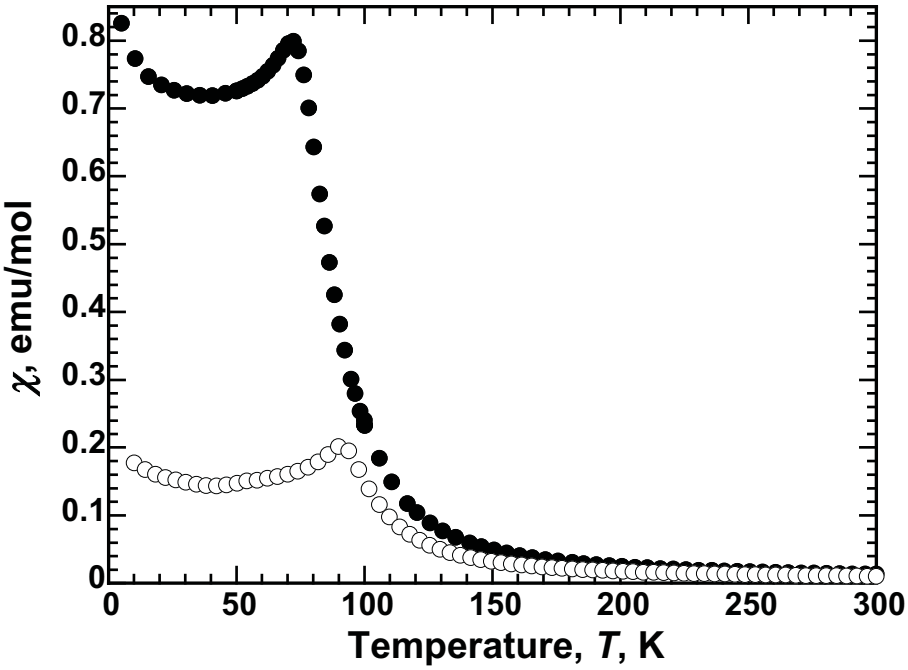

Figure 3.2. $\chi(T)$ for **Mn** (•) and **Fe** (◦) in a 1000 Oe applied field.

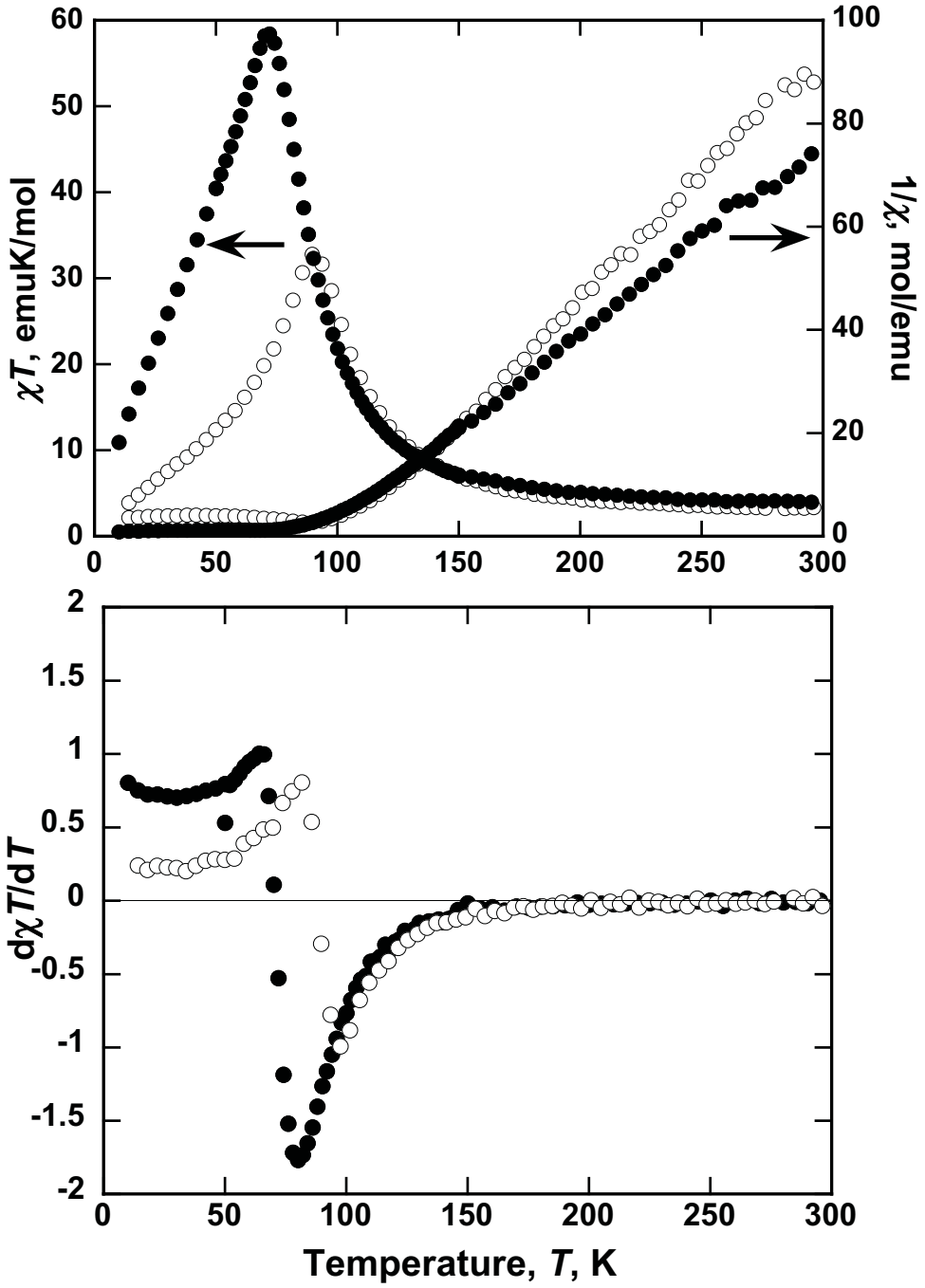

Figure 3.3. $\chi T(T)$ and $\chi^{-1}(T)$ data (top) and $d\chi T/dT$ (bottom) for **Mn** (•) and **Fe** (◦).

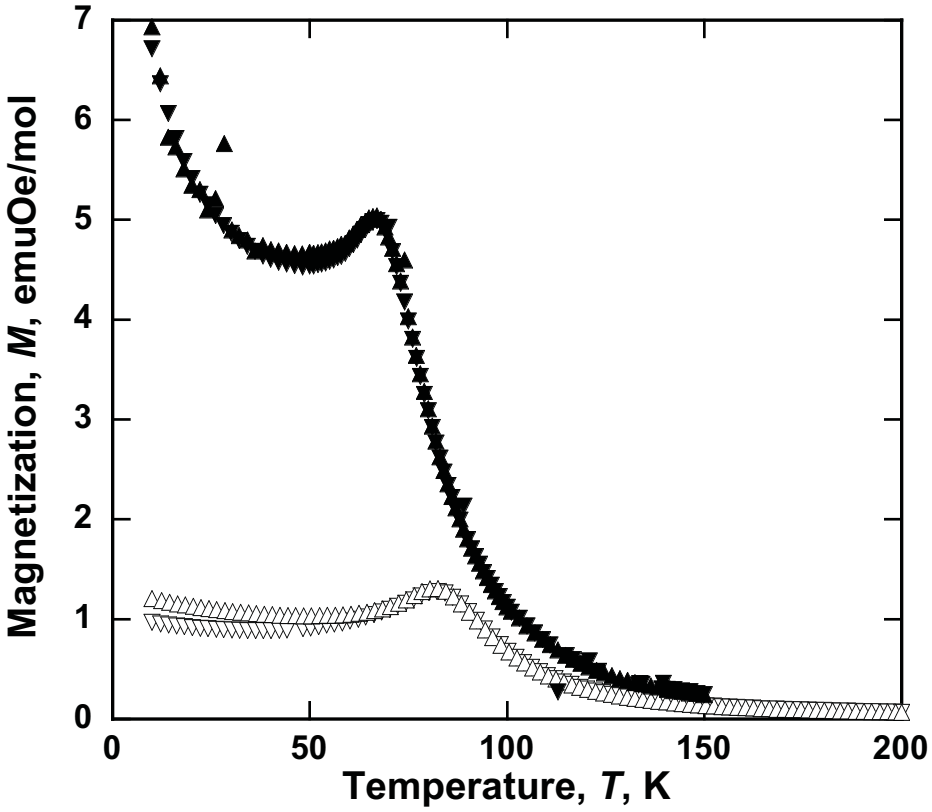

Figure 3.4. $M_{ZFC}(T)$ (▼) and $M_{FC}(T)$ (▲) data for **Mn** and $M_{ZFC}(T)$ (▽) and $M_{FC}(T)$ (△) for **Fe** .

$M(T)_r$, was measured in zero field after cooling the sample in an applied field of 5 Oe; however the data are essentially zero throughout the entire temperature range. The lack of an observed bifurcation temperature, as well as the insignificant remanant magnetization values, further support bulk antiferromagnetic ordering.

The 5 K field-dependent magnetization, $M(H)$, for **Mn** lacks any observable hysteresis and linearly increases up to ~16,000 Oe as expected for an antiferromagnet. At ~19,500 Oe **Mn** undergoes a spin flop transition and begins to approach saturation reaching a maximum value of 19,700 emuOe/mol at 9T, Figure 3.5. This value is lower than the 22,340 emuOe/mol expected for antiferromagnetic coupling between high spin Mn^{II}, $S = 5/2$, and $[TCNE]^{\cdot -}$, $S = 1/2$ within the ferrimagnetic layers. The saturation value varied between samples with a range of 17,500 to 20,400 emuOe/mol with an average value of 19,500 emuOe/mol. Hysteresis was not observed for any sample of **Mn**.

The AC susceptibility data were frequency dependent and confirmed antiferromagnetic ordering for **Mn** in which a peak from the real, in-phase, $\chi'(T)$, was observed but not for the imaginary, out-of-phase, $\chi''(T)$, Figure 3.6. As discussed in chapter 1, a response in $\chi''(T)$ indicates irreversibility due to dissipative properties or domain wall formation, therefore a lack of response is an indication of an antiferromagnetic ground state. The temperature at which the peak in $\chi'(T)$ occurs is in agreement with the DC susceptibility data, and occurs at 69 K. The peak in $\chi'(T)$ shows small variations between samples, and has a similar temperature range as the DC susceptibility data.

The $\chi(T)$ data for **Fe** increase gradually with decreasing temperature until about 125 K when there is a considerable rise until a maximum is reached at 90 K, Figure 3.2.

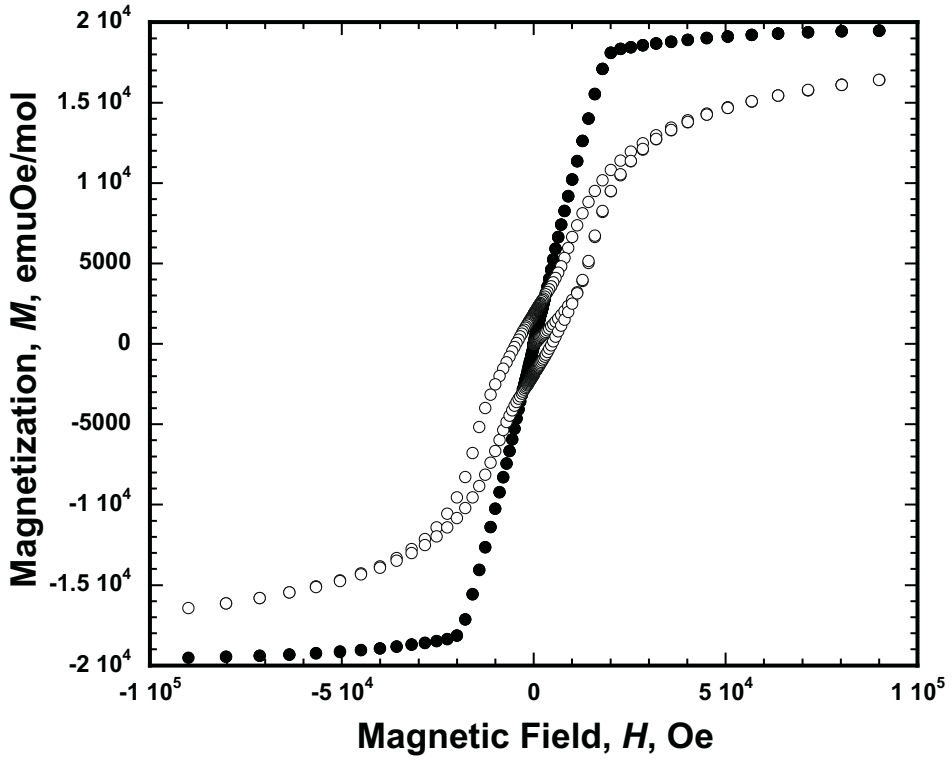

Figure 3.5. 5 K *M*(*H*) data for **Mn** (•) and **Fe** (◦).

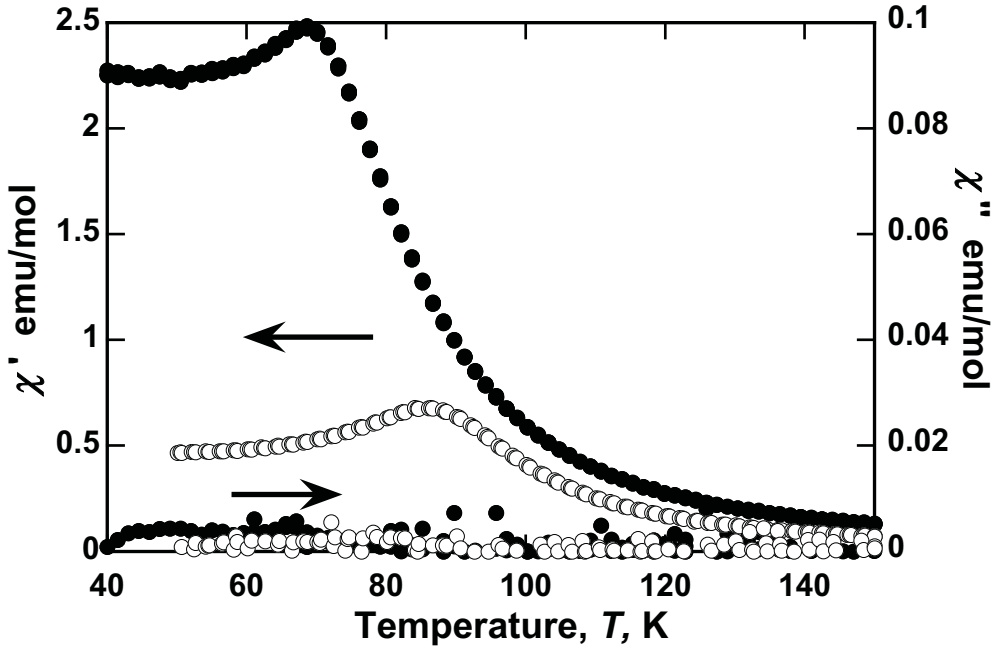

Figure 3.6. $\chi'(T)$ and $\chi''(T)$ for **Mn** (•) and **Fe** (◦).

As occurs for **Mn**, the cusp-shape of $\chi(T)$ for **Fe** is indicative of antiferromagnetic ordering. Also, like for **Mn**, the $d\chi T/dT$ data for **Fe** lacks a peak due to the rapid drop in the $\chi T(T)$ data below 90 K, but is estimated to occur at 84 K, Figure 3.3.

Fe has a room temperature χT-value of 3.12 emuK/mol that is a little less than the expected spin-only value of 3.375 emuK/mol for one high spin, $S = 2$, Fe^{II} and one $S = 1/2$ $[TCNE]^{\cdot -}$, due to antiferromagnetic coupling that occurs at room temperature. $\chi T(T)$ increases slightly with decreasing temperature until ~140 K when it starts to increase more rapidly, reaching a maximum at 90 K, before decreasing toward zero. The peak in both the $\chi(T)$ and $\chi T(T)$ plots suggest bulk magnetic ordering. $\chi^{-1}(T)$ is linear above 150 K, and can be extrapolated to a θ value of 102 K, Figure 3.3, indicating significant short-range ferromagnetic interactions.

The $M_{ZFC}(T)$ and $M_{FC}(T)$ data for **Fe** are coincident, as occurs for **Mn** again indicating an antiferromagnetic ground state, Figure 3.4. Note, however, that several samples exhibited a slight irreversibility at ~86 K. In addition, a small, finite remanant magnetization reaching a plateau at ~78 K was noted for some samples. Contrary to the $\chi(T)$ data, this would suggest that **Fe** has a ferro- or ferrimagnetic ground state. However, it is believed to be due to an impurity that causes incomplete cancellation of moments or spin canting that varies from sample-to-sample and therefore, not representative of the true ground state.

The 5 K $M(H)$ data for **Fe** exhibit a constricted-shaped hysteresis, as previously reported for samples obtained from the other synthetic routes. The $M(H)$ data for **Fe** increase linearly until ~1,100 Oe, after which they rapidly increase to 25,000 Oe when they begin to saturate, Figure 3.5. The 9 T magnetization is 16,500 emuOe/mol which is

comparable to previously reported samples.[13,17] This approaches the expected value of 16,755 emuOe/mol for antiferromagnetic coupling of high spin Fe^{II}, $S = 2$, and $[TCNE]^{\cdot-}$, $S = 1/2$ within the ferrimagnetic layers. However, saturation is not yet achieved, and due to the anisotropy of Fe^{II}, higher values are expected as g should exceed a value of 2.

The sigmoidal shape of the intial $M(H)$ is indicative of a metamagnetic transition, which is not unexpected due to the single ion anisotropy of high spin Fe^{II}.[22] Below ~8000 Oe, **Fe** exhibits a linear increase in $M(H)$ as expected for an antiferromagnetic ground state. Above ~8000 Oe, the $M(H)$ increases more rapidly indicating a field-induced transition to a ferromagnetic-like state, i.e. metamagnetism. The dM/dH versus T data reveals a critical field, H_c, which averages 12,600 Oe at 5 K. The value of H_c varied slightly from sample to sample with a range of 10,900 to 14,300 Oe. This transition is attributed to the weak antiferromagnetic coupling between the layers in **Fe** that is exceeded by the relatively small applied field, which locks the system into a high moment state once the critical field, H_c is reached. Contrary to typical metamagnets,[22,23,] **Fe** exhibits hysteretic behavior, however, several previously reported molecule-based metamagnetic materials have also been reported to exhibit hysteresis.[24]

Although the general sigmoidal shape of hysteresis is always observed,[13,15b] sample to sample variations in the coercive field ranging from 700 to 4,800 Oe as well as the remanant magnetization, M_r ranging from 900 to 18,50 emuOe/mol occur, with the higher values being associated with purer samples.

To further understand the metamagnetic transition,[22] isothermal field-dependent magnetization data were collected at various temperatures for a representative sample of **Fe**, Figure 3.7. The critical field, H_c was taken as the field at which the maximum in the

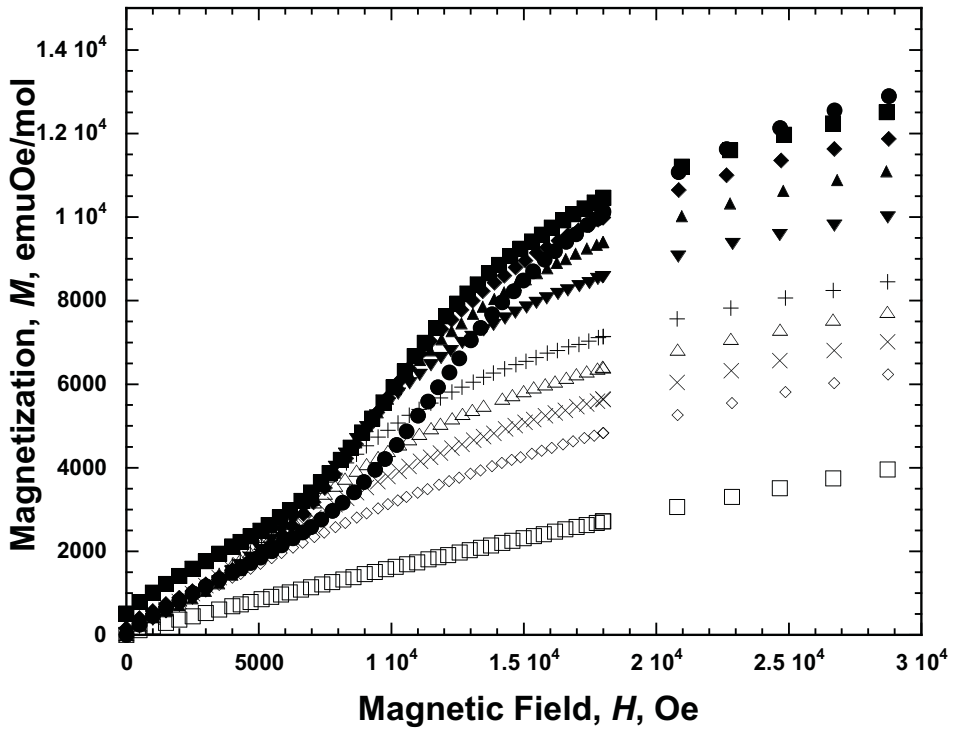

Figure 3.7. Isothermal field *M*(*H*) for **Fe** at 5(●), 20(■), 35(◆), 50(▲), 65(▼), 80(+), 91(△), 93(×), 95(◇), and 110 K(□).

dM/*dH* data occurred, and the phase diagram, $H_c(T)$ is shown in Figure 3.8. A determination of the T_c can be taken to be the temperature at which the field-induced transition disappears, and is ~95 K for this sample. This is unexpectedly more than ten degrees higher than the T_c obtained from the aforementioned methods, and this difference is surprising as these values should coincide,[25] and is under further study. The dashed line indicates the region in which a first-order antiferromagnetic to ferrimagnetic transition occurs, and the solid line indicates a second-order transition. The well-established method for determining the tricritical temperature, T_t is taken to be the temperature at which the two regions (first- and second-order transition) meet.[25] For **Fe**, the tricritical temperature, T_t ~ 62 K. Below T_t, the transitions are characteristic of first-order transitions which is evident from the discontinuity observed in the first derivative of energy curves ($dE/dH = M$) for various temperatures, Figure 3.7. For temperatures above T_t but below the T_c, the transitions are characteristic of continuous, second-order transitions from antiferromagnetic to paramagnetic states.

To validate that both first-and second-order transitions are present, the slope of the *dM*/*dH* curve was evaluated in a field range around the critical field for the various measurements at different temperatures, Figure 3.9. Discontinuity is observed indicating two different regions. Below T_t, the slope of *dM*/*dH* decreases with increasing temperature, above T_t, the slope increases with increasing temperature. The magnetic phase diagram for **Fe** is typical for a Class 1 metamagnet.[22,25]

The AC susceptibility data were frequency independent in which a peak in $\chi'(T)$, but not in $\chi''(T)$, was observed. As temperature is decreased, the $\chi'(T)$ data increases until it reaches a maximum value at 86 K, Figure 3.6. This is in accord with **Fe** exhibiting an

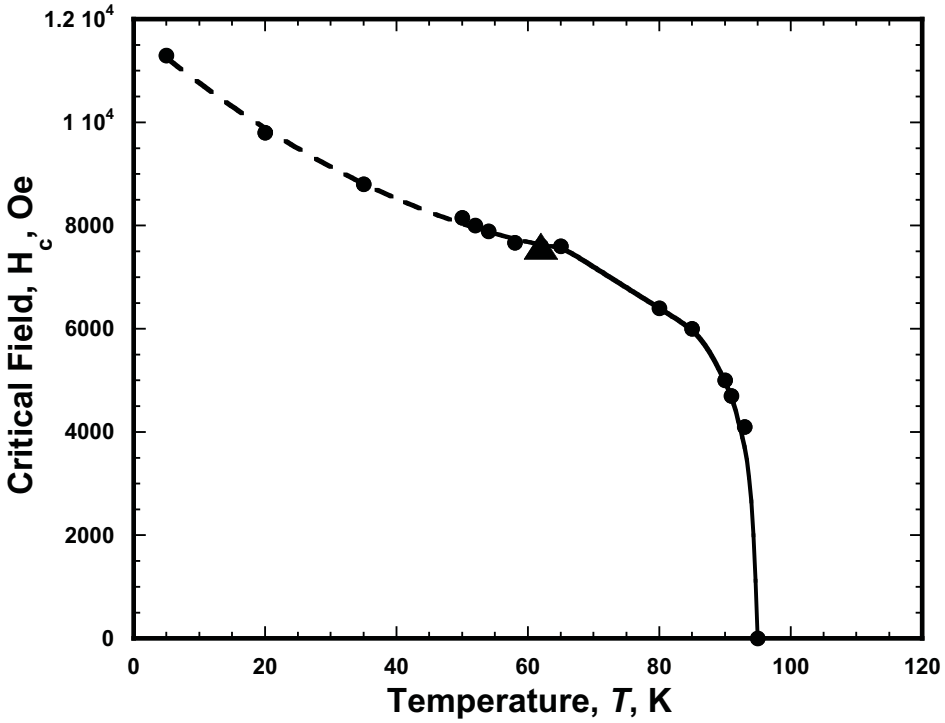

Figure 3.8. $H_c(T)$ magnetic phase diagram for **Fe** showing the tricritical temperature, T_t (▲), where the dashed line indicates the region where first-order transitions occur and the solid line indicates the region where second-order transitions occur. The lines are guides for the eyes.

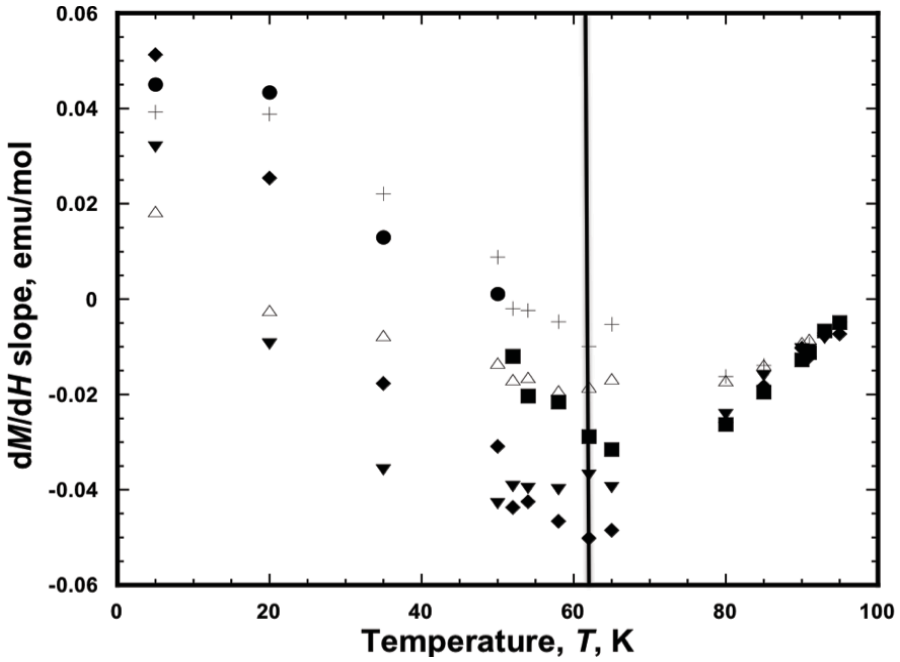

Figure 3.9. The *dM*/*dH*(*T*) for several field ranges for **Fe** showing two discontinuous regions. 5 – 11(•), 5 – 15(■), 8 – 11(◆), 8 – 12(▼), 11 – 17(△), and 12 – 17 kOe(+). The line represents the tricritcal point distinguishing the first- and second-order transitions.

antiferromagnetic ground state. Slight variations in the χ'(T) data were observed from sample-to-sample in which a weak feature was sometimes present. This would indicate bulk ferro- or ferrimagnetic ordering, again, which is attributed to spin canting or incomplete cancellation of spin arising from impurities.

Conclusion

Mn and **Fe** are attributed to having direct antiferromagnetic exchange coupling between the M^{II} (S = 5/2 for **Mn**, S = 2 for **Fe**) and the μ_4-[TCNE]$^{\cdot-}$ (S = 1/2) spin sites with leading to 2-D ferrimagnetic layers. These ferrimagnetic layers are antiferromagnetically coupled via the 5-atom conjugated -N≡C-C-C≡N- superexchange pathways leading to a bulk antiferromagnet. However, both **Mn** and **Fe** do not appear to be simple collinear antiferromagnets as their magnetization data are more complex. This is evident in the rising magnetization at low temperatures (< 25 K) in $M_{ZFC}(T)$ and $M_{FC}(T)$, and in the positive θ value obtained from the $\chi T(T)$ data for both **Mn** and **Fe**. This suggests that there may be a gradual spin rearrangement to a ferromagnetic-like state. Nonetheless, based on the dχT/dT data, an ordering temperature was determined to be 67 and 84 K for **Mn** and **Fe**, respectively. The evidence for antiferromagnetic ordering is supported by: (1) the classic cusp-shape that is observed in the $\chi(T)$ data, (2) the absence of a bifurcation temperature in the coincident $M_{ZFC}(T)$ and $M_{FC}(T)$ data, (3) no remanant magnetization, $M_r(T)$, and (4) no response in χ'(T) data. **Mn** exhibits $M(H)$ data typical for antiferromagnets and lacks irreversibility. The $M(H)$ data for **Fe** on the other hand, shows more complex behavior indicating a field-induced metamagnetic transition from an antiferromagnetic ground state to a high moment, ferromagnetic state. A critical

field, H_c of 14,000 Oe is required to overcome the weak antiferromagnetic coupling between the layers at 5 K. The metamagnetic transition in **Fe** is attributed to the single ion anisotropy of high spin Fe^{II} and is not observed for **Mn** due to the isotropic high spin Mn^{II} ion.

References

(1) Miller, J. S.; Calabrese, J. C.; Epstein, A. J.; Bigelow, R. W.; Zhang, J. H.; Reiff, W. M. *J. Chem. Soc., Chem. Commun.* **1986**, 1026.

(2) Miller, J. S.; Calabrese, J. C.; Rommelmann, H.; Chittipeddi, S. R.; Zhang, J. H.; Reiff, W. M.; Epstein, A. J. *J. Am. Chem. Soc.* **1987**, *109*, 769.

(3) Ovcharenko, V. I.; Sagdeev, R. Z. *Russ. Chem. Rev.* **1999**, *68*, 345.

(4) Blundell, S. J.; Pratt, F. L. *J. Phys.: Condens. Matter* **2004**, *16*, R771.

(5) Miller, J. S. *Chem. Soc. Rev.* **2011**, *40*, 3266.

(6) Miller, J. S. *Angew. Chem. Int. Ed.* **2006**, *45*, 2508.

(7) Miller, J. S.; Calabrese, J. C.; McLean, R. S.; Epstein, A. J. *Adv. Mater.* **1992**, *4*, 498.

(8) Pokhodnya, K. I.; Bonner, M.; Her, J.-H.; Stephens, P. W.; Miller, J. S. *J. Am. Chem. Soc.* **2006**, *126*, 15592.

(9) Lapidus, S. H.; McConnell, A. C.; Stephens, P. W.; Miller, J. S. *Chem. Comm.* **2011**, *47*, 7602.

(10) Stone, K. H.; Stephens, P. W.; McConnell, A. C.; Shurdha, E.; Pokhodnya, K. I.; Miller, J. S. *Adv. Mater.* **2010**, *22*, 2514.

(11) Manriquez, J. M.; Yee, G. T.; McLean, R. S.; Epstein, A. J.; Miller, J. S. *Science* **1991**, *252*, 1415.

(12) Miller, J. S. *Polydedron* **2009**, *28*. 1596.

(13) Zhang, J.; Ensling, J.; Ksenofontov, V.; Gütlich, P.; Epstein, A. J.; Miller, J. S. *Angew. Chem. Int. Ed.* **1998**, *37*, 657.

(14) Pokhodnya, K. I.; Petersen, N.; Miller, J. S. *Inorg. Chem.* **2002**, *41*, 1996.

(15) (a) Wynn, C. M.; Girtu, M. A.; Zhang, J.; Miller, J. S.; Epstein, A. J. *J. Phys. Rev. B.* **1998**, *58*, 8508. Pejakovic, D.; Kitamura, C.; Miller, J. S.: Epstein, A. J. *Phys. Rev. Lett.* **2002**, *88*, 57202/1. Pejakovic, D.; Epstein, A. J.; Kitamura, C.; Miller, J. S. *J. Appl. Phys.* **2002**, *91*, 7176. (b) Girtu, M. A.; Wynn, C. M.; Zhang, J.; Miller, J. S.; Epstein, A. J. *Phys. Rev. B.* **2000**, *61*, 492.

(16) Shurdha, E.; Lapidus, S. H.; Stephens, P. W.; Moore, C. E.; Rheingold, A. L.; Miller, J. S. submitted.

(17) Her, J.-H.; Stephens, P. W.; Pokhodnya, K. I.; Bonner, M.; Miller, J. S. *Angew. Chem. Int. Ed.* **2007**, *46*, 1521.

(18) Bell, J. D.; McConnell, A. C.; Miller, J. S. unpublished results.

(19) Carlin, R. L. *Magnetochemistry*; Springer-Verlag: Berlin, 1986, p. 121.

(20) (a) Aharen, T.; Greedan, J. E.; Ning, F.; Imai, T.; Michaelis, V.; Zhou, S. H.; Wiebe, C. R.; Cranswick, L. M. D. *Phys. Rev. B.* **2009**, *80*, 134423. (b) Cage, B.; Nguyen, B.; Dalal, N. *Sol. State Commun.* **2011**, *119*, 597.

(21) Fisher, M. E. *Philos. Mag.* **1962**, *7*, 1721.

(22) Stryjewski, E.; Giordano, N. *Adv. Phys.* **1977**, *26*, 487.

(23) Taliaferro, M. L.; Palacio, F.; Miller, J. S. *J. Mater. Chem.* **2006**, *16*, 2677.

(24) (a) Zhang, D.; Wang, H.; Chen. Y.; Ni, Z.-H.; Tian, L.; Jiang, J. *Inorg. Chem.* **2009**, *48*, 11215. Sun, Q.; Cheng, A.; Wang, Y.-Q.; Ma, Y.; Gao, E.-Q. *Inorg. Chem.* **2011**, *50*, 8144. (b) Colacio, E.; Ghazi, M.; Stoeckli-Evans, H.; Lloret, F.; Moreno, J.; Perez, C. *Inorg. Chem.* **2001**, *40*, 4876. (c) Yang, C.; Wang, Q.-L.; Qi, J.; Ma. Y.; Yan, S.-P.; Yang, G.-M.; Cheng, P.; Liao, D.-Z. *Inorg. Chem.* **2011**, *50*, 4006. (d) Keene, T.; Light, M.; Hursthouse, M.; Price, D. *Dalton Trans.* **2011**, *40*, 2983. (e) Miyasaka, H.; Izawa, T.; Takahashi, N.; Yamishita, M.; Dunbar, K. *J. Am. Chem. Soc.* **2006**, *128*, 11358.

(25) (a) Schmidt, V. A.; Friedberg, S. A. *Phys. Rev. B.* **1970**, *1*, 2250. (b) Jacobs, I. S.; Lawrence, P. E. *Phys. Rev.* **1967**, *164*, 866. (c) Vettier, C.; Alberts, H. L.; Bloch, D. *Phys. Rev. Lett.* **1973**, *31*, 1414. (d) Shum. W. W.; Schaller, J. N.; Miller, J. S. *J. Phys. Chem. C.* **2008**, *112*, 7936.

CHAPTER 4

A MEAN FIELD ANALYSIS OF THE EXCHANGE COUPLING (*J*) FOR 2- AND 3-D STRUCTURED TETRACYANOETHENIDE ($TCNE^{\cdot-}$)-BASED MAGNETS

Abstract

Mean field expressions, based on the simple Heisenberg model, were derived to correlate the inter- and intralayer exchange coupling to the critical temperature, T_c, for several TCNE (tetracyanoethylene) based magnets with extended 2- and 3-D structure types. These expressions were used to estimate the exchange coupling, *J*, for 2-D ferrimagnetic $[M^{II}(TCNE)(NCMe)_2]^+$ (M = Mn, Fe), 3-D antiferromagnetic $Mn^{II}(TCNE)[C_4(CN)_8]_{1/2}$, and 3-D ferrimagnetic $Mn^{II}(TCNE)_{3/2}(I_3)_{1/2}$. The type and magnitude of the exchange coupling are in accord with previously reported magnetic data.

Introduction

Several organic-based magnets[1,2,3] with TCNE in its mono-reduced form, $[TCNE]^{\cdot-}$, have been reported.[3,4] Their structures, based on the perspective of extended bonding, span from isolated, ionic $[TCNE]^{\cdot-}$ [zero-dimensional (0-D) bonding] to 3-D

extended network structures, possessing μ_4-[TCNE]$^{\cdot-}$. Examples that contain manganese cations include: 0-D $[Mn^{III}(C_5Me_5)_2]^+[TCNE]^{\cdot-}$,[5] 1-D $[Mn^{III}TPP]^+[TCNE]^{\cdot-}$ (TPP = tetraphenylporphrin),[6] 2-D $Mn^{II}(TCNE)I(OH_2)$,[7] and 3-D $Mn^{II}(TCNE)_{3/2}(I_3)_{1/2}$.[8] The family member with the highest magnetic ordering temperature, T_c, which exceeds room temperature, is $V[TCNE]_x$.[9] It is, however, amorphous and its structure has been elusive, although it is proposed to be 3-D.[10] In addition to these examples, other structurally characterized material in the family have been reported.[8,11-15]

Prototype 2- and 3-D structured TCNE-based magnetic materials are a) $[Fe^{II}(TCNE)(NCMe)_2][FeCl_4]$[11], Figure 4.1, and $[M^{II}(TCNE)(NCMe)_2][SbF_6]$ (M = Mn, Fe)[12] that have S = 1/2 μ_4-[TCNE]$^{\cdot-}$ extended network bonding in 2-D; b) $M^{II}(TCNE)[C_4(CN)_8]_{1/2}\bullet zCH_2Cl_2$ (M = Mn,[8] Fe[15])[16] that possess extended network bonding in 2-D via S = 1/2 μ_4-[TCNE]$^{\cdot-}$ in which these layers are bridged by S = 0 μ_4-$[C_4(CN)_8]^{2-}$, i.e. extended network bonding in 3-D, Figure 4.2; and c) $Mn^{II}(TCNE)_{3/2}(I_3)_{1/2}\bullet z$THF[8] that contains extended network bonding in 3-D via S = 1/2 μ_4-[TCNE]$^{\cdot-}$, Figure 4.3. The T_c ranges from 67 to 171 K, Table 4.1.

Each of these 2- and 3-D organic-based magnets possess S = 1/2 μ_4-[TCNE]$^{\cdot-}$ that is antiferromagnetically coupled to four high spin M^{II} ions (S = 5/2 for Mn^{II}, S = 2 for Fe^{II}) by direct exchange. This leads to extended, non-frustrated antiferromagnetically coupled layers. As a consequence, the 2-D structured magnets order as ferrimagnets.[11,12] $Mn^{II}(TCNE)_{3/2}(I_3)_{1/2}$ has an additional S = 1/2 μ_4-[TCNE]$^{\cdot-}$ linking the layers. This linkage is also antiferromagnetically coupled, which leads to extended 3-D, non-frustrated, antiferromagnetic coupling within and between the layers and orders as a ferrimagnet.[8]

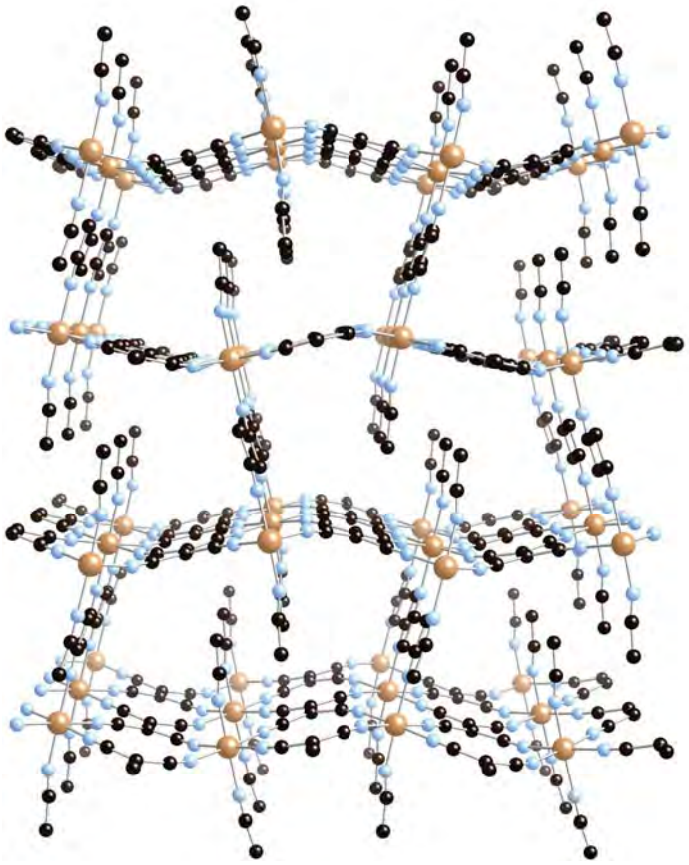

Figure 4.1. 2-D Extended network bonding via μ_4-$[TCNE]^{\bullet-}$ observed for $[Fe^{II}(TCNE)(NCMe)_2]^+$ in $[Fe^{II}(TCNE)(NCMe)_2][FeCl_4]$ (**1c**) (Fe = gold; C = black, N = blue).[11] The ordered anions reside in the channels and have been removed for clarity. (Structure type **A** vide infra.)

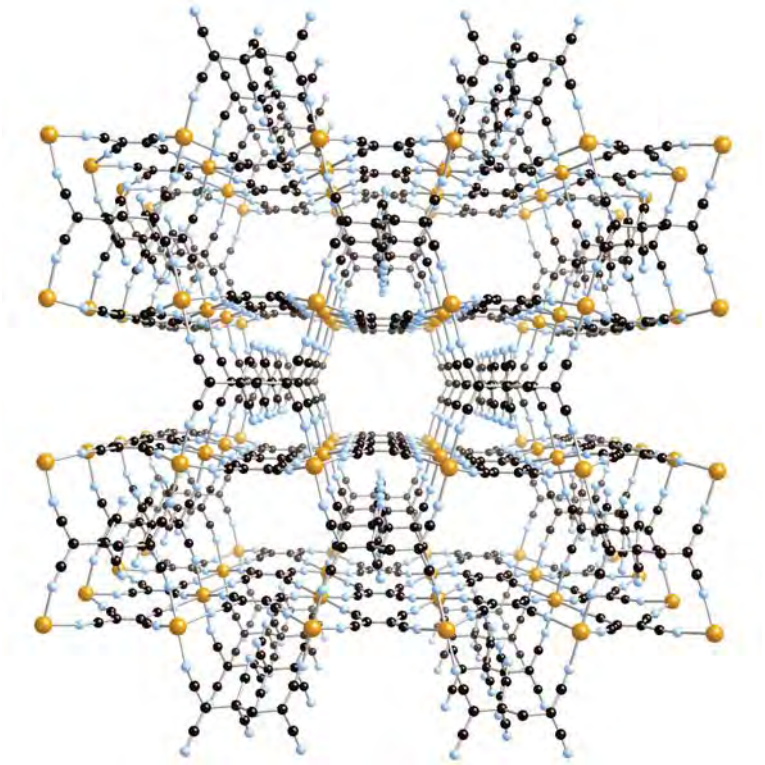

Figure 4.2. 3-D Extended network bonding via 2-D μ_4-$[TCNE]^{\bullet-}$ in which these layers are bridged by μ_4-$[C_4(CN)_8]^{2-}$ that is reported for $M^{II}(TCNE)[C_4(CN)_8]_{1/2}\bullet zCH_2Cl_2$ (M = Mn,[8] Fe[15]) (**2**) (M = gold; C = black, N = blue). The disordered solvent resides in the channels and have been removed for clarity. (Structure type **B** vide infra.)

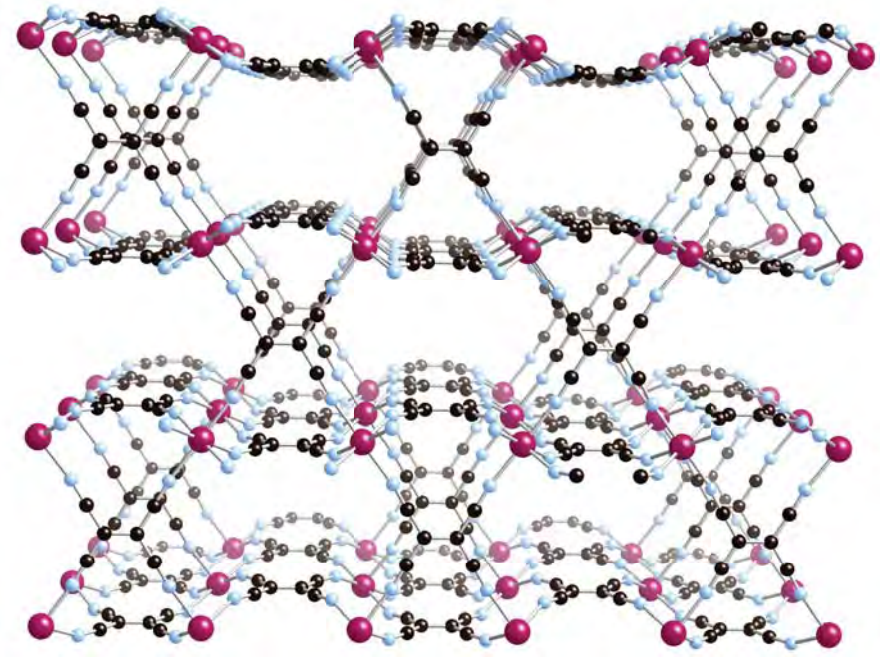

Figure 4.3. Extended network bonding via μ_4-$[TCNE]^{\bullet -}$ in 3-D present for $Mn^{II}(TCNE)_{3/2}(I_3)_{1/2}\bullet z$THF (**3**) (Mn = red; C = black, N = blue).[8] The ordered solvent and ordered anion I_3^- reside in the channels and have been removed for clarity. (Structure type $\mathbf{C_2}$ vide infra.)

Table 4.1. Summary of structurally characterized 2- and 3-D TCNE-based magnets and their T_c's.

Magnet		Bonding Dimensionality	T_c, K	Type [a]	ref
$[Fe^{II}(TCNE)(NCMe)_2][FeCl_4]$	**1c**	2-D	90	FI	11
$[Mn^{II}(TCNE)(NCMe)_2][SbF_6]$	**1a**	2-D	67	FI	12
$[Fe^{II}(TCNE)(NCMe)_2][SbF_6]$	**1b**	2-D	96	FI	12
$Mn^{II}(TCNE)[C_4(CN)_8]_{1/2}\bullet zCH_2Cl_2$	**2**	3-D	67* 69** 68.2***	AF	8, 16
$Fe^{II}(TCNE)[C_4(CN)_8]_{1/2}\bullet zCH_2Cl_2$		3-D	84	AF/MM	16
$Mn^{II}(TCNE)_{3/2}(I_3)_{1/2}\bullet z$THF	**3**	3-D	171	FI	8

[a] FI = Ferrimagnet, AF = Antiferromagnet, MM = metamagnetic behavior. * Determined from the "Fischer heat capacity" peak. ** Determined from the peak in $\chi'(T)$. *** Determined from the spin-flip transition in $M(H)$. (vide infra.)

$M^{II}(TCNE)[C_4(CN)_8]_{1/2}$ has the same layered structure and magnetic coupling, but the layers are linked via $S = 0$ μ_4-$[C_4(CN)_8]^{2-}$. Consequently, $M^{II}(TCNE)[C_4(CN)_8]_{1/2}$ has a 3-D extended network structure. This diamagnetic $[C_4(CN)_8]^{2-}$ anion provides a conjugated -N≡C-C-C≡N- superexchange path that antiferromagnetically couples the ferrimagnetic layers, stabilizing an antiferromagnetic ground state. Due to Fe^{II} being anisotropic, the magnetic ground state has more complex magnetic behavior in which metamagnetism is observed.

An important aspect of understanding organic-based magnets and enhancing their transition temperatures is the identification of the nearest neighbor exchange coupling, *J*, for these magnetic materials. The Mean Field (MF) approximation to the Heisenberg model [$\mathbf{H} = -\Sigma J_{ij} S_i \bullet S_j$ (i > j)], equation 4.1[17,18] has been used extensively to relate T_c to an average *J*

$$T_c = \frac{|J| z S(S+1)}{3k_B}. \tag{4.1}$$

This expression is applicable for isotropic materials with one type of spin site of total spin, *S*. In which *z* is the number of nearest neighbors, and k_B is Boltzmann's constant. The MF result for an isotropic system possessing two different spin sites, *i* and *j*, has also been developed, equation 4.2,[17,19]

$$T_c = \frac{|J| \sqrt{z_i z_j S_i(S_i+1) S_j(S_j+1)}}{3k_B}, \tag{4.2}$$

in which z_i and z_j are the number of nearest neighbors and S_i and S_j are the total spin on sites *i* and *j*, respectively.

While appropriate and providing insightful relations for cubic systems such as Prussian blue analogs,[19a,b] equation 4.2 is not precisely applicable for non-cubic TCNE-based organic-based magnets. With the initial goal to identify the exchange coupling within and between the layers of 2-D and structurally bridged 2-D (3-D via non-spin bearing species), and well as 3-D magnetic materials based on their observed T_c, a MF analysis was performed for the family of magnets described above and reported herein.

MF theory is useful for predicting trends and for qualitative estimates of exchange constants. Although MF theory can overestimate T_c by as much as 40%,[18] it provides better estimates for the ratios of exchange couplings in different materials. The MF analysis for several 2- and 3-D structure-types with general spin, *S*, led to the identification of expressions that relate the exchange couplings to T_c. These expressions are then evaluated using experimental data for 2-D layered $[M^{II}(TCNE)(NCMe)_2][X]$ {M = Mn (**1a**), Fe (**1b**); X = $[SbF_6]^-$; M = Fe, X = $[Fe^{III}Cl_4]^-$ (**1c**)}, 3-D bridged $Mn^{II}(TCNE)[C_4(CN)_8]_{1/2}$ (**2**), and 3-D $Mn^{II}(TCNE)_{3/2}(I_3)_{1/2}$ (**3**) to estimate the values of their exchange couplings.

Mean Field (MF) Expressions

The MF expressions for T_c, using $\mathbf{H} = -\Sigma J_{ij} S_i \bullet S_j$ ($i > j$), are determined for various structure-types: (**A**) 2-D layered system with two spin sites and intralayer coupling, *J*; (**B**) 3-D system with two spin sites and a diamagnetic bridging ligand with intralayer coupling, *J*, and interlayer coupling, *K*; (**C_1** and **D_1**) 3-D system with three spin sites with

intralayer couplings, J and J'; and ($\mathbf{C_2}$ and $\mathbf{D_2}$) 3-D system with two spin sites and with isotropic exchange coupling, J. For all systems, $J < 0$ and $K > 0$ signify ferromagnetic coupling. The derivation of the MF expression for all structure-types is shown in the Appendix.

Structure-type A. The MF solution for the general spin case of a 2-D structure-type **A** material of $M(L^S)(L^{NB})_2$ (M = metal ion; L^S = spin bearing ligand; L^{NB} = non-spin bearing, non-bridging species) composition, Figure 4.4, was constructed. MF theory predicts,

$$T_c = \frac{4}{3k_B} |J| \sqrt{S(S+1)S'(S'+1)}, \tag{4.3}$$

in which J is the coupling between M ($z = 4$) and L^S ($z = 4$) within the layers, S = spin on M, and S' = spin on L^S.

Structure-type B. The MF expression for the general spin case for 3-D structure-type **B** material of $M(L^S)(L)$ (L = non-spin bearing, bridging species) composition, Figure 4.5, is,

$$T_c = \frac{1}{3k_B}[KS(S+1) + \sqrt{K^2[S(S+1)]^2 + 16J^2S(S+1)S'(S'+1)}], \tag{4.4}$$

in which J is the intra-layer coupling between M ($z = 4$) and L^S ($z = 4$), K is the inter-layer coupling between M and M, S = spin on M, and S' = spin on L^S.

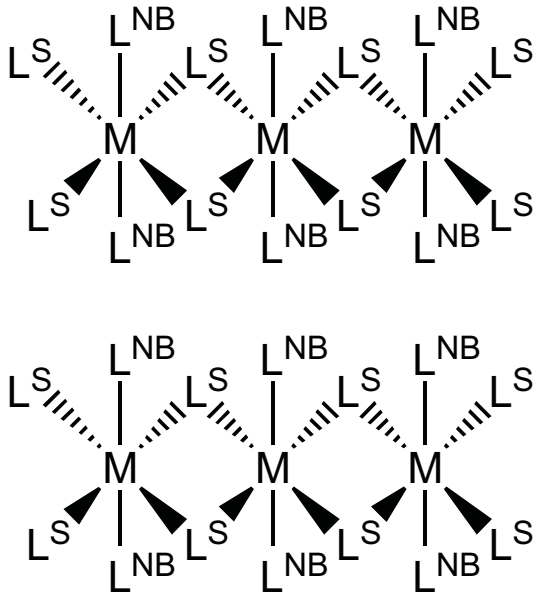

Figure 4.4. Generalized bonding scheme for 2-D layered compounds with formula $M(L^{S})(L^{NB})_2$ of structure-type **A**.

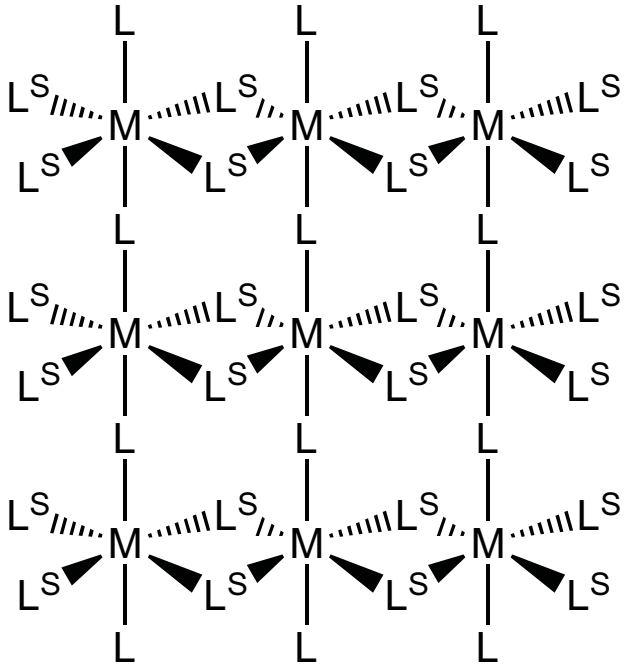

Figure 4.5. Generalized bonding scheme for compounds with formula $M(L^S)(L)$ of structure type **B**.

Structure-type C. The MF expression for the general spin case for 3-D structure-type $\mathbf{C_1}$ material of $M(L^{S1})(L^{S2})_{1/2}$ [M = metal ion (z = 6); L^{S1} = spin bearing ligand (z = 4); L^{S2} = spin bearing species (different than L^{S1}) (z = 4)] composition, Figure 4.6a, is,

$$T_c = \frac{2}{3k_B}\sqrt{S(S+1)[4J^2S'(S'+1) + 2J'^2\,S''(S''+1)]}\,. \tag{4.5}$$

For the case of isotropic coupling ($J \sim J'$) and one spin bearing ligand ($L^{S1} = L^{S2} = L^S$ (z = 4); $S' \sim S''$) of $M(L^S)_{3/2}$ composition and structure-type $\mathbf{C_2}$, Figure 4.6b, equation 4.5 reduces to equation 4.6.

$$T_c = \frac{2}{3k_B}|J|\sqrt{6S(S+1)S'(S'+1)} \tag{4.6}$$

Structure-type D. The MF expression for the general spin case for 3-D structure-type $\mathbf{D_1}$ material of $M(L^{S1})(L^{S2})$ [M = metal ion (z = 6); L^{S1} = spin bearing ligand (z = 4); L^{S2} = spin bearing species (different than L^{S1}) (z = 2)] composition, Figure 4.7a, is

$$T_c = \frac{2}{3k_B}\sqrt{S(S+1)[4J^2S'(S'+1) + J'^2\,S''(S''+1)]}\,. \tag{4.7}$$

For the case of isotropic coupling ($J \sim J'$), $S' = S''$, $M(L^S)_2$ composition, and structure-type $\mathbf{D_2}$, Figure 4.7b, equation 4.7 reduces to equation 4.8. Note that this situation is unlikely as the coordination environments for L^{S1} and L^{S2} are different; thus, $J \sim J'$ is likewise unlikely. Nonetheless, it is useful for comparison purposes.

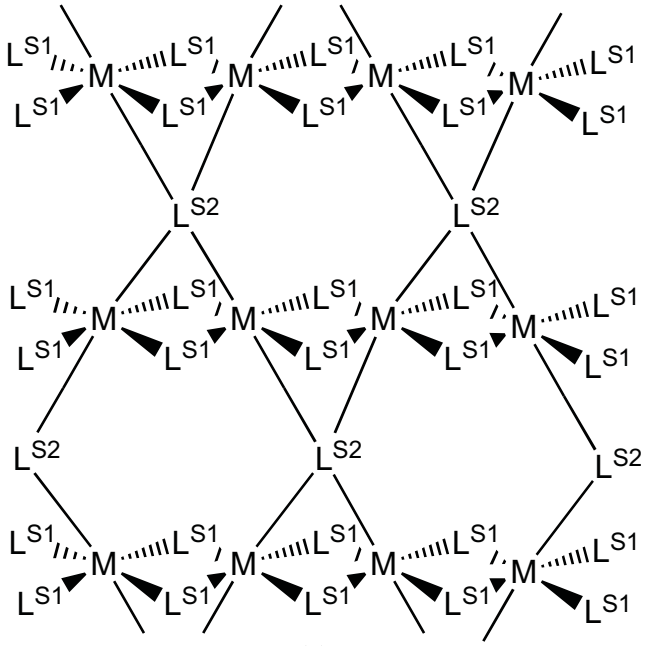

(a)

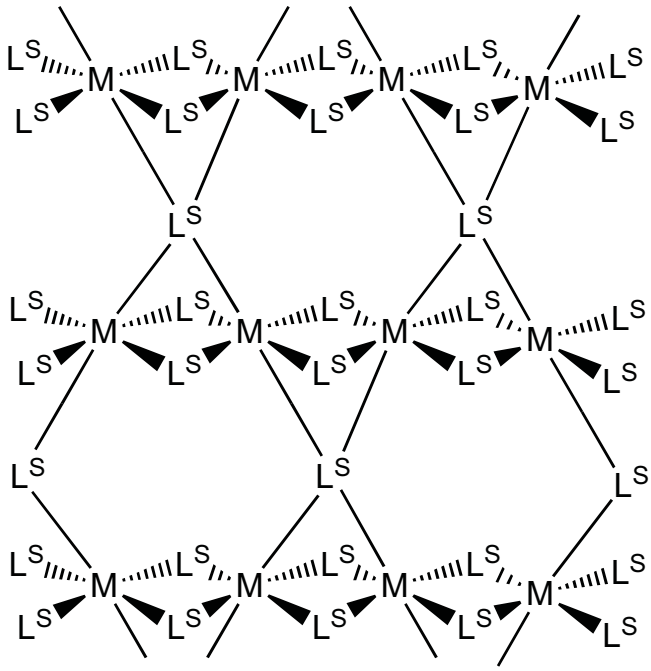

(b)

Figure 4.6. Generalized bonding schemes for $M(L^{S1})(L^{S2})_{1/2}$ of structure-type $\mathbf{C_1}$ (a), and $M(L^{S})_{3/2}$ of structure-type $\mathbf{C_2}$ (b).

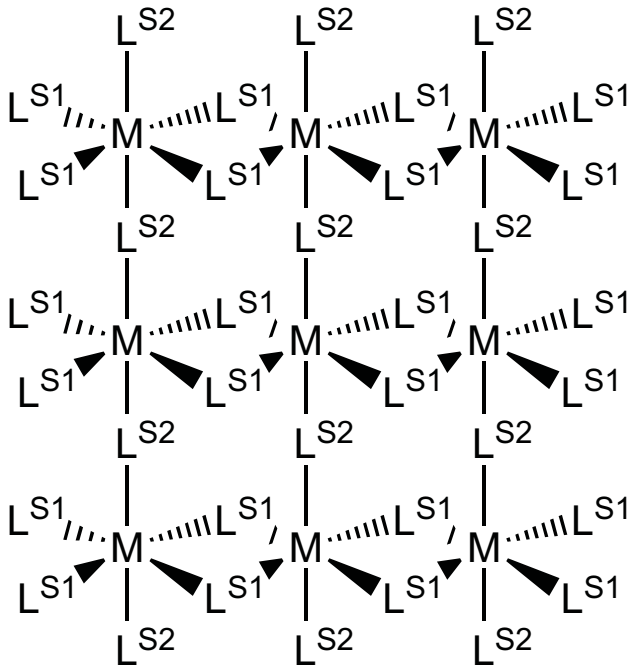

(a)

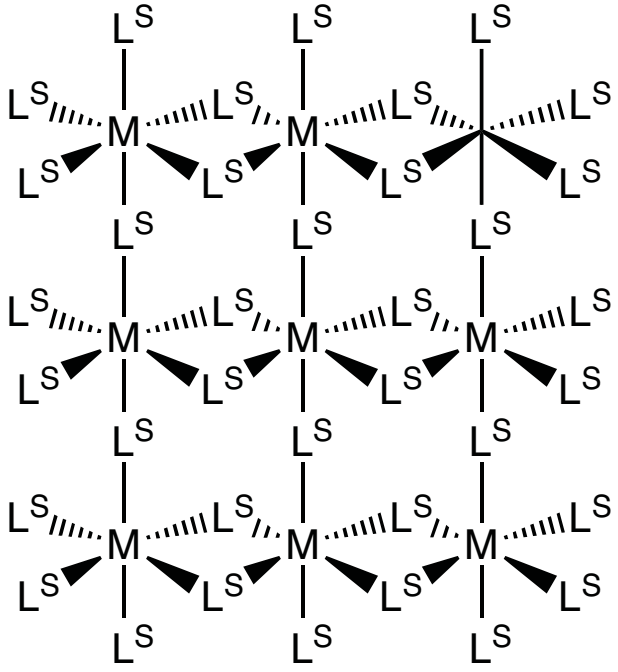

(b)

Figure 4.7. Generalized bonding scheme for $M(L^{S1})(L^{S2})$ of structure-type **D_1** (a), and $M(L^{S})_2$ of structure-type **D_2** (b).

$$T_c = \frac{2}{3k_B} |J| \sqrt{5S(S+1)S'(S'+1)} \tag{4.8}$$

The difference in T_cs between structure-type $\mathbf{C_2}$ and hypothetical structure-type $\mathbf{D_2}$, assuming the identical spins and $J(\mathbf{C_2}) \sim J(\mathbf{D_2})$ can be calculated by equation 4.9, and the ratio is 1.1. Thus, there is a 10% enhancement of T_c if the bridging ligand goes from z = 2 to z = 4, i.e., magnets with structure-type $\mathbf{C_2}$ should have a 10% higher T_c with respect to those with structure-type $\mathbf{D_2}$ for the metal ions, S, and S', or conversely a 10% reduced J would be needed for the same T_c.

$$\frac{T_c(\mathbf{C_2})}{T_c(\mathbf{D_2})} = \frac{J(\mathbf{C_2})}{J(\mathbf{D_2})}\sqrt{\frac{6}{5}} = 1.1\frac{J(\mathbf{C_2})}{J(\mathbf{D_2})} \tag{4.9}$$

A summary of the MF equations for general spin for the aforementioned structural cases **A** to **D** is contained in Table 4.2.

Estimation of Exchange Coupling

The exchange coupling, J, for **1a**, **1b**, and **1c** of structure-type **A** [M = Mn^{II} (**1a**); Fe^{II} (**1b**, **1c**), L^S = μ_4-$[TCNE]^{\cdot-}$; L^{NB} = NCMe; S = 5/2 (**1a**) or 2 (**1b**, **1c**) and S' = 1/2], can be estimated from equation 4.3. Based on previously reported values for T_c of 67, 96, and 90 K for **1a**, **1b**, and **1c**, J/k_B is estimated as 19.6, 33.9, and 31.8 K, respectively. These values are identical to those obtained by using the classical MF expression, equation 4.2, for a two-spin system with isotropic J. Based upon the aforementioned convention, the positive J indicates antiferromagnetic coupling between M^{II} and μ_4-$[TCNE]^{\cdot-}$ for these

Table 4.2. Summary of MF expressions [$\mathcal{H} = -\Sigma J_{ij} S_i \bullet S_j$ (i > j)] for general *S* for 2-D and 3-D structure types **A**, **B**, $\mathbf{C_1}$, $\mathbf{C_2}$, $\mathbf{D_1}$ and $\mathbf{D_2}$.

Formula[a] (structure-type)	Mean Field Expression for T_c [b]
2-D	
$M(L^S)(L^{NB})_2$ (**A**)	$T_c = \frac{4}{3k_B} \lvert J \rvert \sqrt{S(S+1)S'(S'+1)}$
3-D	
$M(L^S)(L)$ (**B**)	$T_c = \frac{1}{3k_B}[KS(S+1) + \sqrt{K^2[S(S+1)]^2 + 16J^2 S(S+1)S'(S'+1)}]$
$M(L^{S1})(L^{S2})_{1/2}$ ($\mathbf{C_1}$)	$T_c = \frac{2}{3k_B}\sqrt{S(S+1)[4J^2 S'(S'+1) + 2J'^2 S''(S''+1)]}$
$M(L^S)_{3/2}$ ($\mathbf{C_2}$)	$T_c = \frac{2}{3k_B} \lvert J \rvert \sqrt{6S(S+1)S'(S'+1)}$
$M(L^{S1})(L^{S2})$ ($\mathbf{D_1}$)	$T_c = \frac{2}{3k_B}\sqrt{S(S+1)[4J^2 S'(S'+1) + J'^2 S''(S''+1)]}$
$M(L^S)_2$ ($\mathbf{D_2}$)	$T_c = \frac{2}{3k_B} \lvert J \rvert \sqrt{5S(S+1)S'(S'+1)}$

[a] M = metal ion; L^S, L^{S1}, and L^{S2} = spin bearing species; L^{NB} = non-spin bearing, non-bridging species. L = non-spin bearing, bridging species

[b] *J* = intra-layer coupling between M and L^S or L^{S1}; *K* = inter-layer M and M coupling; *J'* = inter-layer M and L^{S2} coupling; *S* = spin on M; *S'* = spin on L^S or L^{S1}; *S''* = spin on L^{S2}.

three 2-D compounds that results in ferrimagnetic layers. This agrees with previously reported data.[11,12]

The intra-layer, *J*, and inter-layer, *K*, coupling constants for **2** of structure-type **B** (M = Mn^{II}; L^S = μ_4-$[TCNE]^{\cdot-}$; L = $[C_4(CN)_8]^{2-}$; *S* = 5/2 and *S′* = 1/2), can be estimated from equation 4.4. Since only T_c is known, *J* and *K* cannot be solved individually. Since **1a** and **2** have similar 2-D layers, however, the inter-layer coupling constant, *K*, can be estimated by assuming the value for *J* calculated for **1a** using equation 4.3. This is a reasonable assumption, as both **1a** and **2** possess corrugated sheets of Mn^{II} ions coordinated to four μ_4-$[TCNE]^{\cdot-}$ anions, but due to the *trans* acetonitrile ligands for **1a**, the non-bridging layers are isolated and the intra-layer coupling *K* is negligible, and assumed to be zero. The value of T_c for **2** can vary depending on which method is used to obtain it therefore the value of K/k_B that is estimated will also vary. If the reported value of T_c = 67 K determined from the peak in $d\chi T/dT$ [16] and the estimated value J/k_B = 19.6 K obtained for **1a**, is used then the inter-layer coupling would be K/k_B = 0 K. On the other hand, using the estimated value J/k_B = 19.6 K and T_c = 69 K determined from the peak in $\chi'(T)$ the inter-layer coupling, K/k_B, between the Mn^{II} ions via superexchange in **2** is estimated as -0.67 K. Again using the aforementioned convention, the negative *K* indicates antiferromagnetic coupling between the ferrimagnetic layers, which is expected, and it is much weaker than the intra-layer coupling, *J*, by a factor of 30. This is in accord with the antiferromagnetic ground state. *K* can also be estimated from the 20 kOe critical field for its spin-flip transition[16] using equation 4.10,

$$\frac{K}{k_B} = -\mu_B H_c \frac{(S - S')}{S^2}, \qquad (4.10)$$

in which μ_B = 9.27x10^{-27} J/T, k_B = 1.3807x10^{-23} J/K, H_c = 2 T, S = 5/2 and S'= 1/2. This gives an experimental interlayer exchange value, $|K|/k_B$ of -0.42 K. Using this value for K/k_B and estimated J/k_B = 19.6 K from **1a**, gives a T_c = 68.2 K. Therefore, depending on which method is used to obtain T_c, different values of K can be calculated by this method. Although K obtained via MF theory is in good agreement, it may be overestimated by a factor of 1.5 which is in the range of error for a MF analysis.

$Mn^{II}(TCNE)I(OH_2)$[7] also has the **A** structure-type (M = Mn^{II}, L^S = μ_4-$[TCNE]^{\cdot-}$; L^{NB} = I, OH_2). However, a MF analysis of the exchange coupling, J, is inappropriate as the T_c of 171 K is (a) double that for other structure-type **A** materials, and is (b) the same as compound **3** which has extended 3-D (**C_2**) bonding. Furthermore, the 5.00 Å interlayer separation is substantially reduced (>35%) from the ≳ 8.0 Å interlayer separation for the other type **A** materials, suggesting stronger interlayer coupling. Also, the dissymmetric bonding of the μ_4-$[TCNE]^{\cdot-}$ in $Mn^{II}(TCNE)I(OH_2)$ differs from that observed for other type **A** materials. Since the ground state is not antiferromagnetic, it must be ferromagnetic, perhaps dipolar in origin, which can be substantial for layered systems.[20] Hence, the interlayer coupling, K, cannot be neglected for $Mn^{II}(TCNE)I(OH_2)$ as was done for the other compounds with this structure-type **A**, and the MF analysis is not appropriate.

Due to the more complex magnetic behavior of $Fe^{II}(TCNE)[C_4(CN)_8]_{1/2}$ (analogous to **2**), the coupling could not be estimated for this compound, i.e. the magnetic behavior is more complicated than MF theory can predict. All forms of MF expressions have $T_c \propto S(S + 1)$. Hence, T_c should be higher for S = 5/2 Mn^{II} with respect to S = 2 Fe^{II} by a factor of 1.46 for identical J values. Hence, the Mn^{II} analog should have a T_c that

exceeds the related Fe^{II} analog. Since the Mn^{II} analog has a lower T_c than the anisotropic Fe^{II} analog, however, a larger $|J|$ must occur for the anisotropic Fe^{II} system. Likewise, the observed trend occurs for the anisotropic $S = 1/2$ Fe^{III} (T_c = 4.8 K)[21] and $S = 1$ Mn^{III} (T_c = 8.8 K)[5] analogs of $[M(C_5Me_5)_2]^+[TCNE]^-$ that have T_cs that exceed the 3.65 K for the isotropic $S = 3/2$ Cr^{III} analog.[14] Similarly, this trend is noted for 3-D $M^{II}[N(CN)_2]_2$ (M = Cr, Mn, Fe, Co, Ni).[22] Hence, a MF comparison between anisotropic and isotropic systems is usually inappropriate.

The structure of **3** has similar 2-D corrugated layers present for **1a** and **2**. In addition, it contains μ_4-$[TCNE]^-$ ions that bridge the layers through the axial Mn^{II} ions, thereby creating a 3-D network structure with each Mn^{II} bonded to six μ_4-$[TCNE]^-$s. As a first approximation, the inter-layer exchange coupling J' for **3** of structure-type $\mathbf{C_1}$ (M = Mn^{II}; L^{S1} =μ_4-$[TCNE]^-$ within the layers; and L^{S2} = μ_4-$[TCNE]^-$ between the layers; and $S = 5/2$, $S' = 1/2$, and $S'' = 1/2$), can be estimated by using equation 4.5. Again, as only T_c is known, J and J' cannot be solved for individually from this expression. However, using the same methodology that was used for **2**, the intra-layer coupling J, for **3** can be estimated by assuming the value that was calculated for **1a** using equation 4.3. This is reasonable as the structures of **1a** and **3** both contain similar 2-D ferrimagnetic layers. Unfortunately, this procedure gives J'/k_B = 66 K, which is clearly overestimated. A more detailed comparison of the three structures reveals that the 2-D layers of **1a** and **3** differ significantly with respect to the corrugation. This is evident from the ∠Mn-N-C of all three compounds, i.e. the ∠Mn-N-C are 169.2°, 174.3°, and 156.5° for **1a**, **2**, and **3** respectively. This different buckling angle may create different coupling within the layers for **3**, invalidating the assumption that J (**1a**) ~ J (**3**).

A more reasonable approach for **3** is to assume that the intra-layer coupling is comparable to the interlayer coupling, i.e., $J \sim J'$.[8] Thus, the coupling for **3** can be estimated using equation 4.6 for general structure-type $\mathbf{C_2}$ ($M = Mn^{II}$; $L^S = \mu_4$-$[TCNE]^{\cdot-}$; and $S = 5/2$ and $S' = 1/2$), and using the observed 171 K T_c, J/k_B= 41.1 K. This is identical to that obtained by using the simplified MF expression equation 4.2 for a two-spin system with an isotropic J. Thus, **3** with structure-type $\mathbf{C_2}$ has approximately double the exchange coupling that was calculated for **1a** with structure-type **A**. On the other hand the coupling of **3** should be around ~1.5 times that of **1a** based on the coordination environment. Albeit in the range of error for a MF analysis, the larger value may be due to differences in the corrugation and ∠Mn-N-C that leads to enhanced coupling.

It should be noted that the antiferromagnetic exchange coupling for Mn^{II}-μ_4-$[TCNE]^{\cdot-}$ has been reported to be as high as several hundred Kelvin for the $[Mn^{III}(TPP)]^{+}[TCNE]^{-}$ family of organic-based magnets that have T_cs up to 28 K,[23,24] but these values were not determined from a MF analysis and thus cannot be directly compared to the MF results reported herein.

For comparison purposes, J/k_B of 146 K was calculated for the amorphous room temperature $V^{II}(TCNE)_x$ using equation 4.6 and the previously reported T_c of 400 K.[3,9] Since the coordination environment is unknown, it was assumed to be $\mathbf{C_2}$ ($M = V^{II}$; $L^S = \mu_4$-$[TCNE]^{\cdot-}$; $S = 3/2$; and $S' = 1/2$). This agrees with the value of 100 K obtained from an analysis of the temperature dependence of the saturation magnetization by the Bloch law for spin wave theory.[25]

A summary of the exchange couplings for compounds **1** to **3** and $V^{II}(TCNE)_x$ is presented in Table 4.3.

Table 4.3. Summary of the computed antiferromagnetic intra- and interlayer exchange couplings.

Magnet		Type	interlayer coupling, K/k_B, or J'/k_B K	intralayer coupling, J/k_B, K	equation
2-D compounds					
$[Mn(TCNE)(NCMe)_2][SbF_6]$	**1a**	**A**	0[a]	19.6	4.2, 4.3
$[Fe(TCNE)(NCMe)_2][SbF_6]$	**1b**	**A**	0[a]	33.9	4.2, 4.3
$[Fe(TCNE)(NCMe)_2][FeCl_4]$	**1c**	**A**	0[a]	31.8	4.2, 4.3
3-D compounds					
$Mn(TCNE)[C_4(CN)_8]_{1/2}$	**2**	**B**	-0.67 (K) -0.42 (K)[b]	19.6[a]	4.4
$Mn(TCNE)_{3/2}(I_3)_{1/2}$	**3**	$\mathbf{C_2}$	65.6 (J')	19.6[a]	4.5
$Mn(TCNE)_{3/2}(I_3)_{1/2}$	**3**	$\mathbf{C_2}$	41.1 ($J' = J$)	41.1 (J)	4.6, 4.2
$V(TCNE)_x$		$\mathbf{C_2}$ [a] $\mathbf{D_2}$ [a]		146 (J) 160 ($J' = J$) 100 (J)[c]	4.6, 4.2 4.8

[a] Assumed [b] Ref 19 [c] Bloch law[25]

Conclusion

General spin, *S*, MF expressions for several 2- and 3-D structure-types were reported that related the exchange constants and the critical temperature, T_c. The evaluation of the inter- and intra-layer coupling constants for various non-cubic M^{II}-TCNE compounds using these expressions were evaluated. The sign of the inter- and intra-layer coupling constants for compounds studied indicate antiferromagnetic coupling, as observed. For layered $[M^{II}(TCNE)(NCMe)_2]^+$ (M = Mn, Fe) the estimated intralayer coupling constant values, J/k_B, were 19.6 and 32.9 K respectively. This indicates antiferromagnetic coupling between the M^{II} and TCNE anion leading to bulk ferrimagnetic ordering. This agrees with the previously reported magnetic data. For $Mn^{II}(TCNE)[C_4(CN)_8]_{1/2}$ the intra-layer coupling constant was assumed to be the same as compound $[Mn^{II}(TCNE)(NCMe)_2]^+$ since they share similar 2-D layers, and the interlayer coupling constant, K/k_B, was estimated as -0.67 K. This suggests that the interlayer interaction is antiferromagnetic and leads to bulk antiferromagnetic ordering, as observed. Finally, the coupling constant for 3-D $Mn^{II}(TCNE)_{3/2}(I_3)_{1/2}$ was shown to be between 1.5 and 2 times as large as that of analogous 2-D analog $[Mn(TCNE)(NCMe)_2]^+$. This discrepancy may be attributed to the increase of corrugation that is observed in the former with respect to the latter. Therefore, a model that includes the topology is needed in order to provide a more accurate description for these magnetic materials. As noted, MF theory can overestimate T_c as much as 40%, but the ratio of inter-layer and intra-layer coupling (J/K or J/J') should be more quantitatively accurate.

Appendix

Structure-type A. The derivation of the MF expression for general S and S' for a 2-D $M(L^S)L^{NB}_2$ compound [M= metal ion, L^S= spin bearing species, L^{NB} = non spin-bearing, non-bridging species] is shown for structure-type **A**, Figure 4.4. Let $M1$ be the average component of spin on M, $M2$ be the average component of spin on L^S, J/k_B be the interactions between M and L^S. Then M would experience an effective magnetic field,

$$H_{eff} = \frac{4JM2}{k_B}, \tag{4.A1}$$

in which the factor of 4 comes from the 4 surrounding L^S sites. L^S would experience an effective magnetic field,

$$H'_{eff} = \frac{4JM1}{k_B}, \tag{4.A2}$$

in which the factor of 4 comes from the 4 surrounding M sites. The effective Hamiltonian on the M site would be

$$\boldsymbol{H} = H_{eff} S, \tag{4.A3}$$

and the effective Hamiltonian on the L^S site would be

$$\boldsymbol{H}' = H'_{eff} S', \tag{4.A4}$$

To find, $M1$ and $M2$, the self-consistent equations for $M1$ and $M2$ are solved

$$M1 = \frac{\sum_{m=-S}^{S} me^{(-H/T)}}{\sum_{m=-S}^{S} e^{(-H/T)}} = \frac{\sum_{m=-S}^{S} me^{(-H_{eff}m/T)}}{\sum_{m=-S}^{S} e^{(-H_{eff}m/T)}}, \tag{4.A5}$$

$$M2 = \frac{\sum_{m=-S'}^{S'} me^{(-H'/T)}}{\sum_{m=-S'}^{S'} e^{(-H'/T)}} = \frac{\sum_{m=-S'}^{S'} me^{(-H'_{eff}m/T)}}{\sum_{m=-S'}^{S'} e^{(-H'_{eff}m/T)}}. \tag{4.A6}$$

Since H_{eff} and H'_{eff} are small close to T_c, the exponential can be expanded by using the identity exp(x) = 1 + x. Therefore $M1$ reduces to

$$M1 = \frac{\sum_{m=-S}^{S} m(1 - \frac{mH_{eff}}{T_c})}{\sum_{m=-S}^{S} (1 - \frac{mH_{eff}}{T_c})} = \frac{\sum_{m=-S}^{S} m - \frac{H_{eff}}{T_c} \sum_{m=-S}^{S} m^2}{\sum_{m=-S}^{S} 1 - \frac{H_{eff}}{T_c} \sum_{m=-S}^{S} m}, \tag{4.A7}$$

and since the summation is $-S < m < +S$ the term, $\sum_{m=-S}^{S} m = 0$, which further reduces $M1$ to

$$M1 = \frac{-\frac{H_{eff}}{T_c} \sum_{m=-S}^{S} m^2}{\sum_{m=-S}^{S} 1}, \tag{4.A8}$$

Equation 4.A8 can be further simplified to equation 4.A11 by using the identities 4.A9 and 4.A10,

$$\sum_{m=-S}^{S} m^2 = \frac{1}{3}(2S^3 + 3S^2 + S), \tag{4.A9}$$

$$\sum_{m=-S}^{S} 1 = 2S + 1, \tag{4.A10}$$

$$M1 = \frac{-\frac{H_{eff}}{T_c}[\frac{1}{3}(2S^3 + 3S^2 + S)}{2S+1} = -\frac{H_{eff}S(S+1)}{3T_c}, \tag{4.A11}$$

Using the same methodology for $M2$ yields

$$M2 = -\frac{H'_{eff}\,S'(S'+1)}{3T_c}, \tag{4.A12}$$

Next, substituting the equations 4.A1 and 4.A2 (effective field for $M1$ and $M2$, respectively) into 4.A11 and 4.A12, respectively gives

$$M1 = -\frac{(4JM2)S(S+1)}{3k_BT_c}, \tag{4.A13}$$

$$M2 = -\frac{(4JM1)S'(S'+1)}{3k_BT_c}, \tag{4.A14}$$

To solve for T_c the 2 linear equations (4.A13 and 4.A14) with 2 unknowns ($M1$ and $M2$) can be solved by writing it as

$$\underline{\underline{A}}\,\underline{v} = \underline{0} \tag{4.A15}$$

in which $\underline{v}$ is a 2 component vector,

$$\underline{v} = \begin{pmatrix} M1 \\ M2 \end{pmatrix}, \tag{4.A16}$$

and $\underline{\underline{A}}$ is a 2 x 2 matrix,

$$\underline{\underline{A}} = \begin{pmatrix} a-1 & b \\ c & d-1 \end{pmatrix}. \tag{4.A17}$$

A solution exists if Det($\underline{\underline{A}}$) = 0, giving

$$(a-1)(d-1) - bc = 0. \tag{4.A18}$$

From equations 4.A13 and 4.A14, the coefficients are

$$\begin{aligned} a &= 0 \\ b &= -\frac{4JS(S+1)}{3k_BT_c} \\ c &= -\frac{4JS'(S'+1)}{3k_BT_c} \\ d &= 0 \end{aligned}, \tag{4.A19}$$

and

$$(0-1)(0-1)-(-\frac{4JS(S+1)}{3k_BT_c})(-\frac{4JS'(S'+1)}{3k_BT_c})=0. \tag{4.A20}$$

Finally, solving for T_c gives

$$T_c = \frac{4}{3k_B}J\sqrt{S(S+1)S'(S'+1)}. \tag{4.A21}$$

Structure-type B. The derivation of the MF expression for general S and S' for a 3-D M(L^S)(L) compound [M= metal ion, L^S= spin bearing species, L = non spin-bearing, bridging species] is shown for structure-type **B**, Figure 4.5. Let $M1$ be the average component of spin on M, $M2$ be the average component of spin on L^S, J/k_B be the interactions between M and L^S, and K/k_B be the interactions between M and M. Then M would experience an effective magnetic field,

$$H_{eff} = \frac{4JM2-2KM1}{k_B}, \tag{4.A22}$$

in which the factor of 4 comes from the 4 surrounding L^S sites and the factor of 2 comes from the 2 M sites. Likewise, L^S would experience an effective magnetic field,

$$H'_{eff} = \frac{4JM1}{k_B}, \tag{4.A23}$$

in which the factor of 4 comes from the 4 surrounding M sites. The effective Hamiltonians for M and L^S are the same as structure-type **A**, equations 4.A3 and 4.A4 respectively.

Substituting equations 4.A22 and 4.A23 into the self-consistent equations for $M1$ and $M2$ (equations 4.A11 and 4.A12 from structure-type **A**, respectively) gives

$$M1 = -\frac{(4JM2 - 2KM1)S(S+1)}{3k_B T_c}, \tag{4.A24}$$

and

$$M2 = -\frac{(4JM1)S'(S'+1)}{3k_B T_c}. \tag{4.A25}$$

Again, the 2 linear equations (4.A24 and 4.A25) with 2 unknowns ($M1$ and $M2$) can be solved by writing it as

$$\underline{\underline{A}}\,\underline{v} = \underline{0}, \tag{4.A26}$$

in which $\underline{v}$ is a 2 component vector,

$$\underline{v} = \begin{pmatrix} M1 \\ M2 \end{pmatrix}, \tag{4.A27}$$

and $\underline{\underline{A}}$ is a 2 x 2 matrix,

$$\underline{\underline{A}} = \begin{pmatrix} a-1 & b \\ c & d-1 \end{pmatrix}. \tag{4.A28}$$

A solution exists if Det($\underline{\underline{A}}$) = 0, giving

$$(a-1)(d-1) - bc = 0 \tag{4.A29}$$

From 4.A24 and 4.A25 the coefficients are

$$\begin{aligned} a &= \frac{2KS(S+1)}{3k_B T_c} \\ b &= -\frac{4JS(S+1)}{3k_B T_c} \\ c &= -\frac{4JS'(S+1)}{3k_B T_c} \\ d &= 0 \end{aligned}, \tag{4.A30}$$

and

$$(\frac{2KS(S+1)}{3k_BT_c}-1)(0-1)-[(-\frac{4JS(S+1)}{3k_BT_c})(-\frac{4JS'(S'+1)}{3k_BT_c})]=0. \quad (4.A31)$$

Finally, solving for T_c gives

$$T_c=\frac{1}{3k_B}[KS(S+1)+\sqrt{K^2[S(S+1)]^2+16J^2S(S+1)S'(S'+1)}]. \quad (4.A32)$$

Structure-type C_1. The derivation of the MF expression for general S, S', and S'' for a 3-D $M(L^{S1})(L^{S2})_{1/2}$ compound [M= metal ion, L^{S1}= spin bearing species, L^{S2} = spin bearing species (different than L^{S1})] is shown for structure-type **C_1**, Figure 4.6a. Let $M1$ be the average component of spin on M, $M2$ be the average component of spin on L^{S1}, $M3$ be the average component of spin on L^{S2}, J/k_B be the interactions between M and L^{S1}, and J'/k_B be the interactions between M and L^{S2}. Then M would experience an effective magnetic field,

$$H_{eff}=\frac{4JM2+2J'M3}{k_B}, \quad (4.A33)$$

in which the factor of 4 comes from the 4 surrounding L^{S1} sites and the factor of 2 comes from the 2 surrounding L^{S2} sites. The effective field for L^{S1} and L^{S2} are respectively

$$H'_{eff}=4JM1, \quad (4.A34)$$

$$H''_{eff} = 4J' M1, \tag{4.A35}$$

in which the factor of 4, in both equation 4.A34 and 4.A35, comes from the 4 surrounding M sites. The effective Hamiltonian for M and L^{S1} are the same as structure-type **A**, equations 4.A3 and 4.A4 respectively and the effective Hamiltonian for L^{S2} is

$$\boldsymbol{H}'' = H''_{eff} S''. \tag{4.A36}$$

Substituting equations 4.A34 and 4.A35 into the self-consistent equations for $M1$ and $M2$ (equations 4.A11 and 4.A12 from structure-type **A**, respectively) gives

$$M1 = -\frac{(4JM2 - 2KM1)S(S+1)}{3k_B T_c}, \tag{4.A37}$$

$$M2 = -\frac{(4JM1)S'(S'+1)}{3k_B T_c}. \tag{4.A38}$$

and, the self-consistent equation for $M3$ will be

$$M3 = -\frac{(4J' M1)S''(S''+1)}{3k_B T_c}. \tag{4.A39}$$

The three linear equations (4.A37, 4.A38 and 4.A39) with three unknowns ($M1$, $M2$, and $M3$) can be solved by writing it as

$$\underline{\underline{A}}\underline{v} = \underline{0}, \tag{4.A40}$$

in which $\underline{v}$ is a 3 component vector,

$$\underline{v} = \begin{pmatrix} M1 \\ M2 \\ M3 \end{pmatrix}, \tag{4.A41}$$

and $\underline{\underline{A}}$ is a 3 x 3 matrix,

$$\underline{\underline{A}} = \begin{pmatrix} a-1 & b & c \\ d & e-1 & f \\ g & h & i-1 \end{pmatrix}, \tag{4.A42}$$

so a solution exists if Det($\underline{\underline{A}}$) = 0 giving

$$(a-1)[(e-1)(i-1)-hf] - d[b(i-1)-hc] + g[bf-(e-1)c] = 0. \tag{4.A43}$$

From equations, 4.A37, 4.A38, and 4.A39 the coefficients are

$$
\begin{aligned}
a &= 0 \\
b &= -\frac{4JS(S+1)}{3k_BT_c} \\
c &= -\frac{2J'S(S+1)}{3k_BT_c} \\
d &= -\frac{4J'S'(S'+1)}{3k_BT_c} \\
e &= 0 \\
f &= 0 \\
g &= -\frac{4J'S''(S''+1)}{3k_BT_c} \\
h &= 0 \\
i &= 0
\end{aligned}
\quad , \tag{4.A44}
$$

which gives

$$
-1 + \frac{16J^2S(S+1)S'(S'+1)}{9k_BT_c} + \frac{8J'^2S(S+1)S''(S''+1)}{9k_BT_c} = 0. \tag{4.A45}
$$

Solving for T_c gives

$$
T_c = \frac{2}{3k_B}\sqrt{S(S+1)[4J^2S'(S'+1) + 2J'^2S''(S''+1)]}\,. \tag{4.A46}
$$

Structure-type $\mathbf{C_2}$. The MF expression for general S and S' for a 3-D $M(L^S)_{3/2}$ compound [M= metal ion, L^S= spin bearing species shown for structure-type $\mathbf{C_2}$, Figure 4.6b can be derived using the same methodology as used for structure-type $\mathbf{C_1}$. However, the MF expression that relates T_c to the coupling constant J for $\mathbf{C_2}$ is equation 4.A47,

$$T_c = \frac{2}{3k_B}|J|\sqrt{6S(S+1)S'(S'+1)}\,, \tag{4.A47}$$

which is a reduced form of equation 4.A46 for the case of isotropic coupling and one spin bearing ligand, i.e. $J \sim J'$ and $L^{S1}=L^{S2}=L^2$ ($S'' \sim S'$).

Structure-type $\mathbf{D_1}$. The derivation of the MF expression for general S, S', and S'' for a 3-D $M(L^{S1})(L^{S2})$ compound [M= metal ion, L^{S1}= spin bearing species, L^{S2} = spin bearing species (different than L^{S1})] is shown for structure-type $\mathbf{D_1}$, Figure 4.7a. Let $M1$ be the average component of spin on M, $M2$ be the average component of spin on L^{S1}, $M3$ be the average component of spin on L^{S2}, J/k_B be the interaction between M and L^{S1}, and J'/k_B be the interaction between M and L^{S2}. Then M would experience an effective magnetic field,

$$H_{eff} = \frac{4JM2 + 2J'M3}{k_B}, \tag{4.A48}$$

in which the factor of 4 comes from the 4 surrounding L^{S1} sites and the factor of 2 comes from the 2 surrounding L^{S2} sites. The effective magnetic fields for L^{S1} and L^{S2} are respectively

$$H'_{eff} = 4JM1, \tag{4.A49}$$

$$H''_{eff} = 2J'M1, \tag{4.A50}$$

in which the factor of 4, in 4.A49 comes from the 4 surrounding M sites and the factor of 2, in 4.A50, comes from the 2 surrounding M sites. The effective Hamiltonians for M and L^{S1} are the same as structure-type **A**, equations 4.A3 and 4.A4, respectively, and the effective Hamiltonian for L^{S2} is

$$\boldsymbol{H}'' = H''_{eff}\, S''. \tag{4.A51}$$

Substituting equations 4.A49 and 4.A50 into the self-consistent equations for $M1$ and $M2$ (equations 4.A11 and 4.A12 from structure-type **A**, respectively) gives

$$M1 = -\frac{(4JM2 - 2KM1)S(S+1)}{3k_B T_c}, \tag{4.A52}$$

$$M2 = -\frac{(4JM1)S'(S'+1)}{3k_B T_c}, \tag{4.A53}$$

The self-consistent equation for $M3$ will likewise be

$$M3 = -\frac{(2J'M1)S''(S''+1)}{3k_B T_c}. \tag{4.A54}$$

Again, the three linear equations ($M1$, $M2$, and $M3$) with three unknowns is solved by writing it as

$$\underline{\underline{A}}\underline{v} = \underline{0}, \tag{4.A55}$$

in which $\underline{v}$ is a 3 component vector,

$$\underline{v} = \begin{pmatrix} M1 \\ M2 \\ M3 \end{pmatrix}, \tag{4.A56}$$

and $\underline{\underline{A}}$ is a 3 x 3 matrix,

$$\underline{\underline{A}} = \begin{pmatrix} a-1 & b & c \\ d & e-1 & f \\ g & h & i-1 \end{pmatrix}, \tag{4.A57}$$

A solution exists if Det($\underline{\underline{A}}$) = 0, giving

$$(a-1)[(e-1)(i-1) - hf] - d[b(i-1) - hc] + g[bf - (e-1)c] = 0. \tag{4.A58}$$

From equations, 4.A52, 4.A53, and 4.A54, the coefficients are

$$
\begin{aligned}
a &= 0 \\
b &= -\frac{4JS(S+1)}{3k_BT_c} \\
c &= -\frac{2J'S(S+1)}{3k_BT_c} \\
d &= -\frac{4J'S'(S'+1)}{3k_BT_c} \\
e &= 0 \\
f &= 0 \\
g &= -\frac{2J'S''(S''+1)}{3k_BT_c} \\
h &= 0 \\
i &= 0
\end{aligned}
\quad , \tag{4.A59}
$$

which gives

$$
-1 + \frac{16J^2S(S+1)S'(S'+1)}{9k_BT_c} + \frac{4J'^2S(S+1)S''(S''+1)}{9k_BT_c} = 0. \tag{4.A60}
$$

Solving for T_c gives

$$
T_c = \frac{2}{3k_B}\sqrt{S(S+1)[4J^2S'(S'+1) + J'^2S''(S''+1)]}\,. \tag{4.A61}
$$

Structure-type $\mathbf{D_2}$. The MF expression for general S and S' for a 3-D $M(L^S)_2$ compound [M= metal ion, L^S= spin bearing species] is shown for structure-type $\mathbf{D_2}$, Figure 4.7b can be derived by using the same methodology used for strucuture type $\mathbf{D_1}$. However, the MF expression that relates T_c to the coupling constant J for $\mathbf{D_2}$ is equation 4.A62,

$$T_c = \frac{2}{3k_B}|J|\sqrt{5S(S+1)S'(S'+1)}\,, \tag{4.A62}$$

which is a reduced form of equation 4.A61 for the case of isotropic coupling and one spin bearing ligand, i.e. $J \sim J'$ and $L^{S1}=L^{S2}=L^2$ ($S'' \sim S'$).

References

(1) Ovcharenko, V. I.; Sagdeev, R. Z. *Russ. Chem. Rev.* **1999**, *68*, 345.

(2) Blundell, S. J.; Pratt, F. L. *J. Phys.: Condens. Matter.* **2004**, *16*, R771.

(3) (a) Miller, J. S. *Chem. Soc. Rev.* **2011**, *40*, 3266. (b) Miller, J. S.; Epstein, A. J. *Angew. Chem. Int. Ed.* **1994**, *33*, 385.

(4) Miller, J. S. *Angew. Chem. Int. Ed.* **2006**, *45*, 2508.

(5) Yee, G. T.; Manriquez, J. M.; Dixon, D. A.; McLean, R. S.; Groski, D. M.; Flippen, R. B.; Narayan, K. S.; Epstein, A. J.; Miller, J. S. *Adv. Mater.* **1992**, *3*, 309.

(6) Miller, J. S.; Calabrese, J. C.; McLean, R. S.; Epstein, A. J. *Adv. Mater.* **1994**, *4*, 498.

(7) (a) Lapidus, S. H.; McConnell, A. C.; Stephens, P. W.; Miller, J. S. *Chem. Comm.* **2011**, *47*, 7602. (b) Chapter 2.

(8) (a) Stone, K. H.; Stephens, P. W.; McConnell, A. C.; Shurdha, E.; Pokhodnya, K. I.; Miller, J. S. *Adv. Mater.* **2010**, *22*, 2514. (b) Chapter 2.

(9) Manriquez, J. M.; Yee, G. T.; McLean, R. S.; Epstein, A. J.; Miller, J. S. *Science*, **1991**, *252*, 1415.

(10) Miller, J. S. *Polyhedron* **2009**, *28*, 1596.

(11) Pokhodnya, K. I.; Bonner, M.; Her, J.-H.; Stephens, P. W.; Miller, J. S. *J. Am. Chem. Soc.* **2006**, *126*, 15592.

(12) Olson, C.; Heth, C.; Lapidus, S. H.; Stephens, P. W.; Halder, G. J.; Pokhodnya, K. I. *J. Chem. Phys.* **2011**, *135*, 024503.

(13) Her, J.-H.; Stephens, P. W.; Ribas-Ariño, J.; Novoa, J. J.; Shum, W. W.; Miller, J. S. *Inorg. Chem.* **2009**, *48*, 3296.

(14) Miller, J. S.; McLean, R. S.; Vazquez, C.; Calabrese, J. C.; Zuo, F.; Epstein, A. J. *J. Mater. Chem.* **1993**, *3*, 215.

(15) Her, J.-H.; Stephens, P. W.; Pokhodnya, K. I.; Bonner, M.; Miller, J. S. *Angew. Chem. Int. Ed.* **2007**, *46*, 1521.

(16) (a) McConnell, A. C.; Shurdha, E.; Bell, J. D.; Miller, J. S. submitted. (b) Chapter 3.

(17) Néel, L. *Ann. Phys. (Paris)* **1948**, *3*, 137.

(18) White, R. M. *Quantum Theory of Magnetism;* Springer: Berlin, 2007, pp. 149-153.

(19) (a) Verdaguer, M.; Bleuzen, A.; Marvaud, V.; Vaissermann, J.; Seuleiman, M.; Desplances, C.; Scuiller, A.; Train, C.; Garde, R.; Gelly, G.; Lomenech, C.; Rosenman, I.; Veillet, P.; Cartier, C.; Villain, F. *Coord. Chem. Rev.* **1999**, *190-192,* 1023. (b) Tanaka, H.; Okawa, N.; Kawai, T. *Solid State Commun.* **1999**, *110*, 191. (c) Greedan, J. E.; Chien, C.-L.; Johnston, R. G. J. *Solid State Commun.* **1976**, *19*, 155. (d) Greedan, J. E. *J. Phys. Chem. Solids* **1971**, *32*, 819. (e) Kimishima, Y.; Ichiyanagi, Y.; Shimizu, K.; Mizuno, T. *J. Magn. Magn. Mater.* **2000**, *210*, 244.

(21) Drillon, M.; Panissod, P.; Rabu, P.; Souletie, J.; Ksenofontov, V.; Gütlich, P. *Phys. Rev. B* **2002**, *65*, 104404. Drillon, M.; Panissod, P. *J. Magn. Magn. Mater.* **1998**, *188*, 93. Drillon, M.; Panissod, P. in *Magnetisim – Molecules to Materials*; Miller, J. S.; Drillon, M., Eds.; Wiley-VCH: Weinheim, 2003, Vol. 4, p. 233.

(22) Miller, J. S.; Calabrese, J. C.; Rommelmann, H.; Chittipeddi, S. R.; Zhang, J. H.; Reiff, W. M.; Epstein, A. J. *J. Am. Chem. Soc.* **1987**, *109*, 769.

(23) (a) Manson, J. L. in *Magnetism: Molecules to Materials V*, Miller, J. S. and Drillon, M. Eds.; Wiley-VCH: New York, 2001, pp. 70-101. (b) Kmety, C. R.; Manson, J. L.; Huang, Q.-Z.; Lynn, J. W.; Erwin, R. W.; Miller, J. S.; Epstein, A. J. *Mol. Chryst. Liq. Crys. A* **1999**, *334*, 631. (c) Kohout, J.; Jager, L.; Hvastijova, M.; Kozisek, J. *J. Coord. Chem.* **2000**, *51*, 169. (d) Batten, S. R.; Murray, K. S. *Coord. Chem. Rev.* **2003**, *246*, 103.

(24) Ribas-Ariño, J.; Novoa, J. J.; Miller, J. S. *J. Mater. Che.* **2006**, *16*, 2600.

(25) Hibbs, W.; Rittenberg, D. K.; Sugiura, K.-I.; Burkhart, B. M.; Morin, B. G.; Arif, A. M.; Liable-Sands, L.; Rheingold, A. L.; Sundaralingam, M.; Epstein, A. J.; Miller, J. S. *Inorg. Chem.* **2001**, *40*, 1915.

(26) Pokhodnya, K. I.; Epstein, A. J.; Miller, J. S. *Adv. Mater.* **2000**, *12*, 410.

CHAPTER 5

PRESSURE-INDUCED MAGNETIC BEHAVIOR OF METAL-TETRACYANOETHYLENE COMPOUNDS

Abstract

The pressure dependent magnetizations of three metal-TCNE (TCNE = tetracyanotheylene) molecule-based magnets, namely, $Mn^{II}(TCNE)_{3/2}(I_3)_{1/2}$ and $M^{II}(TCNE)[C_4(CN)_8]_{1/2}$ (M = Mn, Fe) are reported. $Mn^{II}(TCNE)_{3/2}(I_3)_{1/2}$ exhibits a reversible enhancement of critical temperature, T_c, from 171 K at ambient pressure to 273 K at 14.3 kbar. Compounds, $M^{II}(TCNE)[C_4(CN)_8]_{1/2}$ (M = Mn, Fe) both exhibit quasi-reversible pressure-induced magnetic transitions from antiferromagnetic to ferri- or ferromagnetic.

Introduction

As stated previously, magnets are ubiquitous facets of technology and the design and investigation of new magnetic material that have potential technological application is an expanding area of current research.[1,2,3,4] This avenue of research led to the discovery of the first organic-based magnet, $[Fe(C_5Me_5)_2]^{\cdot+}[TCNE]^{\cdot-}$ and subsequently, the first

room-temperature organic-based magnet, $V(TCNE)_x$. [5,6] One component of that research is the study of the relationship between the structural and magnetic properties of a material. The use of pressure and how it effects the bulk magnetic properties is of particular interest[7] because it allows the investigator to smoothly change the structural parameters of the material.

The reaction of $MnI_2(THF)_3$ and TCNE in CH_2Cl_2 led to an unprecedented structure with μ_4-$[TCNE]^{\cdot-}$ in 3-D of $Mn^{II}(TCNE)_{3/2}(I_3)_{1/2}\bullet z$THF composition.[8] $Mn^{II}(TCNE)_{3/2}(I_3)_{1/2}$ (**1**) exhibits long-range magnetic ordering with a critical temperature, T_c = 171 K. Within the layers, each Mn^{II}, S = 5/2, is antiferromagnetically coupled to four μ_4-$[TCNE]^{\cdot-}$, S = 1/2, creating ferrimagnetic layers. In addition, there are μ_4-$[TCNE]^{\cdot-}$ that bridge the layers that are antiferromagnetically coupled to each Mn^{II}, S = 5/2, leading to bulk ferrimagnetic ordering.

The reaction of $M^{II}(NCS)_2(OCMe)_2$ (M = Mn,[9] Fe[10]) and $(NBu_4)(TCNE)$ in CH_2Cl_2 resulted in the discovery of a new synthetic route for $M^{II}(TCNE)_2\bullet zCH_2Cl_2$ that produced material with a single magnetic phase. The structure of $M^{II}(TCNE)_2\bullet zCH_2Cl_2$ showed that the Mn (**2**) and Fe (**3**) analogs are isostructural and contain corrugated layers of M^{II} bonded to four μ_4-$[TCNE]^{\cdot-}$ that are antiferromagnetically coupled and these layers are bridged by the diamagnetic μ_4-$[C_4(CN)_8]^{2-}$ dimer and best formulated as $M^{II}(TCNE)[C_4(CN)_8]_{1/2}$. It was shown through detailed magnetic susceptibility measurements that **2** and **3** have complex antiferromagnetic ground states.[11]

The relationship between pressure and bulk magnetic properties is not fully understood, however, enhancement of the exchange coupling is expected due to the contraction of bonds under applied pressure. This, in turn, is expected to enhance the

critical temperature, T_c, as it is directly related to the exchange coupling. With the goal of further understanding the role of pressure and to investigate the nature of the magnetic transitions, the pressure dependence of the temperature dependent magnetizations, $M(T,P)$ and of the field dependent magnetizations, $M(H,P)$ were measured for compounds **1**, **2**, and **3** and are reported herein.

Experimental Section

$Mn^{II}(TCNE)_{3/2}(I_3)_{1/2}$[8] (**1**) and $M^{II}(TCNE)[C_4(CN)_8]_{1/2}$ [Mn[9] (**2**), Fe[10] (**3**)] were prepared as previously reported and ~1 mg was loaded into a Teflon™ sample holder. In addition to the sample, ~3 mg of a cylindrical 1.0 mm diameter piece of lead (Alfa Aesar, 99.998%) and ~2 mg of decalin were added to the Teflon holder. The decalin was used as a hydrostatic pressure fluid and the lead was used as an internal pressure standard. At each pressure the superconducting T_c of lead was used as a calibration of applied pressure as the T_c dependence of pressure of lead is known and has been shown to exhibit a linear relationship.[12] The Teflon holder was loaded into a Kyowa Seisakusho beryllium-copper hydrostatic pressure cell with zirconia pistons and o-rings, Figure 5.1. Pressure was applied by using a Kyowa Seisakusho CR-PSC-KY05-1 pressure cell apparatus (pressure range $\leq$ 16 kbar), with WG-KY03-3 pressure sensor. An Aikoh Engineering Model-0218B digital sensor was used as a digital readout for pressure.

All magnetic measurements were performed using a Quantum Design MPMS-5XL 5T SQUID magnetometer equipped with a reciprocating sample measurement system, low field option, and continuous low temperature control with enhanced thermometry features. The temperature dependence of the magnetization was obtained by

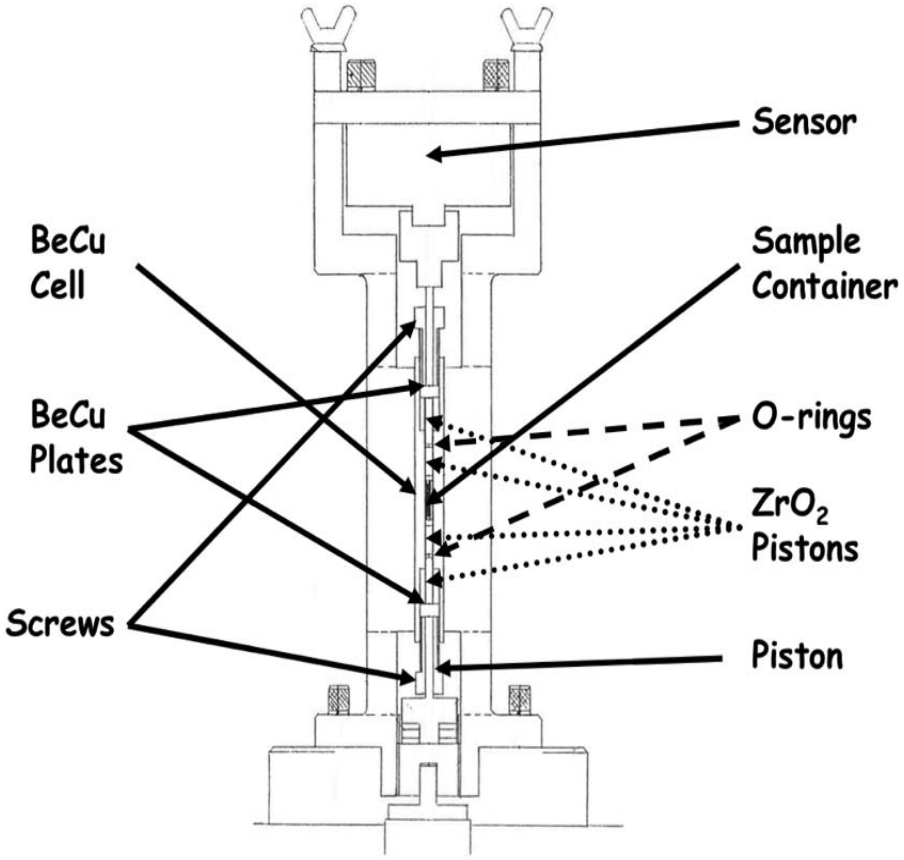

Figure 5.1. Kyowa Seisakusho CR-PSC-KY05-1 BeCu pressure cell apparatus.

cooling in zero-applied field and collecting data upon warming. The remnant magnetization was measured in zero applied field upon warming after cooling below T_c in an applied field of 5 Oe. Isothermal field dependent magnetization was obtained by cooling in zero applied field down to 8 or 10 K and collecting data as field is varied. **1**, **2**, and **3** were each placed separately inside a gelatin capsule for ambient pressure measurements. The gelatin capsule ambient pressure data were then compared to the pressure cell ambient pressure data and a minor adjustment was made to correct for the diamagnetic contribution from the pressure cell.

Results and Discussion

$Mn^{II}(TCNE)_{3/2}(I_3)_{1/2}$ (1). The zero field cooled, $M_{ZFC}(T,P)$ and field cooled, $M_{FC}(T, P)$ magnetizations, up to 14.3 kbar, were measured between 8 and 300 K, Figure 5.2. The bifurcation temperature, T_b, at ambient pressure was found to be 171 K indicating a point of irreversibility. T_b increases continually with increasing pressure by 59% up to a maximum value of T_b = 272 K at a pressure of 14.3 kbar, the upper limit of this study, Figure 5.3. The magnitude of the field cooled magnetization, at low temperature, exhibits a slight decrease with the application of pressure, from a value of 1710 emuOe/mol at ambient pressure to a value of 1420 emuOe/mol at 14.3 kbar.

The remnant magnetization, $M_r(T,P)$, up to 14.3 kbar was measured between 8 and 300 K, Figure 5.4. At ambient pressure, $M_r(T,P)$ is coincident with $M_{FC}(T,P)$ and, upon extrapolation to zero, reaches a temperature intercept of 171 K, which corresponds to the T_c. Upon application of pressure, $M_r(T,P)$ follows the same trend as $M_{FC}(T,P)$ and continues to be coincident. T_c increases continually with increasing pressure by 63% up

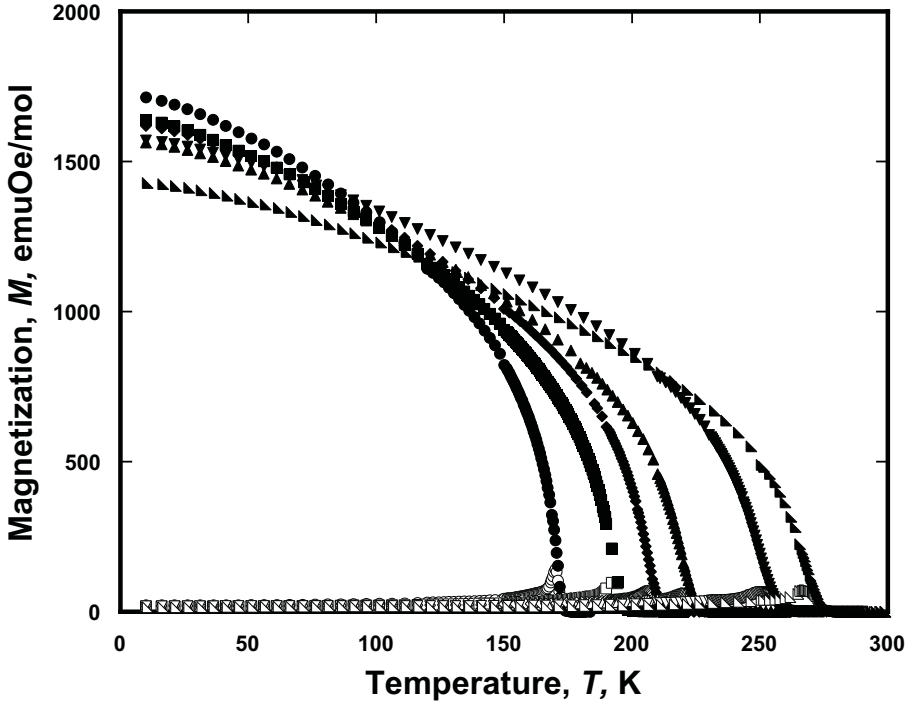

Figure 5.2. $M_{ZFC}(T,P)$ and $M_{FC}(T,P)$ for $Mn^{II}(TCNE)_{3/2}(I_3)_{1/2}$ (**1**). Ambient pressure ZFC (○), FC (●); 1.30 kbar ZFC (□), FC (■); 2.96 kbar ZFC (◇), FC (◆); 5.00 kbar ZFC (△), FC (▲); 10.4 kbar ZFC (▽), FC (▼); and 14.3 kbar ZFC (◺), FC (◣).

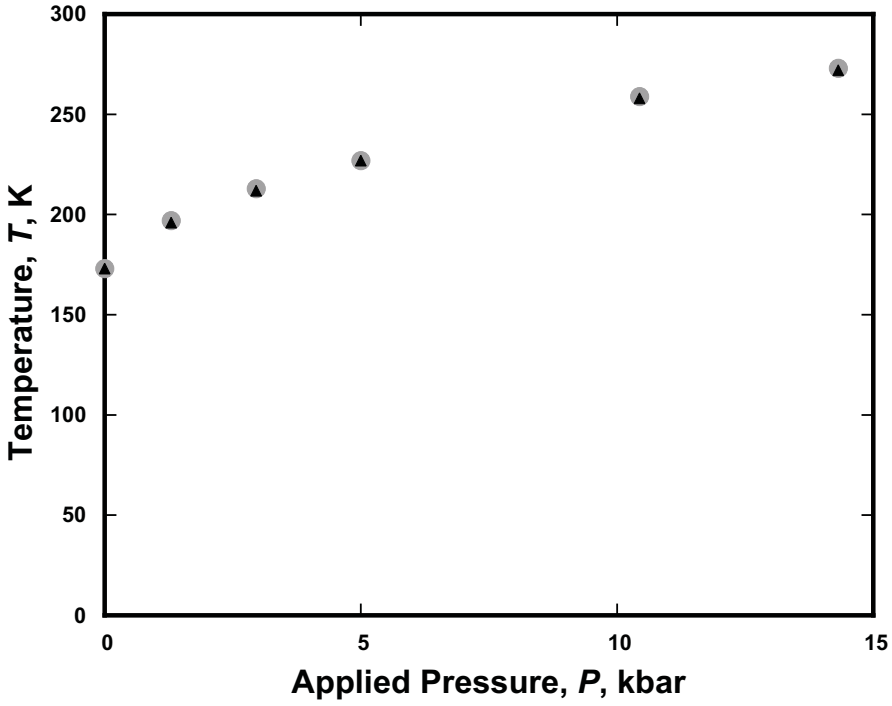

Figure 5.3. $T_c(P)$ (▲) and $T_b(P)$ (●) for $Mn^{II}(TCNE)_{3/2}(I_3)_{1/2}$ (**1**).

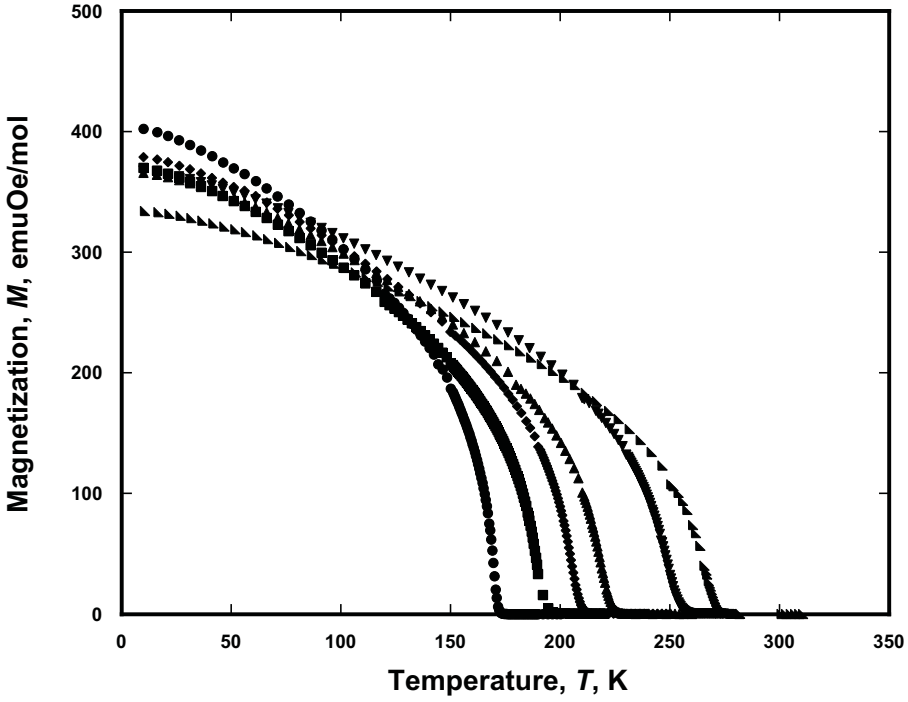

Figure 5.4. $M_r(T,P)$ for $Mn^{II}(TCNE)_{3/2}(I_3)_{1/2}$ (**1**). Ambient pressure (●), 1.30 kbar (■), 2.96 kbar (◆), 5.00 kbar (▲), 10.4 kbar (▼), and 14.3 kbar (◣).

to a maximum value of T_c = 273 K at a pressure of 14.3 kbar, Figure 5.3. The same slight depression of magnetization values at low temperatures that was observed in $M_{FC}(T,P)$ is also exhibited in $M_r(T,P)$.

The isothermal field-dependent magnetization, $M(H,P)$ at 10 K was measured up to 14.3 kbar, Figure 5.5. At ambient pressure **1** exhibits a coercive field, H_{cr}, of 600 Oe; remnant magnetization, M_r, of 8000 emuOe/mol; and a saturation magnetization, M_s, of 21,800 emuOe/mol. The shape of the hysteresis curve changed only slightly upon the application of pressure with the H_{cr} values increasing while the M_r and M_s values exhibiting minimal changes. H_{cr} increases continually with increasing pressure by 46%, up to a maximum of H_{cr} = 880 Oe at 14.3 kbar.

All $M_{ZFC}(T,P)$, $M_{FC}(T,P)$, $M_r(T,P)$ and $M(H,P)$ measurements were re-measured, upon the release of pressure at ambient conditions, after reaching the maximum pressure of 14.3 kbar. The values of the original magnetic properties including, T_b, T_c, H_{cr}, M_r, and M_s were observed upon the release of pressure, proving the reversibility of the process. A comparison of the original ambient pressure measurement of the temperature dependent remnant magnetization, $M_r(T, P)$ to the ambient pressure measurement after release from 14.3 kbar is shown in Figure 5.6.

Compound **1** is attributed to have a direct-coupled 3-D magnetic motif with antiferromagnetic coupling between the Mn^{II} and μ_4-$[TCNE]^{-}$ within the layers as well as between the layers, leading to bulk ferrimagnetic ordering.[8] Therefore, the increase in T_c with the application of pressure is somewhat expected due to the bonds contracting and thus creating enhancement of the cross-sectional overlapping of the orbitals responsible for spin coupling.[13]

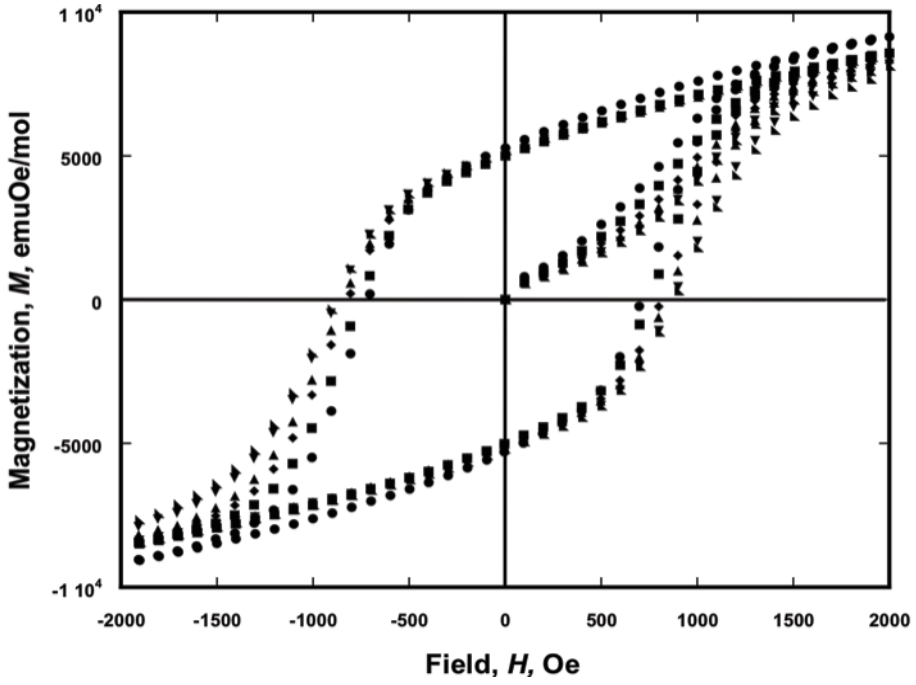

Figure 5.5. $M(H,P)$ for $Mn^{II}(TCNE)_{3/2}(I_3)_{1/2}$ (**1**). Ambient pressure (●), 1.30 kbar (■), 2.96 kbar (◆), 5.00 kbar (▲), 10.4 kbar (▼), and 14.3 kbar (◣).

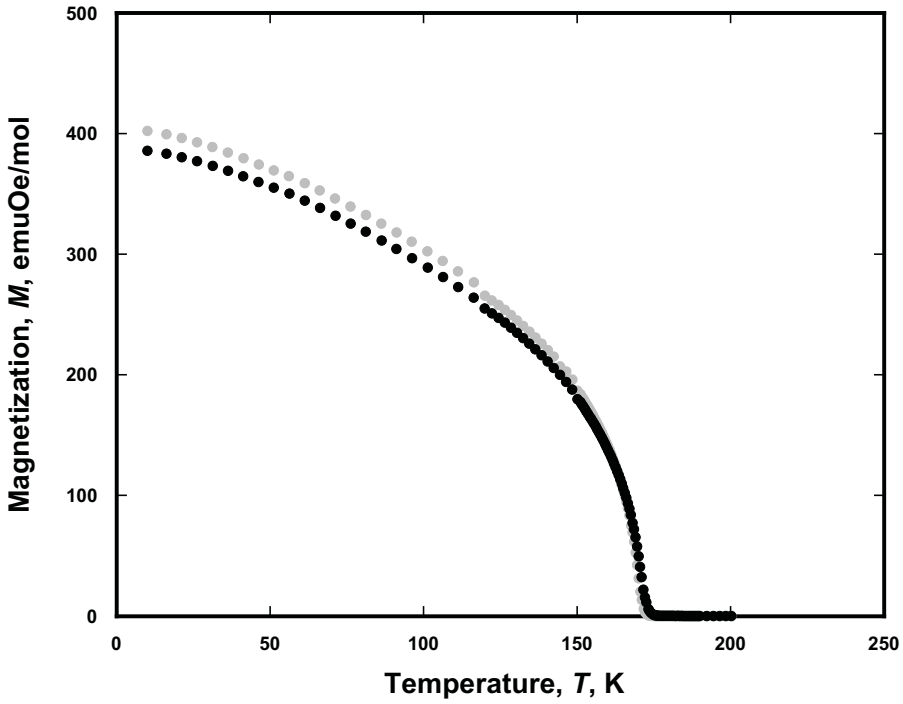

Figure 5.6. $M_r(T, P)$ for $Mn^{II}(TCNE)_{3/2}(I_3)_{1/2}$ (**1**) at ambient pressure (●) and ambient pressure after released (●) depicting the reversibility in the process.

The reproducibility of **1** was investigated by re-measuring the $M_{ZFC}(T,P)$, $M_{FC}(T,P)$, $M_r(T,P)$ and $M(H,P)$ for an additional sample. Although the exact numbers differ, the same trends are observed in $T_c(P)$, $T_b(P)$, and $H_{cr}(P)$ Figure 5.7, for both samples.

$Mn^{II}(TCNE)[C_4(CN)_8]_{1/2}$ (2). The $M_{ZFC}(T,P)$ and $M_{FC}(T,P)$ magnetizations up to 12.6 kbar were measured between 8 and 200 K, Figure 5.8. The ambient pressure $M_{ZFC}(T,P)$ and $M_{FC}(T,P)$ are coincident and lack a bifurcation temperature, T_b, and thus also lack any irreversibility, and contain a broad maxima at 68 K. Upon the initial application of pressure of only 0.95 kbar the $M_{ZFC}(T,P)$ and $M_{FC}(T,P)$ no longer are coincident and exhibit a T_b of 30 K. T_b reaches a maximum value of 105 K upon the application of 12.6 kbar, Figure 5.9.

The $M_r(T,P)$ up to 12.6 kbar was also measured between 8 and 200 K, Figure 5.10. At ambient pressure, $M_r(T,P)$ exhibits atypical behavior in that at low temperature it is negative and reaches a maximum value of only 0.41 emuOe/mol at ~62 K, indicative of its bulk antiferromagnetic properties. $M_r(T,P)$ behaves more typically with the application of the initial pressure of 0.95 kbar and upon extrapolation to zero, gives a T_c of ~25 K. T_c increases continually with increasing pressure up to a maximum T_c ~97 K at a pressure of 12.6 kbar, Figure 5.9.

The $M(H,P)$ at 10 K was measured up to 12.6 kbar, Figure 5.11. At ambient pressure **2** does not exhibit a hysteresis and has an M_s of 20,400 emuOe/mol. This value is less than the expected saturation magnetization of 22,340 emuOe/mol for antiferromagnetic coupling. $M(H,P)$ changes significantly upon the application of pressure leading to an induced hysteretic behavior. Below 3.88 kbar the $M(H,P)$ shape is

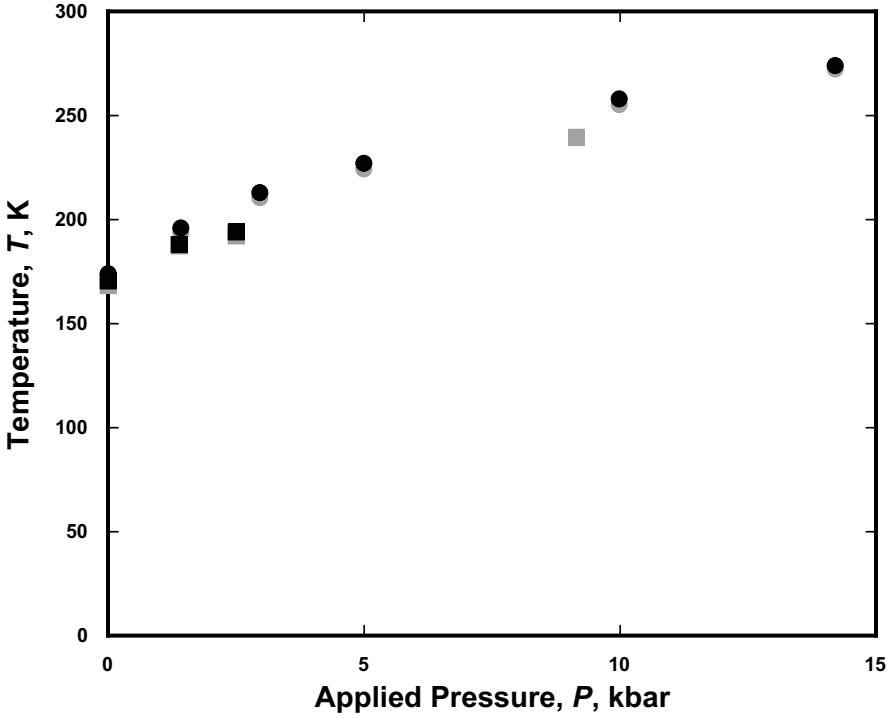

Figure 5.7. Plot of $T_c(P)$ for sample 1 (•) and sample 2 (■); and $T_b(P)$ for sample 1 (•) and sample 2 (■) for $Mn^{II}(TCNE)_{3/2}(I_3)_{1/2}$ (**1**).

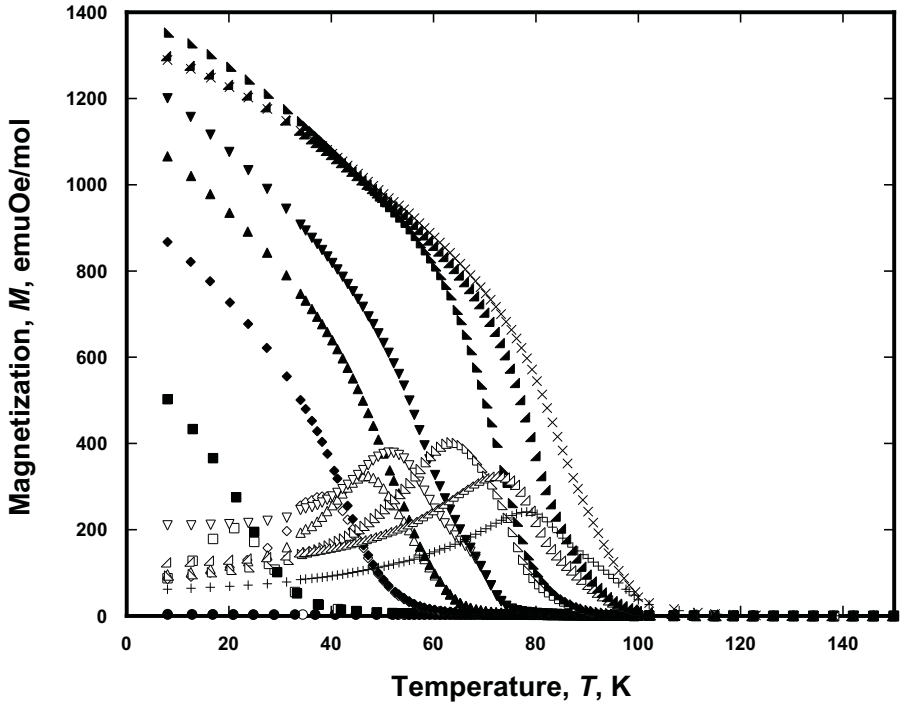

Figure 5.8. $M_{ZFC}(T,P)$ and $M_{FC}(T,P)$ for $Mn(TCNE)[C_4(CN)_8]_{1/2}$ (**2**). Ambient pressure ZFC (○), FC (●); 0.95 kbar ZFC (□), FC (■); 3.88 kbar ZFC (◇), FC (◆); 4.95 kbar ZFC (△), FC (▲); 6.37 kbar ZFC (▽), FC (▼); 8.86 kbar ZFC (◺), FC (◣); 10.8 kbar ZFC (◿), FC (◢); and 12.6 kbar ZFC (+), FC (×).

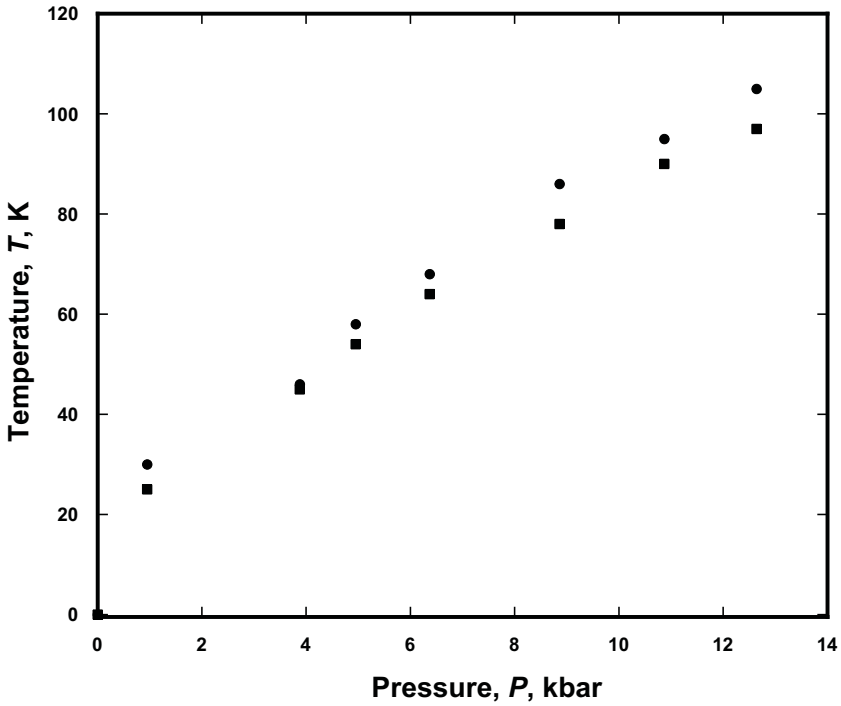

Figure 5.9. $T_c(P)$ (■) and $T_b(P)$ (●) for $Mn^{II}(TCNE)[C_4(CN)_8]_{1/2}$ (**2**).

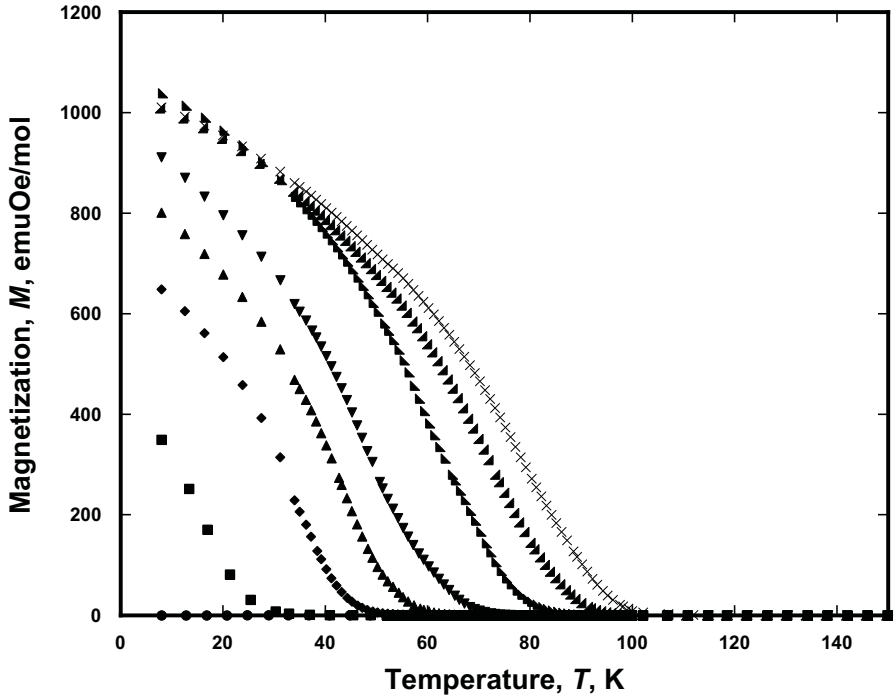

Figure 5.10. $M_r(T,P)$ for $Mn(TCNE)[C_4(CN)_8]_{1/2}$ (**2**). Ambient pressure (●), 0.95 kbar (■), 3.88 kbar (◆), 4.95 kbar (▲), 6.37 kbar (▼), 8.86 kbar (◣), 10.8 kbar (◢), and 12.6 kbar (×).

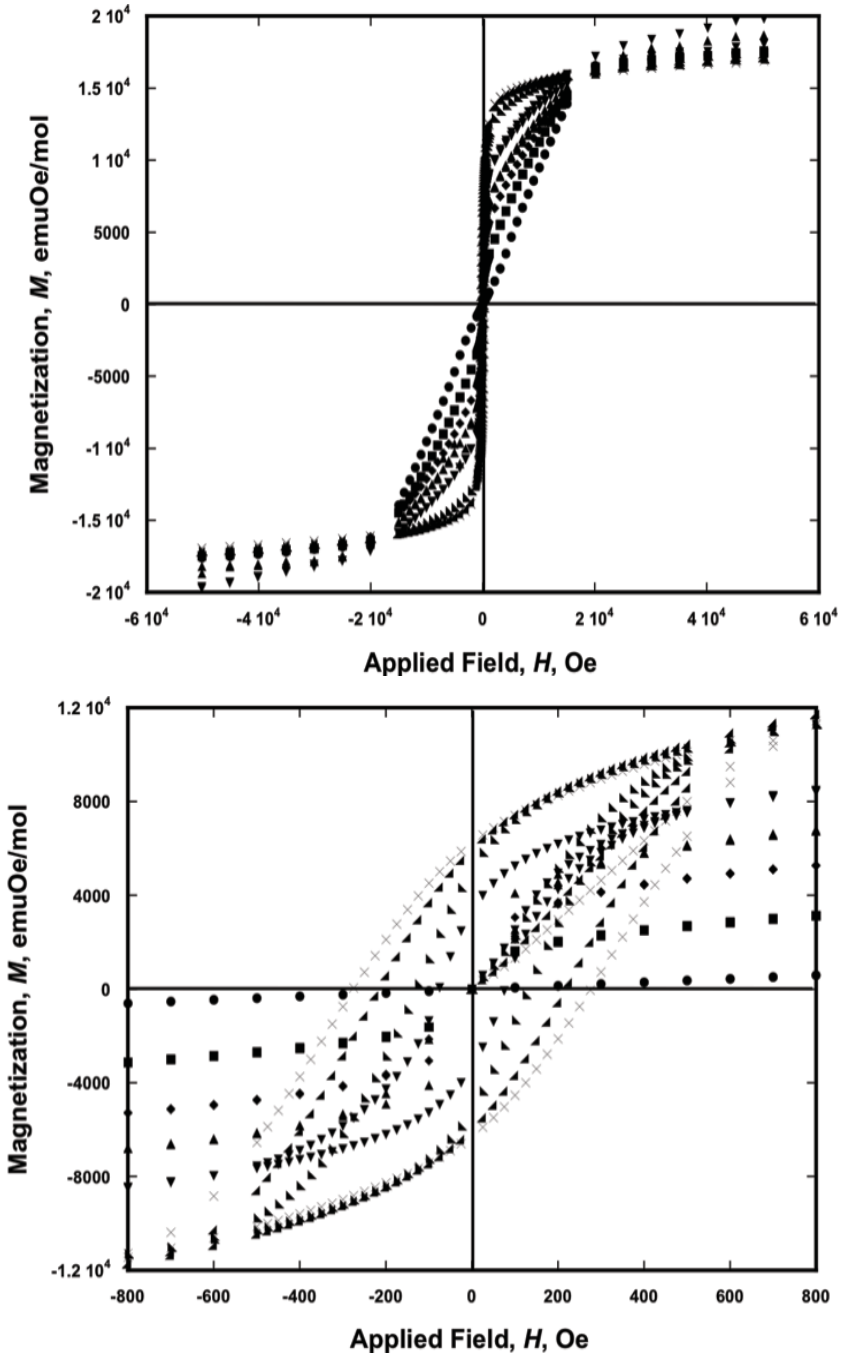

Figure 5.11. *M*(*H*,*P*) (top) and zoom-in showing hysteresis (bottom) for $Mn^{II}(TCNE)[C_4(CN)_8]_{1/2}$ (**2**). Ambient pressure (●), 0.95 kbar (■), 3.88 kbar (◆), 4.95 kbar (▲), 6.37 kbar (▼), 8.86 kbar (◣), 10.8 kbar (◢), and 12.6 kbar (×).

similar to the ambient pressure $M(H,P)$ in that there is no observed H_{cr} or M_r and the M_s exhibits a slight decrease. Above 3.88 kbar the $M(H,P)$ exhibits a coercive field, H_{cr} and remnant magnetization, M_r and both continually increase with the increase of pressure, Figure 5.12.

The application of pressure on **2** is qualitatively a reversible process in that when the pressure is released the induced ferrimagnetic behavior disappears and the original antiferromagnetic properties are retained, i.e., there is no bifurcation temperature in the $M_{ZFC}(T,P)$ and $M_{FC}(T,P)$ data, the magnititude of $M_r(T, P)$ is small for the entire temperature range, and the hysteretic behavior that is induced with pressure is no longer observed, Figure 5.13. Although the original antiferromagnetic ground state is retained, the exact values and shape of $M_{ZFC}(T,P)$, $M_{FC}(T,P)$, $M_r(T, P)$, and $M(H,P)$ change slightly.

The observed behavior can be attributed to an increase in the coupling between the 2-D ferrimagnetic layers. The drastic change in the shape of the $M_{ZFC}(T,P)$ and $M_{FC}(T,P)$ measurement suggests that the dominant interactions, between the layers, change with the application of pressure going from an antiferromagnet to a ferrimagnet. This is in agreement with the remnant data in which the ambient pressure measurement shows little or no remnant magnetization, however with the application of pressure shows significant remnant magnetization typical of ferrimagnets. The $M(H,P)$ data also are in accord with this exhibiting the lack of hysteresis at ambient pressure and upon the application of pressure exhibiting hysteresis indicative of ferrimagnetic ordering. In addition to the pressure-induced transition from antiferromagnetic to ferrimagnetic behavior the decrease in bond lengths increases the superexchange that occurs between

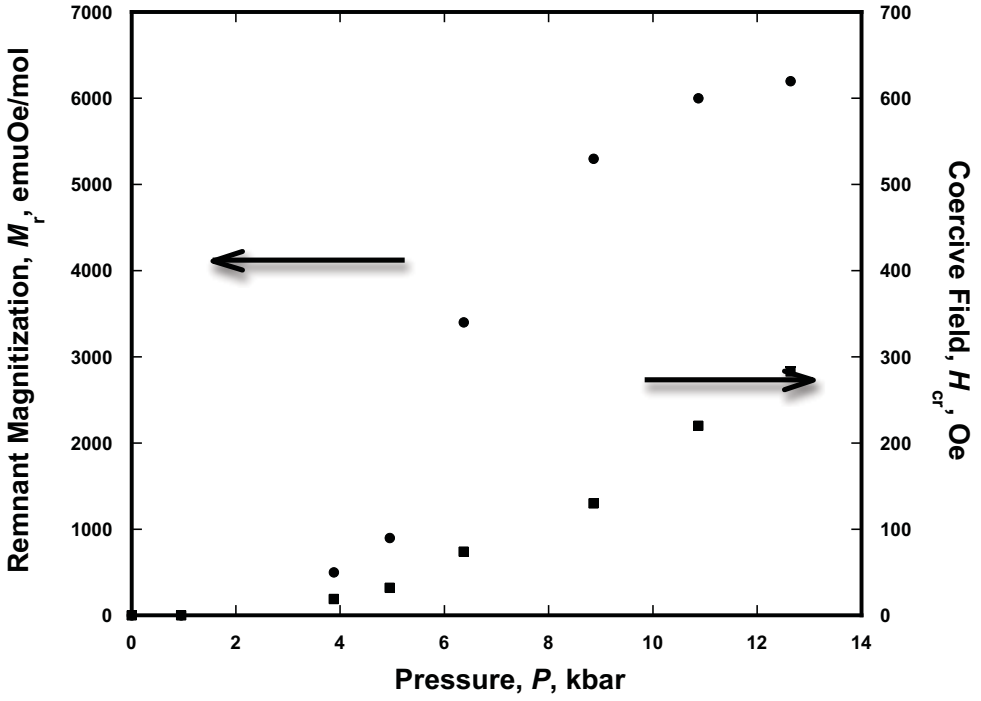

Figure 5.12. $H_{cr}(P)$ (■) and $M_r(P)$ (●) for $Mn^{II}(TCNE)[C_4(CN)_8]_{1/2}$ (**2**).

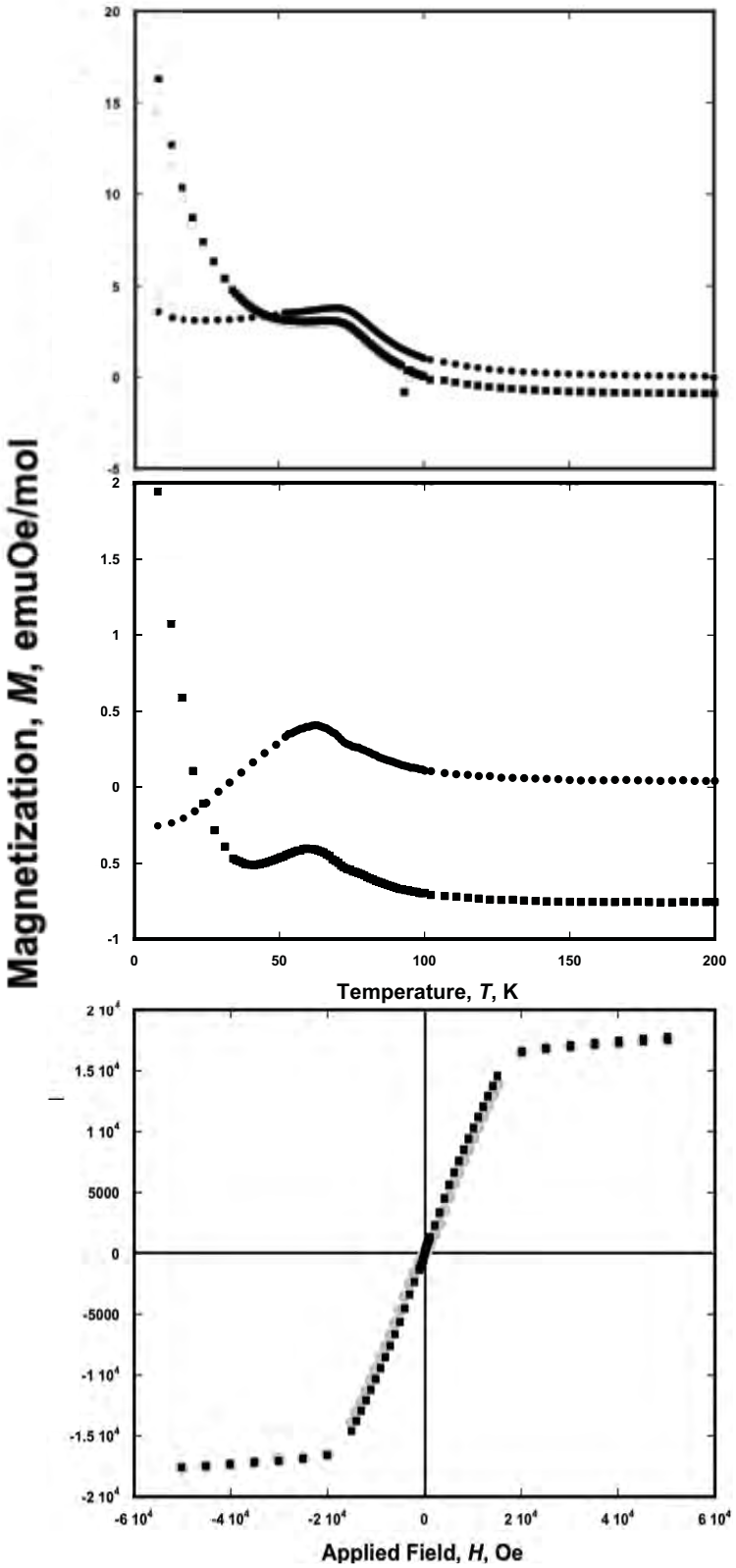

Figure 5.13. $M_{ZFC}(T,P)$ and $M_{FC}(T,P)$ at ambient pressure (●), after release (■) (top); $M_r(T,P)$ ambient pressure (●), after release (■) (middle); and $M(H,P)$ ambient pressure (●), ambient pressure (■) (bottom) for (**2**) showing the quasi-reversible behavior.

the 2-D layers, thus leading to an increase in T_c. Pressure-induced magnetic transitions have been previously reported for other magnetic materials including antiferromagnetic (AFM) to ferri- or ferromagnetic (FM)[14] as observed for **2**, (AFM) to paramagnetic (PM),[15] and FM to AFM.[16]

The reproducibility of **2** was investigated by re-measuring the $M_{ZFC}(T,P)$, $M_{FC}(T,P)$, $M_r(T,P)$ and $M(H,P)$ for an additional sample. Although the exact numbers differ, the same pressure-induced magnetic transition from antiferromagnetic to ferrimagnetic is observed. Similar trends are observed in $T_b(P)$ and $H_{cr}(P)$, Figure 5.14, however the values for sample 2 are significantly reduced. This is attributed to sample 2 being less pure than the original sample that was measured. Further pressure studies on purer samples are needed in order to fully understand the reproducibility of **2**.

$Fe^{II}(TCNE)[C_4(CN)_8]_{1/2}$ (3). Temperature dependent magnetization, $M(T,P)$, up to 12.3 kbar was measured between 8 and 200, Figure 5.15. Because of the weak signal of the $M(T,P)$ data for **3**, the $M_{ZFC}(T)$ and $M_{FC}(T)$ could not be measured. In order to achieve a reasonable signal, an applied field of 10,000 Oe as well as a shortened scan length of 2.0 cm (reduced from typical 6.0 cm scan) was used. The possible addition of an inert paramagnetic material into the sample space in order to increase signal was also considered, however a successful candidate was not identified. Since a fairly large applied field was used, the data collected may not be representative of ground state behavior; therefore the analysis of the data was qualitative. The ambient pressure $M(T,P)$ is indicative of antiferromagnetic ordering and contains a maximum value of ~1700 emuOe/mol at ~100 K which is taken to be the T_c. This differs from that reported in Chapter 3 for this material. This is due to the unpredictable nature of this material and is

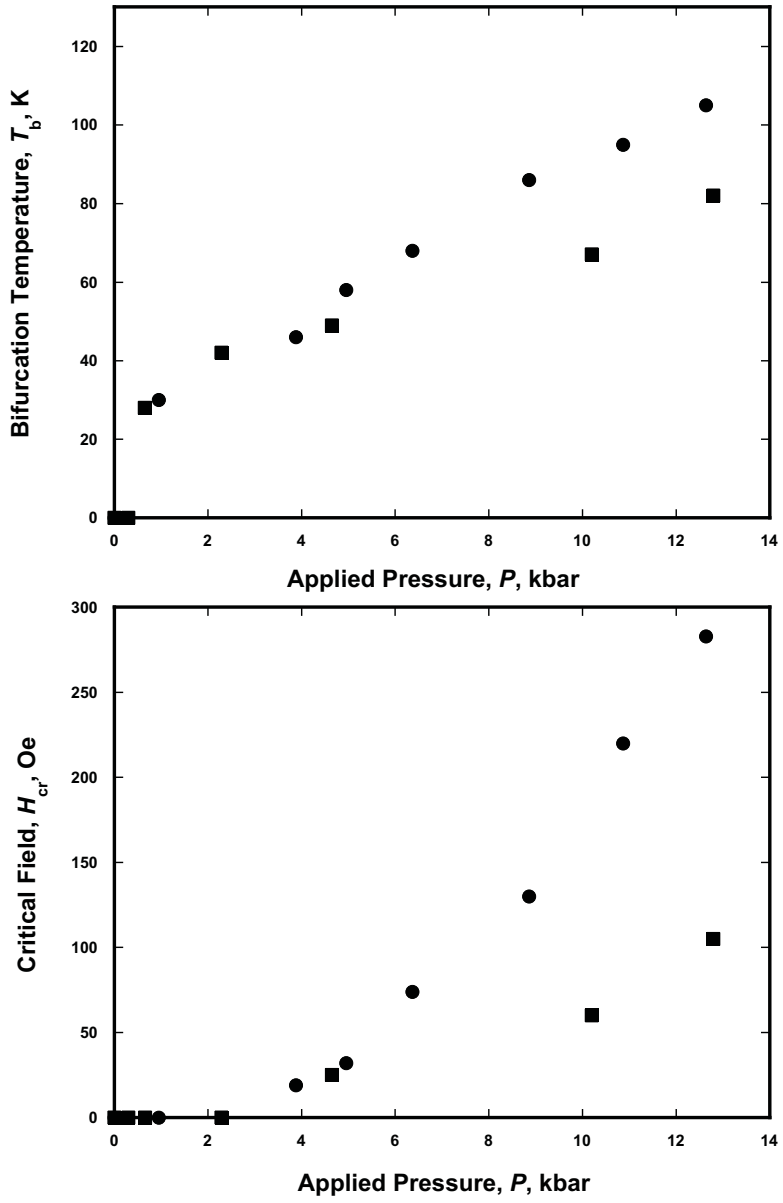

Figure 5.14. Plot of $T_b(P)$ (top) and $H_{cr}(P)$ (bottom) for sample 1 (•) and sample 2 (■) of **2**.

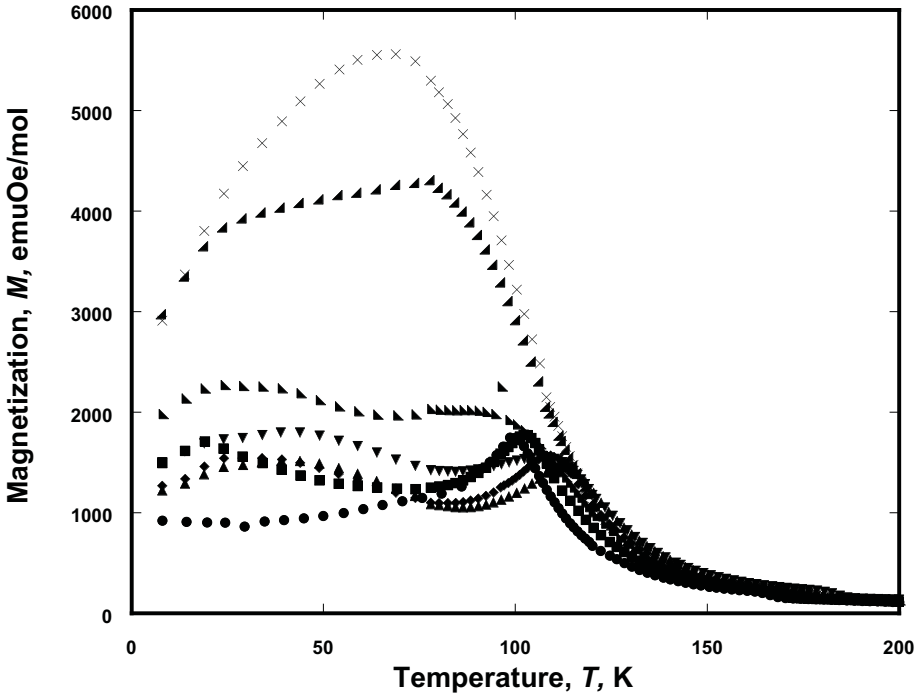

Figure 5.15. $M(T,P)$ of $Fe^{II}(TCNE)[C_4(CN)_8]_{1/2}$ (**3**). Ambient pressure (●), 1.10 kbar (■), 2.95 kbar (◆), 5.31 kbar (▲), 7.43 kbar (▼), 9.58 kbar (◣), 11.8 kbar (◢), and 12.3 kbar (×).

in accord with the sample-to-sample variation observed with the magnetic properties.[11] Upon application of pressure, the magnitude of $M(T,P)$ increases, as does the temperature of the peak. The shape of $M(T,P)$ changes dramatically, leading to two distinct pressure regions. Below 7.43 kbar, the shape of $M(T,P)$ is indicative of bulk antiferromagnetism and the T_c increases as pressure increases. However, above 7.43 kbar the shape of $M(T,P)$ changes drastically, signifying a change in the dominant magnetic interactions in the system. In this high pressure region, the peak of the $M(T,P)$ is no longer distinguishable and therefore a comparison of the onset of $M(T,P)$ is used for this region. A plot showing the dependence of T_c ($P < 7.43$ kbar) and onset temperature is shown in Figure 5.16. As was stated in Chapter 3, the $d\chi T/dT$ data at ambient pressure for **3** lack a peak typically observed, nonetheless for this particular sample, is estimated to occur at 97 K. As pressure is increased, the temperature at which the peak of $d\chi T/dT$ data occur, increases until a pressure of about 7.43 kbar. Above 7.43 kbar, the shape of the $d\chi T/dT$ data changes in that a peak is no longer distinguishable. This signifies a change in the dominant interactions in the system to something other than antiferromagnetic, Figure 5.17.

The $M(H,P)$ at 8 K was measured up to 12.3 kbar, Figure 5.18. At ambient pressure **3** exhibits a constricted hysteresis loop that is indicative of a Class-I metamagnet[17] with a M_r = 720 emuOe/mol and H_{cr} = 2000 Oe. The shape of $M(H,P)$ changes significantly with the application of pressure in which $M(H,P)$ begins to "open up", with both the M_r and H_{cr} values increasing. Again, two distinct pressure regions are observed in that below 7.43 kbar, $M(H,P)$ continues to retain its constricted shape, however above 7.43 kbar, $M(H,P)$ exhibits a more typical hysteretic shape. A plot of the

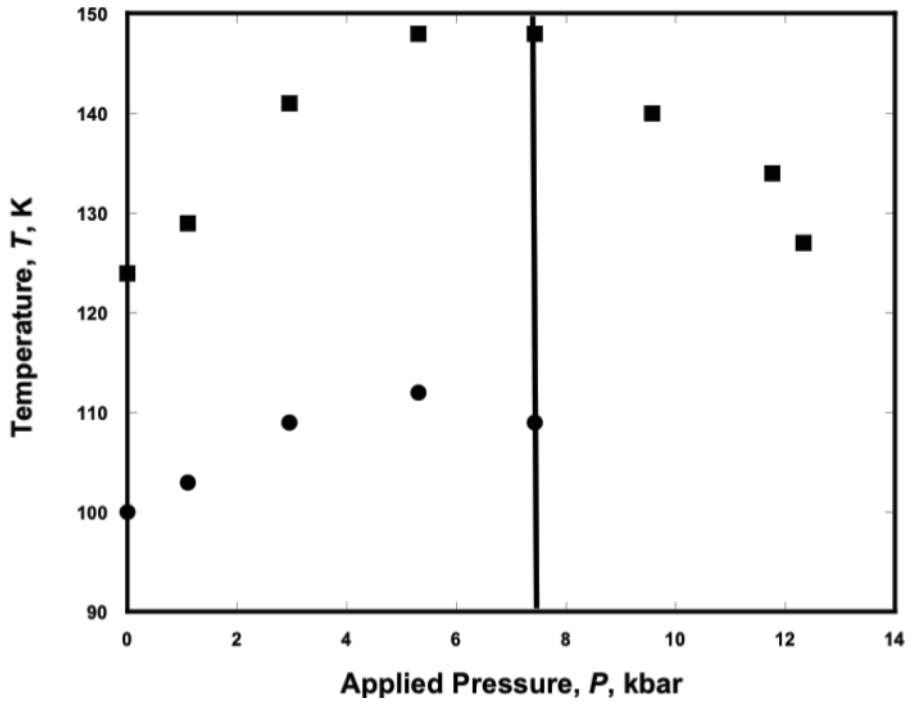

Figure 5.16. Onset Magnetization temperature versus Applied pressure for $Fe^{II}(TCNE)[C_4(CN)_8]_{1/2}$ (**3**) showing the two distinct regions.

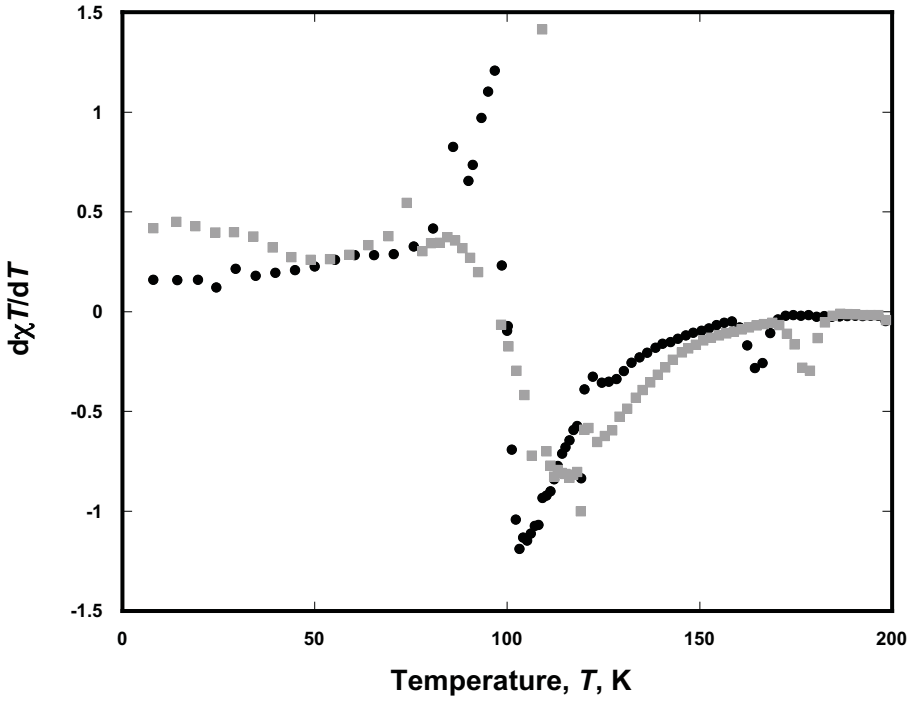

Figure 5.17. Plot of dχT/dT for two selected pressures illustrating the change in shape for the two regions. Ambient pressure (•) and 7.43 kbar (■).

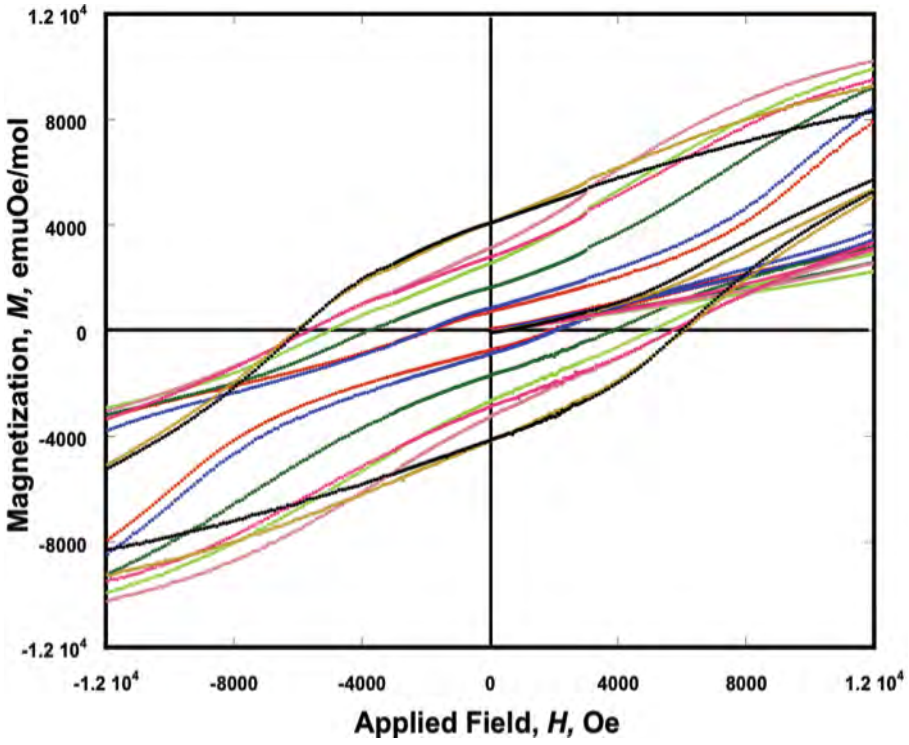

Figure 5.18. $M(H,P)$ for $Fe^{II}(TCNE)[C_4(CN)_8]_{1/2}$ (**3**). Ambient pressure (●), 1.10 kbar (●), 2.95 kbar (●), 5.31 kbar (●), 7.43 kbar (●), 9.58 kbar (●), 11.8 kbar (●), and 12.3 kbar (●).

remnant magnetization, M_r, values and coercive field, H_{cr}, values versus pressure is shown in Figure 5.19, clearly depicting the two regions.

The application of pressure on **3**, like **2** is qualitatively a reversible process in that when the pressure is released the induced ferrimagnetic behavior disappears and the original antiferromagnetic properties are recovered, Figure 5.20. The magnitude and shape of the $M(T,P)$ curve are comparable for both the ambient pressure and the ambient pressure after release. However, the released ambient pressure data show a low temperature phase that is not present in the original ambient pressure data. The isothermal field dependent data, $M(H,P)$ are also comparable for both the ambient pressure and the after release ambient pressure in that they both show the constricted hysteresis shape. However, the values of M_r and H_{cr} are higher in magnitude in the ambient pressure after release data than in the original ambient pressure data. This suggests that the pressure-induced change in coupling is reversible. However, the application of pressure does create a minor irreversible change in **3** perhaps causing spin-canting or slight structural changes.

The observed behavior can be attributed to a change in the interlayer coupling between the 2-D ferrimagnetic layers. This is concluded to occur around or above 7.43 kbar of applied pressure. The drastic change in the shape of the $M(T,P)$ measurement upon the application of pressure suggests a change in the dominant interactions of **3**. This is in agreement with the $M(H,P)$ data in which, upon the application of pressure, the shape goes from constricted to non-constricted, indicating a change in the coupling. Although the nature of the pressure-induced transition is not fully understood, it is estimated to be a transition from antiferromagnetic to ferrimagnetic. This is a reasonable

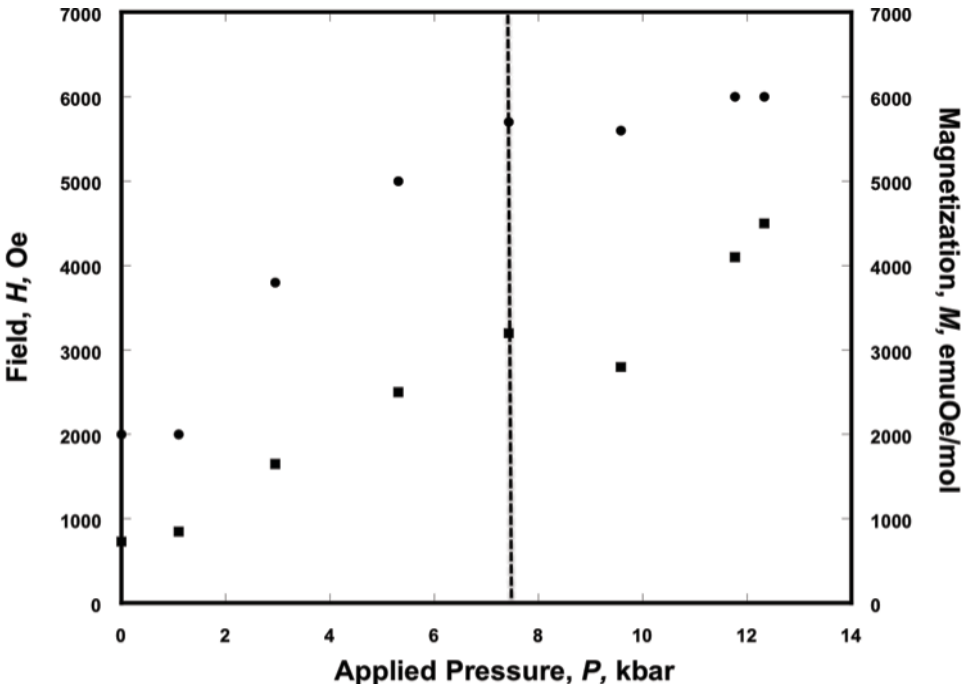

Figure 5.19. $H_{cr}(P)$ and $M_r(P)$ for $Fe^{II}(TCNE)[C_4(CN)_8]_{1/2}$ (**3**) showing the two distinct regions.

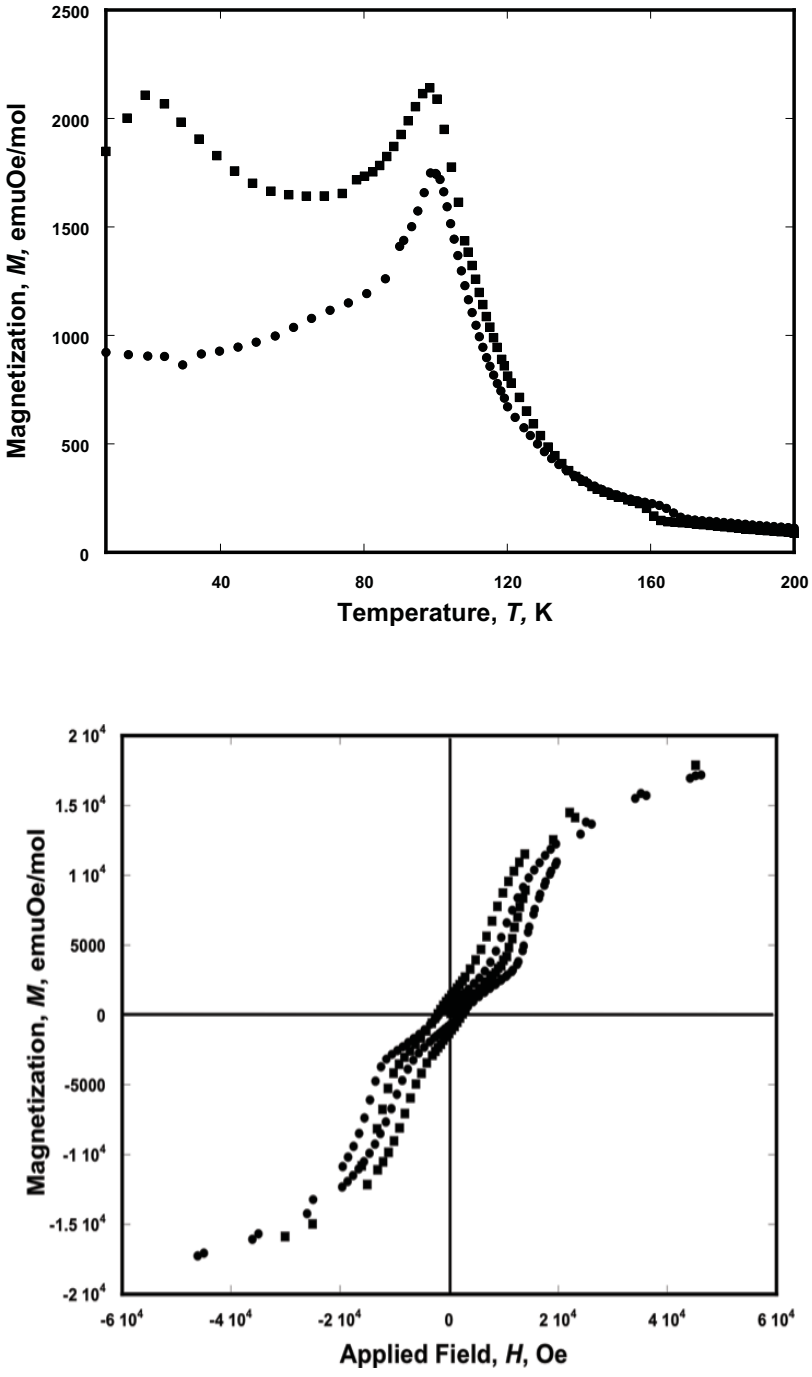

Figure 5.20. *M*(*T*,*P*) ambient pressure (●), ambient pressure after release (■) (top); *M*(*H*,*P*) ambient pressure (●), ambient pressure after release (■) (middle).

assumption since **2** and **3** are isostructural and both contain the same antiferromagnetic ground state. Therefore, the nature of the pressure-induced transition should be similar in both. This is in agreement with the pressure dependent data for **2** in which a pressure-induced transition, from antiferromagnetic to ferrimagnetic, was also observed. This is a qualitatively reversible process in that the observed $M(T,P)$ and $M(H,P)$, at ambient pressure after release, retain their original shapes, however with slight differences in values of magnetic properties.

The reproducibility of **3** was investigated by re-measuring the $M(T,P)$ and $M(H,P)$ curves for an additional sample. Although the exact numbers differ, the same pressure-induced magnetic transition, from antiferromagnetic to ferrimagnetic, exists for both samples. The $M(H,P)$ data for both samples are in agreement in that they both lose their constricted shape at ~ 7 kbar. Similar trends are observed in the onset $T(P)$ and $H_{cr}(P)$, Figure 5.21, although the values for sample 2 are significantly reduced. This is attributed to sample 2 being less pure than the original sample that was measured. Further pressure studies on purer samples are needed in order to fully understand the reproducibility of **3**.

Conclusion

The pressure dependent magnetization of three metal-TCNE molecule-based magnets $\{Mn^{II}(TCNE)_{3/2}(I_3)_{1/2}$ (**1**); $Mn^{II}(TCNE)[C_4(CN)_8]_{1/2}$ (**2**); and $Fe^{II}(TCNE)[C_4(CN)_8]_{1/2}$ (**3**)}are reported. At ambient pressure, **1** orders as a ferrimagnet with a T_c = 171 K and under pressure exhibits a reversible enhancement of T_c up to a maximum of 273 K at 14.3 kbar. Both **2** and **3** order as antiferromagnets at ambient pressure and exhibit a quasi-reversible pressure-induced magnetic transition from

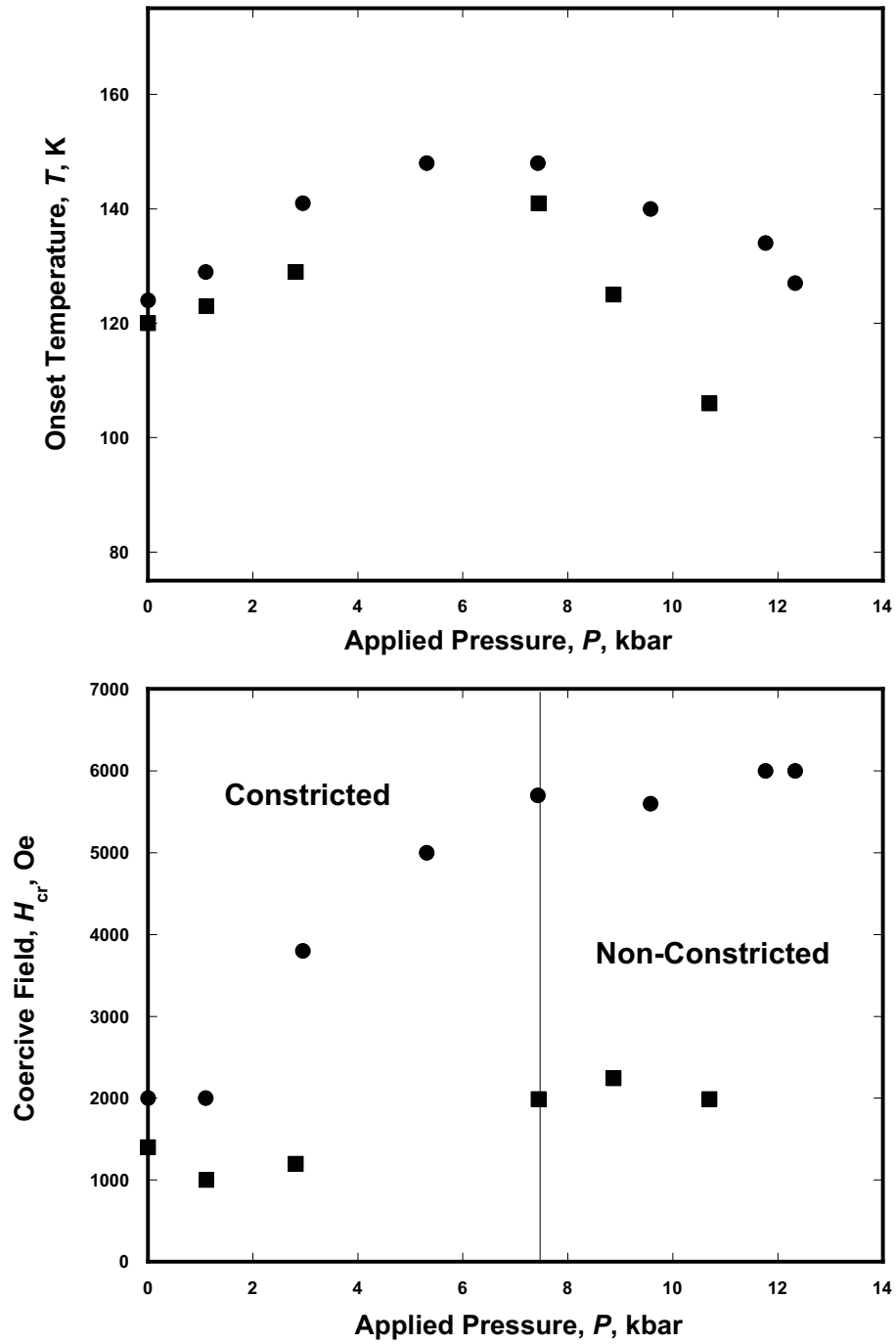

Figure 5.21. Plot of onset $T(P)$ (top) and $H_{cr}(P)$ (bottom) for sample 1 (•) and sample 2 (■) for **3**.

antiferromagnetic to ferri- or ferromagnetic. The reproducibility of the pressure dependencies of all three compounds is under further investigation.

References

(1) (a) Ovcharenko, V. I.; Sagdeev, R. Z. *Russ. Chem. Rev.* **1999**, *68*, 345. (b) Crayson, J. A.; Devine, J. N.; Walton, J. C. *Tetrahedron* **2000**, *56*, 7829. (c) Gatteschi, D. *Adv. Mater.* **1994**, *6*, 635.

(2) (a) Miller, J. S.; Epstein, A. J. *Chem & Industry* **1996**, *2*, 49. (b) Miller, J. S.; Epstein, A. J. *Angew. Chem. Int. Ed. Engl.* **1994**, *33*, 385. (c) Miller, J. S. *Chem. Eng. News* **1995**, *October 2*, 30. (d) Kahn, O. *Molecular Magnetism;* VCH: Weinheim, 1993. (e) Miller, J. S.; Epstein, A. J. *J. Chem. Commun.* **1998**, 1319.

(3) Verdaguer, M.; Girolami, G. in *Magnetism: Molecules to Materials, V*, Miller, J. S. and Drillon, M.; Eds.; Wiley-VCH: Weinheim, 2004, p. 283.

(4) (a) Pejakovic, D. A.; Kitamura, C.; Miller, J. S.; Epstein, A. J. *Phys. Rev. lett.* **2002**, *88*, 057202. (b) Ohkoshi, S.; Yorozu, S.; Sato, O.; Iyoda, T.; Fujishima, A.; Hashimoto, K. *Appl. Phys. Lett.* **1997**, *70*, 1040. (c) Ogaway, Y.; Koshihara, S.; Koshino, K.; Ogawa, T.; Urano, C.; Takagi, H. *Phys. Rev. B* **2000**, *84*, 3181

(5) (a) Miller, J. S.; Calabrese, J. C.; Epstein, A. J.; Bigelow, R. W.; Zhang, J. H.; Reiff, W. M. *J. Chem. Soc. Chem. Commun.* **1986**, 1026. (b) Miller, J. S.; Calabrese, J. C.; Rommelmann, H.; Chittipeddi, S.; Epstein, A. J.; Zhang, J. H.; Reiff W. M. *J. Am. Chem. Soc.* **1987**, *109*, 769.

(6) Manriquez, J. M.; Yee, G. T.; McLean, R. S.; Epstein, A. J.; Miller, J. S. *Science* **1991**, *252*, 1415.

(7) (a) Umeo, K.; Yamane, H.; Kubo, H.; Muro, Y.; Nakamura, F.; Suzuki, T.; Takabatake, T.; Sengupta, K.; Forthaus, M. K.; Abd-Elmeguid, M. M. *Phys. Rev. B* **2012**, *85*, 033101/1. (b) Marcano, N.; Algarabel, P. A.; Fernandez, J. R.; Magen, C.; Morellon, L.; Singh, N. K.; Schlagel, D. L.; Gschneidner Jr., K. A.; Pecharsky, V. K.; Ibarra, M. R. *Phys. Rev. B* **2012**, *85*, 024408/1. (c) Pajerowski, D. M.; Stamatatos, T. C.; Mukherjee, S. Knowles, E. S.; Bencomo, M.; Meisel, M. W.; Christou, G. *Polyhedron* **2010**, *29*, 2462.

(8) (a) Stone, K. H.; Stephens, P. W.; McConnell, A. C.; Shurdha, E.; Pokhodnya, K. I.; Miller, J. S. *Adv. Mater.* **2010**, *22*, 2514. (b) Chapter 2.

(9) (a) Pokhodnya, K. I.; Bonner, M.; Her, J.-H.; Stephens, P. W.; Miller, J. S. *J. Am. Chem. Soc.* **2006**, *126*, 15592. (b) Chapter 3.

(10) (a) Shurdha, E.; Lapidus, S. H.; Stephens, P. W.; Moore, C. E.; Rheingold, A. L.; Miller, J. S. submitted. (b) Chapter 3.

(11) (a) McConnell, A. C.; Shurdha, E.; Bell, J. D.; Miller, J. S. submitted. (b) Chapter 3.

(12) Clark, M. J.; Smith, T. F. *J. Low Temp. Phys.* **1978**, *32*, 495.

(13) (a) Huang, Z. J.; Cheng, F.; Ren, Y. T.; Xue, Y. Y.; Chu, C. W.; Miller, J. S. *J. Appl. Phys.* **1993**, *37*, 3376. (b) Awaga, K.; Sekine, T.; Okawa, M.; Fujita, W.; Holmes, S. M.; Girolami, G. S. *Chem. Phys. Lett. B* **1998**, *293*, 352. (c) Shum, W. W.; Her, J.-H.; Stephens, P. W.; Lee, Y.; Miller, J. S. *Adv. Mater.* **2007**, *19*, 2910.

(14) (a) Umeo, K.; Yamane, H.; Kubo, H.; Muro, Y.; Takabatake, T. *J. Phys. Conf. Ser.* **2010**, *200*, 012215. (b) Egan, L.; Kamenev, K.; Papanikolaou, D.; Takabayashi, Y.; Margadonna, S. *J. Am. Chem. Soc.* **2006**, *128*, 6034. (c) Yamamoto, T.; Tassel, C.; Kobayashi, Y.; Kawakami, T.; Okada, T.; Yagi, T.; Yoshida, H.; Kamatani, T.; Watanabe, Y.; Kikegawa, T.; Takano, M.; Yoshimura, K.; Kageyama, H. *J. Am. Chem. Soc.* **2011**, *133*, 6036.

(15) Tajiri, T.; Matsumoto, S.; Deguchi, H.; Mito, M.; Takagi, S.; Moriyoshi, C.; Itoh, K.; Koyama, K. *J. Magn. Magn. Mater.* **2007**, *310*, e566.

(16) (a) Yamada, A.; Matsubayashi, K.; Uwatoko, Y.; Kondo, K.; Katano, S.; Kosaka, M. *Solid State Commun.* **2010**, *150*, 725. (b) Mitrofanov, V. Y.; Nikiforov, A. E.; Shashkin, S. Y. *Solid State Commun.* **1997**, *104*, 499. (c) Okada, H.; Koyama, K.; Miura, S.; Yamada, M.; Goto, T.; Makihara, Y.; Fujii, H.; Watanabe, K. *J. Phys. Soc. Jpn.* **2004**, *73*, 1982.

(17) (a) Stryjewski, E.; Giordano, N. *Adv. Phys.* **1977**, *26*, 487. (b) Vos, T. E.; Liao, Y.; Shum, W. W.; Her, J.-H; Stephens, P. W.; Reiff, W. M.; Miller, J. S. *J. Am. Chem. Soc.* **2004**, *126*, 11630. (c) Liao, Y.; Shum, W. W.; Miller, J. S. *J. Am. Chem. Soc.* **2002**, *124*, 9336. (d) Vos, T. E.; Miller, J. S. *Angew. Chem. Int. Ed.* **2005**, *44*, 2416: *Angew. Chem.* **2005**, *117*, 2468.

CHAPTER 6

CONCLUSION AND FUTURE DIRECTIONS

It was shown in this dissertation that the metal-tetracyanoethylene (tetracyanoethylene = TCNE) family of molecule-based magnets (MBM) is very diverse in its structural and magnetic properties. This diversity arises from the versatility of the TCNE ligand as it can have multiple coordination modes and can exist as the neutral species, the reduced radical anion, or as the diamagnetic dimer. This allows for numerous extended bonding schemes in the family of material that have shown to exhibit various magnetic exchange pathways including direct-exchange and superexchange or combinations of both. The metal-TCNE family of material has also shown to exhibit a range of bulk magnetic properties including antiferromagnetism, ferrimagnetism, metamagnetism and pressure-induced ferrimagnetism. Nonetheless, more work is still needed in several areas of this research.

The first area that could be further investigated is the nature of the dipolar interactions in 2-D layered $Mn^{II}(TCNE)I(OH_2)$ (Chapter 2). This could be examined by performing a pressure dependent study. The magnetic ground state of $Mn^{II}(TCNE)I(OH_2)$ is similar to 3-D $Mn^{II}(TCNE)_{3/2}(I_3)_{1/2}$ (Chapter 2) in that they both exhibit bulk ferrimagnetism with critical temperatures, T_cs, at 171 K. It was shown in Chapter 5 that

the T_c of $Mn^{II}(TCNE)_{3/2}(I_3)_{1/2}$ increased with increasing pressure reaching a maximum value of 272 K. However, since $Mn^{II}(TCNE)I(OH_2)$ is a 2-D layered structure, the dependency of T_c on pressure is not expected to mimic its 3-D counterpart. Instead, a reasonable hypothesis is that the dependency of T_c on pressure for $Mn^{II}(TCNE)I(OH_2)$ would mimic 2-D $[Fe^{II}(TCNE)(NCMe)_2][Fe^{III}Cl_4]$ in which there are several different regions observed.[1]

It was also shown that the coupling exchange constants could be estimated for several non-cubic structured materials in the metal-TCNE family of molecule-based magnets (MBMs). This was useful as it allowed a comparison of the strength of coupling could be made between similarly structured materials. A similar analysis could be applied toward other non-cubic structured MBMs. For example, Prussian blue analogs (PBAs) are typically cubic structured, however recently there have been developments toward the syntheses of non-cubic PBAs.[2] A comparison between the coupling strength of the cubic-structured PBAs versus non-cubic PBAs may prove fruitful.

In addition, more work is needed in order to fully investigate the reproducibility of the pressure-induced magnetic behavior of $M^{II}(TCNE)[C_4(CN)_8]_{1/2}$ (M= Mn, Fe). To do this, a higher level of reproducibility in the syntheses of the material is needed. It was shown in Chapter 3 that there was sample-to-sample variation in both the Mn and Fe analogs. Therefore an investigation into the nature of the role of solvent content and reaction conditions is needed. If the reproducibility in the syntheses of the material is not fine-tuned then additional pressure measurements on multiples samples is needed so that average trends and values can be extracted.

Recent work performed by Pokhodnya, et al. led to the discovery of 2-D layered compounds, $[M^{II}(TCNE)(NCMe)_2][SbF_6]$ (M = Mn, Fe, Ni).[3] These materials order as bulk ferrimagnets and have similar structures as the $[Fe^{II}(TCNE)(NCMe)_2][Fe^{III}Cl_4]$ compound. In order to fully investigate the magnetic properties of these materials, detailed magnetic susceptibility measurements, in addition to pressure dependent measurements, are needed. Since $[M^{II}(TCNE)(NCMe)_2][SbF_6]$ (M = Mn, Fe, Ni) share similar structures to $[Fe^{II}(TCNE)(NCMe)_2][Fe^{III}Cl_4]$, their bulk magnetic properties, in addition to their dependence on pressure, should be similar. Finally, using the synthetic route that was reported for $[M^{II}(TCNE)(NCMe)_2][SbF_6]$ (M = Mn, Fe, Ni), analogous 2-D layered materials with the formula $[M^{II}(TCNE)(NCMe)_2][X]$ in which X is $[PF_6]^-$ for example, could be synthesized and their magnetic properties studied.

References

(1) Shum, W. W.; Lee. Y.; Stephens, P. W.; Liu, Z.; Miller, J. S. in preparation.

(2) (a) Kareis, C. M.; Lapidus, S. H; Stephens, P. W.; Miller, J. S. *Inorg. Chem.* **2012**, *51*, 3046. (b) Kareis, C. M.; Lapidus, S. H.; Her, J.-H.; Stephens, P. W.; Miller, J. S. *J. Am. Chem. Soc.* **2012**, *134*, 2246. (c) Her, J.-H.; Stephens, P. W.; Kareis, C. M.; Moore, J. G.; Miller, J. S. *Angew. Chem. Int. Ed.* **2010**, *49*, 7773. (d) Her, J.-H.; Stephens, P. W.; Kareis, C. M.; Moore, J. G.; Min, K. S.; Park, J.-W.; Bali, G.; Kennon, B. S.; Miller, J. S. *Inorg. Chem.* **2010**, *49*, 1524.

(3) Olson, C.; Heth, C.; Lapidus, S. H.; Stephens, P. W.; Halder, G. J.; Pokhodnya, K. I. *J. Chem. Phys.* **2011**, *135*, 024503.